EPA-600/3-77-025
August 1977

Ecological Research Series

APPLICATION OF FOURIER TRANSFORM SPECTROSCOPY TO AIR POLLUTION PROBLEMS

Interim Report – 1976

Environmental Sciences Research Laboratory
Office of Research and Development
U.S. Environmental Protection Agency
Research Triangle Park, North Carolina 27711

RESEARCH REPORTING SERIES

Research reports of the Office of Research and Development, U.S. Environmental Protection Agency, have been grouped into five series. These five broad categories were established to facilitate further development and application of environmental technology. Elimination of traditional grouping was consciously planned to foster technology transfer and a maximum interface in related fields. The five series are:

1. Environmental Health Effects Research
2. Environmental Protection Technology
3. Ecological Research
4. Environmental Monitoring
5. Socioeconomic Environmental Studies

This report has been assigned to the ECOLOGICAL RESEARCH series. This series describes research on the effects of pollution on humans, plant and animal species, and materials. Problems are assessed for their long- and short-term influences. Investigations include formation, transport, and pathway studies to determine the fate of pollutants and their effects. This work provides the technical basis for setting standards to minimize undesirable changes in living organisms in the aquatic, terrestrial, and atmospheric environments.

This document is available to the public through the National Technical Information Service, Springfield, Virginia 22161.

EPA-600/3-77-025
August 1977

APPLICATION OF FOURIER TRANSFORM SPECTROSCOPY TO AIR POLLUTION PROBLEMS

Interim Report - 1976

by

J. G. Calvert
W. H. Chan
E. Niple
R. J. Nordstrom
J. H. Shaw
W. R. Skinner
W. M. Uselman
The Ohio State University
Research Foundation
Columbus, Ohio 43212

Grant Number R803868-1

Project Officer

John Spence
Atmospheric Chemistry and Physics Division
Environmental Sciences Research Laboratory
Research Triangle Park, North Carolina 27711

ENVIRONMENTAL SCIENCES RESEARCH LABORATORY
OFFICE OF RESEARCH AND DEVELOPMENT
U.S. ENVIRONMENTAL PROTECTION AGENCY
RESEARCH TRIANGLE PARK, NORTH CAROLINA 27711

DISCLAIMER

This report has been reviewed by the Environmental Sciences Research Laboratory, U. S. Environmental Protection Agency and approved for publication. Approval does not signify that the contents necessarily reflect the views and policies of the U. S. Environmental Protection Agency, nor does mention of trade names or commercial products constitute endorsement or recommendation for use.

ABSTRACT

A Fourier Transform Spectrometer has been used to explore problems in air pollution. Spectra of air samples at ground level of approximately 10m, 100m, and 1km, and solar spectra obtained for solar zenith angles between 40° and 87° have been obtained in the spectral region from 700 to 3500 cm^{-1} with a spectral resolution of better than 0.2 cm^{-1}. Examples of these spectra in the region from 1100 to 1200 cm^{-1} are presented together with synthetic spectra calculated from the compilation of information concerning the spectral lines of atmospheric gases prepared by the Air Force Geophysical Laboratories. The procedure used to generate these synthetic spectra is described briefly. These atmospheric spectra have been searched for the presence of absorption features of a number of gases including HNO_2, HNO_3, HCOOH. From the absorption features of fluorocarbon-12 near 1160 cm^{-1} in solar spectra, a mean tropospheric abundance of 0.34 ppb has been estimated.

A photochemical cell capable of approximating the solar noon irradiance at ground level between 300 and 400 nm and in which path lengths in excess of 200m can be obtained is described. This cell has been used to study the photoysis of HNO_2 and a value of 0.070 min^{-1} has been obtained for the rate constant.

Spectra of more than 20 gases of importance to air pollution problems, obtained under controlled concentration and pressure conditions and covering the region from 700 to 1500 cm^{-1}, are presented.

The progress in the construction of an absorption cell designed to simulate the environment of the stratosphere is described. This cell can be cooled to $-60^{o}C$ and can be irradiated with short wave-length UV radiation down to 170nm.

This report was submitted in fulfillment of Grant Number R803868-1 by The Ohio State University Research Foundation under the sponsorship of the U.S. Environmental Protection Agency. This report covers the period July 15, 1975, to July 14, 1976.

CONTENTS

Abstract..... iii
Figures..... vi
Tables..... ix
Acknowledgment..... x

1. Introduction..... 1
2. Identification of Trace Atmospheric Constituents..... 2
   Identification of fluorocarbon-12 in solar spectra..... 2
   Exploration of techniques for spectral data reduction and analysis-calculation of synthetic spectra..... 13
   Atlas of ground level air spectra and solar spectra..... 23
3. Design of Absorption Cell to Simulate the Environment of the... Stratosphere..... 35
4. Study of Some Key Reactions of Probable Importance in Photo-... chemical Smog Formation..... 41
   Construction and performance of photochemical cell..... 41
   Photolysis experiments..... 56
5. Library of Spectra..... 66
6. Concerning Problems Identified as a Result of the Present..... Investigation..... 94
   Solar spectra and ground level air spectra analysis..... 94
   nitrous acid band analysis..... 94

References..... 96
Appendices

A. Summary of objectives from 1975 proposal..... 99
B. Papers published or accepted for publication..... 101
C. List of papers presented at meetings..... 102

FIGURES

Number		Page
1	Apparatus used to Collect Solar Spectra	4
2	Low-Resolution Solar Spectrum from 500 to 4200 cm^{-1}	6
3	High-Resolution Spectra of Fluorocarbon-12 (CCl_2F_2) from 800 to 1200 cm^{-1}	7
4	Comparison of Solar Spectra, Laboratory Spectra of Fluorocarbon-12, and Computer Synthesized Solar Spectra (with no FC-12 Absorptance) near 923 and 1161 cm^{-1}	8
5	Transmittance of 5.0×10^{-3} Torr FC-12 and 0, 200 and 700 Torr N_2. Total path length = 170 m	10
6	Peak Absorbance of FC-12 at 1160.9 cm^{-1} as a Function of Optical Density (pl)	12
7	Effect of the Width of the Instrument Function a (cm^1) on Resolution	18
8	Atmospheric Spectra between 1100 and 1128 cm^{-1} (see Table V)	26
8a	Synthetic Atmospheric Spectra between 1100 and 1128 cm^{-1} (see Table VI)	25
9	Atmospheric Spectra between 1124 and 1152 cm^{-1}	28
9a	Synthetic Spectra between 1124 and 1152 cm^{-1}	27
10	Atmospheric Spectra between 1150 and 1178 cm^{-1}	30
10a	Synthetic Spectra between 1150 and 1178 cm^{-1}	29
11	Atmospheric Spectra between 1174 and 1202 cm^{-1}	32
11a	Synthetic Spectra between 1174 and 1202 cm^{-1}	31
12	Schematic Diagrams of the Cell and Bath	37
13	Schematic Diagram of Typical Bellows Connection from Cell to Bath	38
14	Radiation Field Inside Cell	40
15	Optical Transfer System from Interferometer to Photochemical Cell	42
16	Gas Inlet System to 6 m Cell	44

FIGURES (Continued)

Number		Page
17	Gas Handling System for 6 m Cell	45
18a	Spectral Distribution of Fluorescent Lamp Output after Passing through the Glass Walls of the Cell	47
18b	Relative Spectral Distribution of Solar Energy at Ground Level	47
19	Radiant Flux Detector Readings (in $mW/cm^2 \cdot sr$) Measured in a Plane Containing the Cell Axis	48
20	The Theoretical Magnitude of the Rate Constant k, for the Formation of $O(^3p)$ Atoms through NO_2 Photolysis at Different Solar Zenith Angles as Estimated for the Atmosphere of Los Angeles	50
21	A Plot of $\ln(A_o/A_t)$ vs Time for NO_2 Photolysis at Low Pressure $[NO_2]_o$ = 30.4 ppm	52
22	Plot of $[NO_2]$ versus Time of Irradiation in the Photochemical Cell	54
23	Plot of $[NO_2]$ versus Time of Irradiation in the Photochemical Cell	55
24	The Time Dependence of [HONO] and $[CO_2]$ in the Photolysis of an HONO-NO_x-CO Mixture	60
25	The Time Dependence of [HONO] and $[CO_2]$ in the Photolysis of an HONO-NO_x-CO Mixture	61
26	The Time Dependence of [HONO] and $[CO_2]$ in the Photolysis of an HONO-NO_x-CO Mixture	62
27	The Time Dependence of [HONO] and $[CO_2]$ in the Photolysis of an HONO-NO_x-H_2O Mixture	63
28	Chart of Chlorine and Fluorine Addition to Methane	66
29	High-Resolution Spectra of Methane	67
30	High-Resolution Spectra of Methyl-fluoride	68
31	High-Resolution Spectra of Dichloro-methane	69
32	High-Resolution Spectra of Chloroform	70

FIGURES (Continued)

Number		Page
33	High-Resolution Spectra of Fluorocarbon-21	71
34	High-Resolution Spectra of Fluorocarbon-22	72
35	High-Resolution Spectra of Fluoroform	73
36	High-Resolution Spectra of Carbon Tetrachloride	74
37	High-Resolution Spectra of Fluorocarbon-11	75
38	High-Resolution Spectra of Fluorocarbon-12	76
39	High-Resolution Spectra of Carbon Tetrafluoride	77
40	Infrared Spectrum of Hydrogen Peroxide	79
41	Infrared Spectrum of Nitrous Acid	80
42	Infrared Spectrum of Methyl Nitrate	81
43	Infrared Spectrum of Ozone	82
44	Infrared Spectrum of Carbon monoxide	83
45	Infrared Spectrum of Methanol	84
46	Infrared Spectrum of t-Butyl-Alcohol	85
47	Infrared Spectrum of di-t-Butyl-Peroxide	86
48	Infrared Spectrum of t-Butyl-Hydroperoxide	87
49	Infrared Spectrum of 2, 2' - Azoisobutane	88
50	Infrared Spectrum of Azomethane	89
51	Infrared Spectrum of Formic Acid	90
52	Infrared Spectrum of Formaldehyde	91
53	Infrared Spectrum of Acetone	92

TABLES

No.		Page
I	Equivalent Air Masses for Zenith Angles 0° to 90° (from Ref. 16)	16
II	Surface Number Densities at T = 294 K and P = 1013 mbar for Atmospheric Gases with Constant Mixing Ratios	19
III	Midlatitude Summer Atmospheric Model (from Ref. 8)	21
IV	Thickness, Mean Pressure, and Temperature of Layers Used in Slant Path Computation	22
V	Information Concerning Spectra Shown in Figures 8-11	24
VI	Parameters for Synthetic Spectra in Figures 8a-11a	24
VII	Rate Data on the Photolysis of NO_2 at Low Pressure	53
VIII	Theoretical Estimates of First-Order Decay Constants for the Photodecomposition of Some Light-Sensitive Compounds of Interest in this Work (Photochemical Chamber)	58
IX	Absorption Coefficients Determined in this Work (Pressure N_2 = 700 Torr, Temperature = 23 ± 2°, Resolution = 1 cm^{-1}	59
X	Initial Conditions of the HONO Photolysis Experiments	59

ACKNOWLEDGMENTS

We would like to thank Dr. S. Z. Levine and Mr. M. Whitbeck for carrying out computer simulations and for preparing compounds for some of the photolysis experiments.

INTRODUCTION

This report summarizes progress made under EPA Grant No. R803868-1. This grant began in July, 1975, and was a successor to EPA Grant No. R803075-01 which extended from April, 1974, to July, 1975. The work completed under the initial grant is described in the Final Report dated August, 1975.

During the first year an Infrared Fourier Transform Spectrometer (IFTS) was made operational and used in conjunction with a 21 m multiple traversal cell to study infrared spectra of atmospheric gases and several pollutant gases including: NO, NO_2, HNO_2. Some preliminary solar spectra between 3 and 20 μm were also obtained.

The kinetics of the formation and decay of nitrous acid were followed by monitoring bands of NO, NO_2, and cis- and trans-HNO_2. Rate constants for the reactions were derived and a mechanism accounting for the formation of HNO_2 in the atmosphere was proposed.

In addition to these studies a six-meter multiple traversal cell in which path lengths up to 300 m can be obtained was constructed.

This cell is surrounded with fluorescent tubes with output in the region from 300 to 450 nm. The cell irradiance in this region closely simulates the solar irradiance at ground level in spectral distribution and intensity.

The work performed under the present grant has built on the experience gained during the first year of work, and the progress made in several areas is described in this report.

IDENTIFICATION OF TRACE ATMOSPHERIC CONSTITUENTS

Among the objectives of this work is the search for evidence of trace gas constituents in the atmosphere and the estimation of their abundances and variabilities. Infrared techniques are among the most unambiguous and sensitive methods for identifying traces of gases, especially if high-resolution spectra of long atmospheric paths are available. We have obtained relatively high resolution (0.125 cm^{-1})spectra of various path lengths of ground level air and also solar spectra. Analyses of these spectra are being made and the present status of these investigations is described below.

IDENTIFICATION OF FLUOROCARBON-12 IN SOLAR SPECTRA

Concern over the atmospheric concentrations and fates of halogen-substituted methanes has grown since the first report of the potential influence of these compounds in the stratosphere. A variety of techniques has been employed to measure trace pollutants such as fluorocarbon-11 (FC-11, CCl_3F) and fluorocarbon-12 (FC-12, CCl_2F_2). Gas chromatography has been used extensively by several research groups throughout the world to record in situ concentrations of these compounds at a variety of altitudes.[2-5]

Although gas chromatography is a popular method for investigating atmospheric pollutants, several forms of infrared spectroscopy are also being used to identify trace gases. By using infrared Fourier transform spectroscopy and a cryogenic procedure for concentrating trace pollutants, Hanst et al.[6] detected background levels of several pollutants including FC-11 and FC-12. Murcray et al.[7] performed in situ infrared measurements in the stratosphere, and detected FC-11 and FC-12 as well as HNO_3 with a grating instrument on a balloon flight at 30 km.

We have initiated a project to record high-resolution spectra of the infrared transmission of solar radiation through the atmosphere to detect trace pollutants. The solar spectra were recorded using Fourier transform spectroscopy from a ground-based station in Columbus, Ohio. Nominal resolution for this instrument is 0.125 cm^{-1}.

Data were recorded over a two-month period in September and October, 1975. Preliminary analysis of these solar spectra indicates the presence of FC-12 in the atmosphere. This analysis was made by comparing these solar spectra with laboratory spectra of FC-12 and also by comparing the observed solar spectra with computer synthesized solar spectra which exclude absorption features due to trace pollutants. These synthetic spectra were generated from the Air Force Cambridge Research Laboratories (AFCRL) Atmospheric Absorption Line Parameters Compilation.[8] This compilation is available on magnetic tape.

Results of these comparisons indicate that there are absorption features in our collected solar spectra which are not present in the computer-generated spectra. Furthermore, these absorption peaks agree in both position and relative intensity with several absorption peaks of FC-12.

Equipment

A sketch of the apparatus used to collect the solar spectra is shown in Fig. 1. Solar radiation incident on the first coelostat mirror (CM_1) is reflected to the second coelostat mirror (CM_2). This second mirror reflects the radiation down through an opening in the roof and into the laboratory. Both coelostat mirrors are 30 cm diameter flats.

The first coelostat mirror is equipped with a clock drive which rotates the mirror to track the motion of the sun. The coelostat thus provides a fixed beam of solar radiation into the laboratory. Mirror M_3 reflects the vertical beam to an optical table where mirrors M_4 and M_5 are positioned to direct the radiation into the Michelson interferometer. Both of these mirrors are rectangular flats.

An aperture A reduces the beam diameter to approximately 2.5 cm before the radiation enters the interferometer. This aperture aids in alignment of the beam into the interferometer in the following way. The beam splitter is removed from the interferometer and mirrors M_4 and M_5 are adjusted until the 2.5 cm diameter beam falls in the center of the 5 cm diameter interferometer mirror, and the beam which is reflected from the interferometer mirror passes back through the optical system and out the aperture. In this fashion, the beam is made reasonably perpendicular to the mirror surface. The beam splitter is then replaced.

Mirror M_6 directs the radiation which exits the interferometer into the detector. For this study, a copper-doped germanium photoconductor operated at liquid helium temperature was used. The spectral range of this detector extends from 300 cm^{-1} to 3500 cm^{-1}. However, because of sampling limitations involved in high-resolution Fourier transform spectroscopy, the spectral range was limited by an optical filter to the region 300 cm^{-1} to 1500 cm^{-1}. The detector assembly is equipped with optics which focus parallel radiation onto the 1 mm square detecting crystal.

The output from the detector is digitized by a 15-bit analog-to-digital converter, and the interferogram is computed into a spectrum by a Nova 1200 minicomputer. This computer has 8K of core and has a 128K, fixed-head disc and a 9-track, high-density magnetic tape unit as peripheral equipment. The computed spectra are stored on the magnetic tape and can be recalled at any future time for plotting on a digital plotter. The entire system was supplied by Digilab, Inc.

High-resolution spectra of FC-12 were recorded with the same Fourier transform instrument. A Nernst glower was used as the infrared source. Radiation from the glower was collimated into the interferometer. The radiation leaving the interferometer passed through a multiple traversal cell and was collected by the copper-doped germanium detector.

The absorption cell was constructed entirely of glass and stainless steel. The mirror system in the cell was designed by Hanst[6] and the base path length between the mirrors is approximately 5.3 meters. The spectra of FC-12 were recorded by using a variety of path lengths within the cell.

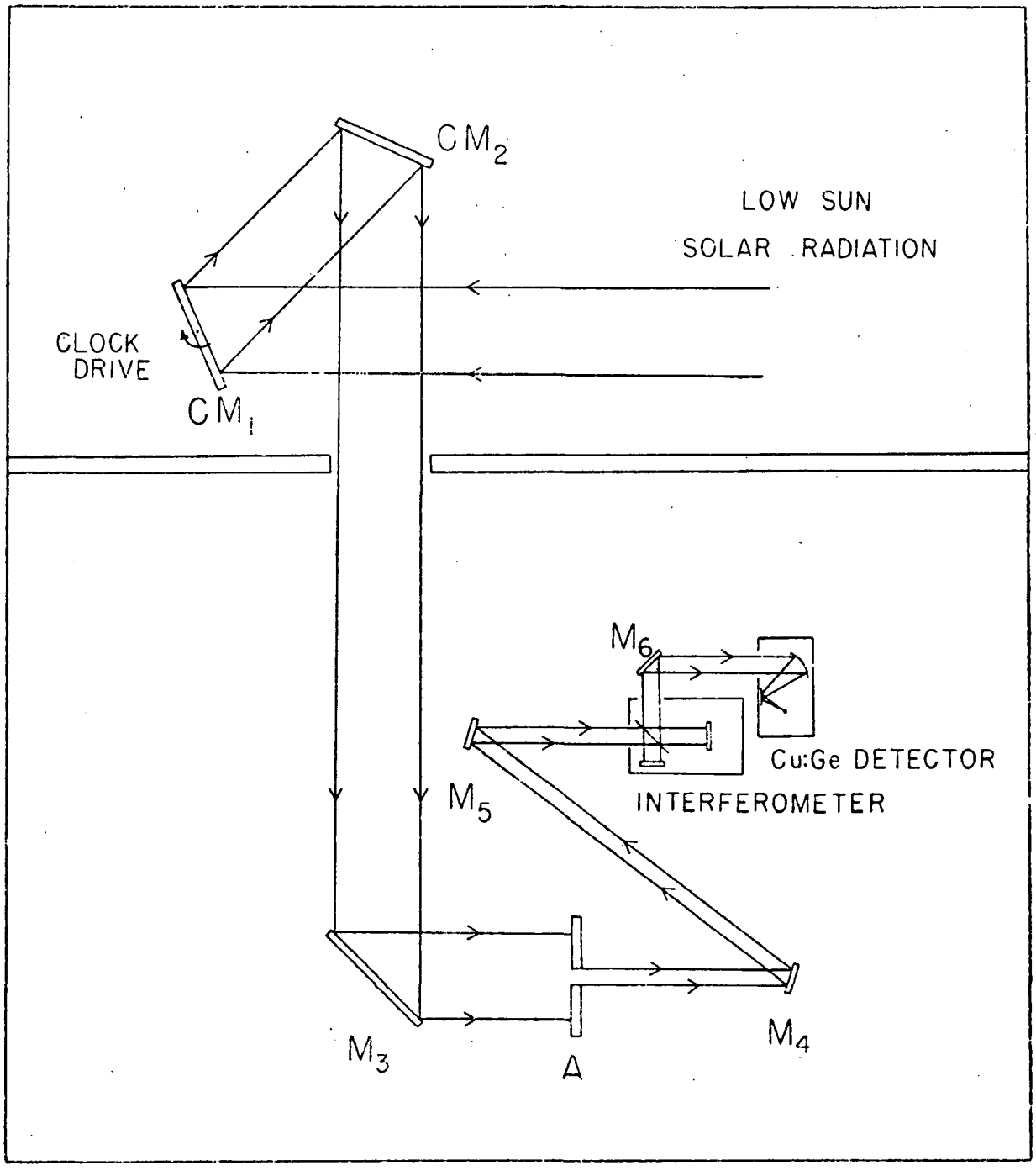

Figure 1. Apparatus used to collect solar spectra

Detection of Fluorocarbon-12

Figure 2 shows a low-resolution survey spectrum of the atmospheric transmission of infrared solar radiation from 500 cm^{-1} to 4200 cm^{-1}. This plot shows that the resident atmospheric gases, most notably H_2O and CO_2 are totally absorbing in several regions, dividing the spectrum into limited infrared "windows." If pollutants are to be detected in the atmosphere by observing infrared solar spectra, it is necessary that their infrared absorptions fall within an atmospheric transmission window. Even within a window, however, interference from partially absorbing lines can obscure the detection of trace gases.

A high-resolution solar spectrum is rich with a complexity of absorbing lines. In order to sort out which of these lines, if any, are due to an atmospheric contaminant, it is necessary to make extensive comparisons of the solar spectrum with various laboratory spectra. Many gases have been selected for comparison, however at this time only FC-12 has been identified in the solar spectra.

Figure 3 shows two high-resolution transmission spectra of FC-12 in the region of the 1000 cm^{-1} solar window. Nominal resolution for these spectra is 0.125 cm^{-1}. Several features stand out as being ideal signatures for possible identification of FC-12 in solar spectra. These features are the very strong, narrow absorptions near 923 cm^{-1} and 1161 cm^{-1}. which are possibly due to Q-branch transitions. Narrow absorption spikes such as these might be separable at high resolution from absorption features of the resident atmospheric gases.

Figure 4 shows several comparisons which were made to verify that FC-12 is indeed present in our solar spectra. The two spectral regions where the narrow FC-12 absorptions occur are plotted. The top spectrum in each region is FC-12 at low concentration. Below this spectrum is one of the many solar spectra which were collected. The solar angle to the zenith was approximately 45° for this spectrum. In the region near 923 cm^{-1} there is a strong water absorption which partially masks the position of the FC-12 absorption features. Nevertheless, three distinctive absorption characteristics are evident in the solar spectrum which might be attributed to FC-12. Murcray et al.[7] have previously identified these absorption features as belonging to FC-12.

The region near 1161 cm^{-1} appears to be a much better spectral region in which to observe atmospheric FC-12. From the laboratory spectrum, it is clear that the FC-12 absorption in this region is approximately twice as strong as the strongest feature near 923 cm^{-1} which leads to a more sensitive detection. Also, the region around 1161 cm^{-1} is free from water vapor interference. The moderately strong and regular absorption lines in this region of the solar spectrum are due to N_2O. Weaker absorption lines are due to O_3. Figure 4 shows an absorption line in the solar spectrum which coincides with the strong absorption of FC-12.

Although these four absorption lines in the solar spectrum coincide with the positions of FC-12 absorptions, it would be most informative to compare the solar spectrum with a similar spectrum which definitely had no FC-12 present. This comparison was accomplished by first generating synthetic solar spectra. Results of this computer synthesis are shown in Fig. 4. The spectrum below

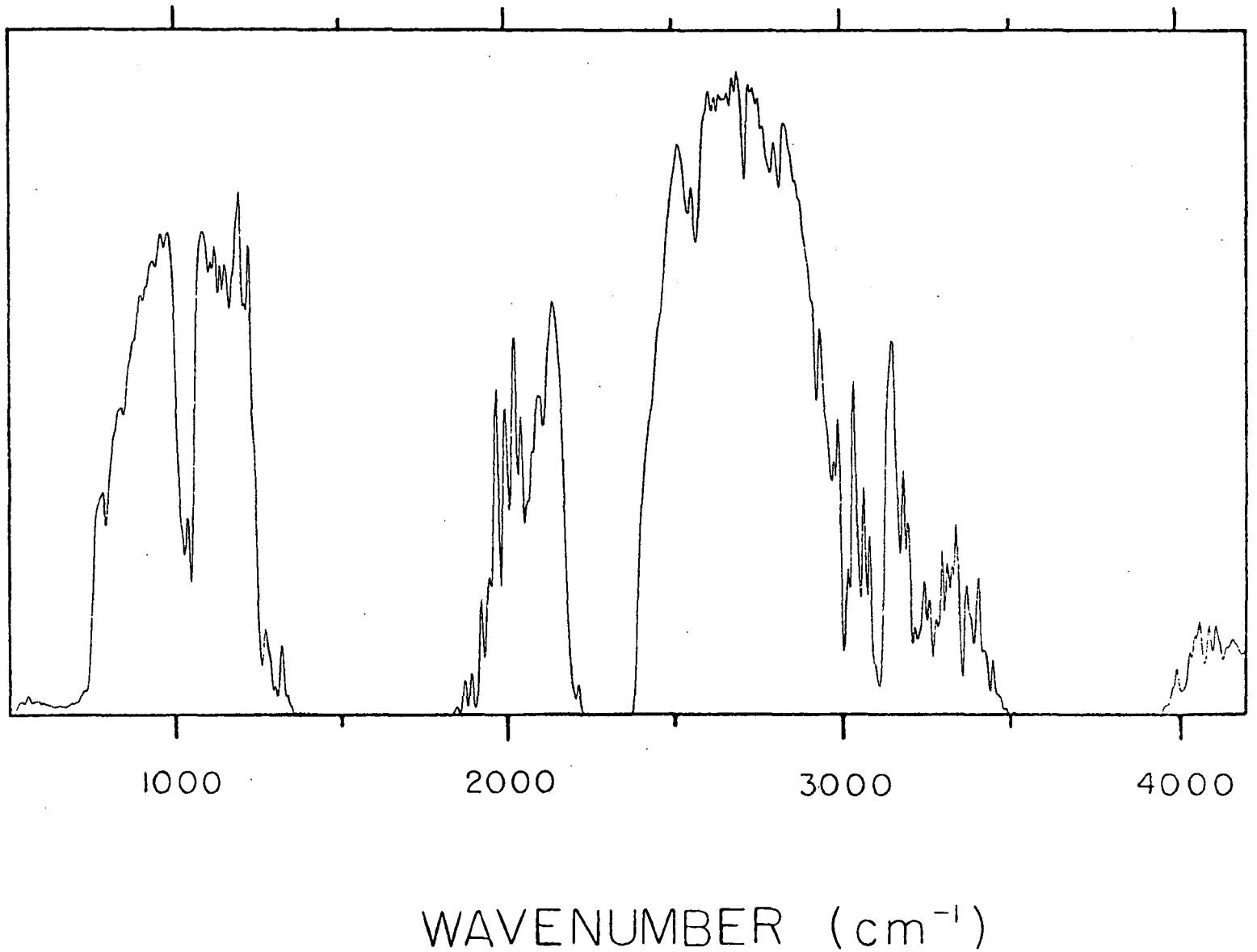

Figure 2. Low-resolution solar spectrum from 500 to 4200 cm^{-1}

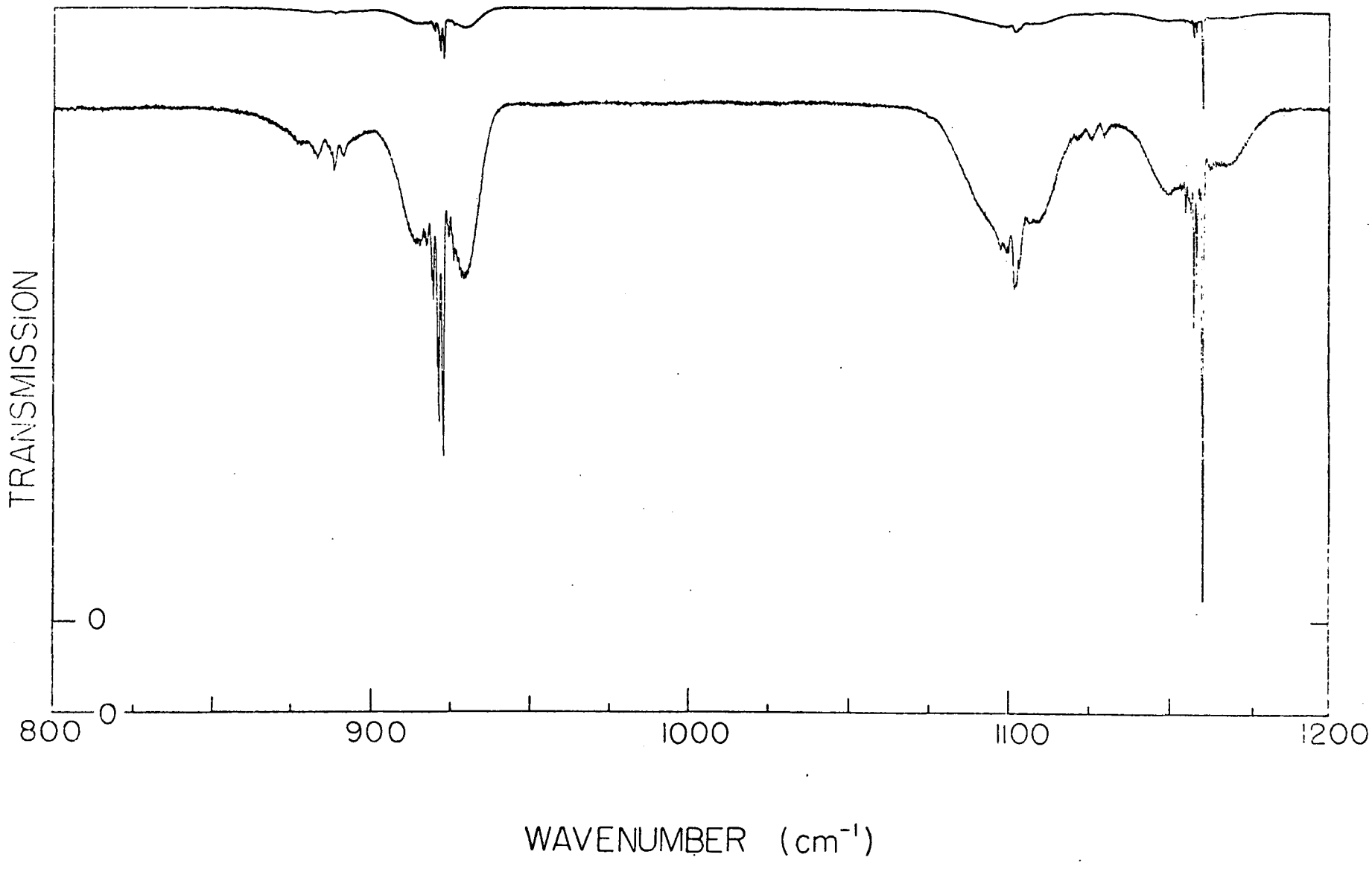

Figure 3. High-resolution spectra of fluorocarbon-12 (CCl_2F_2) from 800 to 1200 cm^{-1}

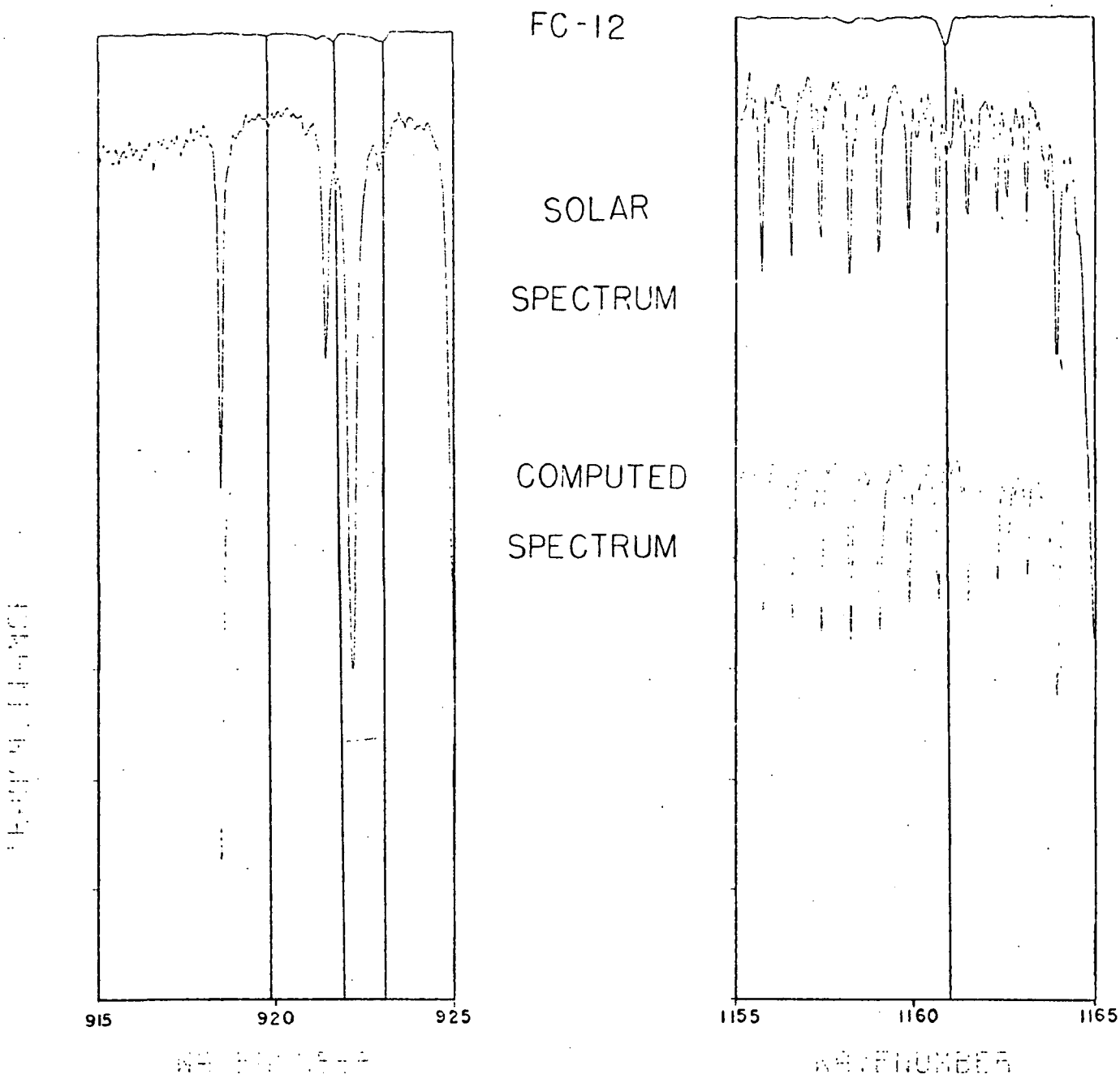

Figure 4. Comparison of solar spectra, laboratory spectra of fluorocarbon-12, and computer synthesized solar spectra (with no FC-12 absorptance) near 923 and 1161 cm^{-1}

the collected solar spectrum is a computer generated solar spectrum; the method for generating this spectrum is discussed below.

In the computerized spectrum it was found that the water vapor absorption line marked with the asterisk (*) did not coincide with the same line in our collected spectrum. The collected spectra were examined to determine if the position of this line was consistent within the collected data. It was found that the collected data, recorded periodically over two months, were self-consistent and therefore it was decided to move this line in the synthetic spectrum to lower frequencies by approximately 0.25 cm^{-1} to obtain the agreement shown in the figure. In the 10 wavenumber region around 1161 cm^{-1} there is good correlation between the collected and computed spectra for over 70 lines.

In both spectral regions the absorption features which have been tentatively identified as belonging to FC-12 are missing in the synthetic spectrum. The fact that these features are absent in the computed spectrum and the fact that all other absorption features in the synthetic spectrum show good agreement with the collected spectrum places much credibility to the assignment of these four features as being due to FC-12 absorption.

Analysis

In order to estimate the atmospheric concentration of FC-12, laboratory spectra of known concentrations of FC-12 were recorded. However, several features of the absorption of solar radiation by the atmosphere cannot be reproduced in a laboratory absorption cell. One such feature is the vertical profile of temperature and pressure of the atmosphere as the radiation approaches the surface of the Earth. The resulting solar transmission spectrum is a composite of transmissions of strata of air, each at a different temperature and pressure. Another feature of solar spectra which cannot be duplicated in a laboratory environment is the fluctuation of absorber concentration along the optical path.

No temperature variation studies could be performed with our absorption cell. However, since the bands of FC-12 which appear in Fig. 4 are fundamental bands,[9] large changes in the appearance of the transmission spectrum with temperature are not expected.[10]

A careful study of the dependence of the absorption bands of FC-12 as a function of total cell pressure was performed. A known amount of FC-12 was introduced into the cell and a spectrum was recorded. High-purity nitrogen gas was then injected into the cell to bring the total pressure up to some desired amount and another spectrum was recorded. The total pressure was increased in this manner from a few Torr up to atmospheric pressure.

Results of this pressure study are shown in Fig. 5. As this figure indicates, there is no dramatic change in the appearance of the transmission spectrum as the total pressure within the cell is varied over this wide range. The fact that these spectra show very little broadening with pressure is fortunate when it comes to analyzing the solar spectra data to determine the atmospheric FC-12

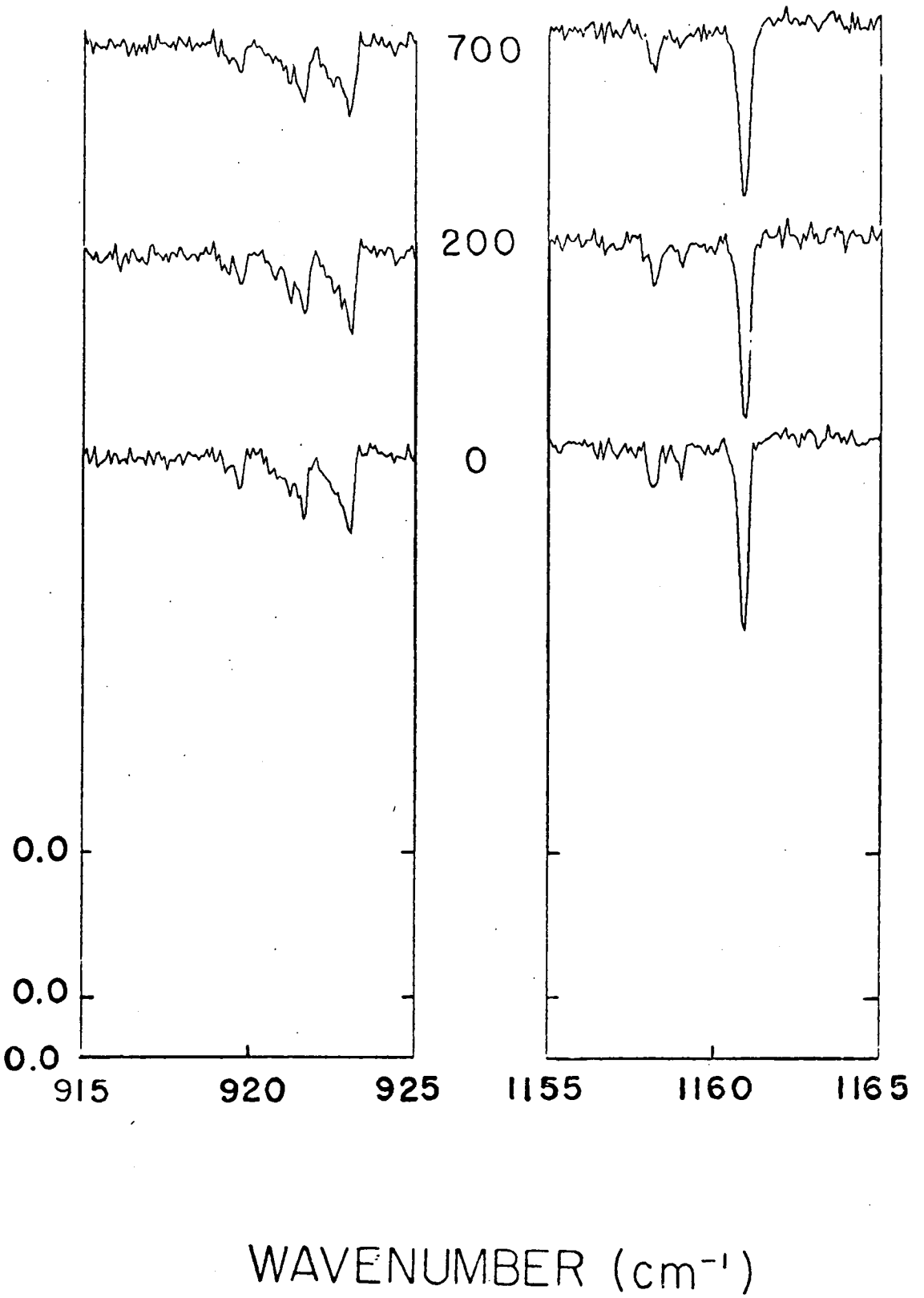

Figure 5. Transmittance of 5.0×10^{-3} Torr FC-12 and 0, 200, and 700 Torr N_2. Total path length = 170 m

concentration. Essentially, the entire atmosphere can be considered to be a homogeneous host for the trace pollutant since all strata of the atmosphere have the same effect on the FC-12 spectra. Furthermore, if FC-12 is assumed to be uniformly mixed in the troposphere,[4] and assuming that the small amount of FC-12 in the stratosphere contributes negligibly to the absorption in the solar spectrum, the problem of calibrating the amount of this fluorocarbon contaminant in the atmosphere is greatly simplified.

Several methods for determining the atmospheric concentration of FC-12 from solar spectra are being investigated. Perhaps the most obvious technique is to compare the center frequency transmissions of each of the four suspected FC-12 peaks in the solar spectrum with laboratory spectra of known amounts of the compound. This technique requires that all spectra be recorded at the same resolution and does not take account of possible overlap of spectral features.

The spectral transmittance of a gas can be expressed as

$$T(\nu) = \exp\,[-K(\nu)\ \rho \cdot l], \tag{1}$$

where $K(\nu)$ is the absorption coefficient at frequency ν, ρ is the number density of absorber molecules in molecules/cm^3, and l is the path length (in cm) of the radiation through the absorber. The absorbance $A(\nu)$ is defined as $\ln[T(\nu)]$. Therefore,

$$A(\nu) = K(\nu) \cdot \rho \cdot l. \tag{2}$$

A plot of absorbance at a given frequency ν_0 vs. the product $\rho \cdot l$ for an absorber should give a straight line with an intercept at the origin and a slope $K(\nu_0)$.

Since the absorption features of FC-12 near 923 cm^{-1} are masked by water vapor, a good calibration of this pollutant cannot be made in this region. The strong, narrow spike at 1160.9 cm^{-1} was used instead. Absorbance data were extracted from the FC-12 laboratory spectra, and plotted against the $\rho \cdot l$ product; this plot is shown in Fig. 6. The optical density $\rho \cdot l$ is in molecules/cm^2. It is clear from this plot that the data can be represented by a straight line. The line chosen in the plot is an estimated fit based on the confidence placed on the individual data points. This fit yields an intercept which, within experimental error, passes through the origin. The slope of the line is 8.9×10^{-18} (molecule/cm^2)$^{-1}$, or 240 (atm $\cdot$ cm)$^{-1}$.

In measuring the absorbance from the solar spectrum a background level must be assumed, and the overlap of the FC-12 absorption feature with N_2O and O_3 makes this difficult. Nevertheless, from the solar spectrum in Fig. 4, an atmospheric optical density of 1.3×10^{16} molecules/cm^2 can be estimated. As indicated earlier, the solar zenith angle was approximately 45° for this spectrum. Assuming the approximate height of the troposphere to be 10 km, a partial pressure of FC-12 at 3.4×10^{-10} atm can be calculated.

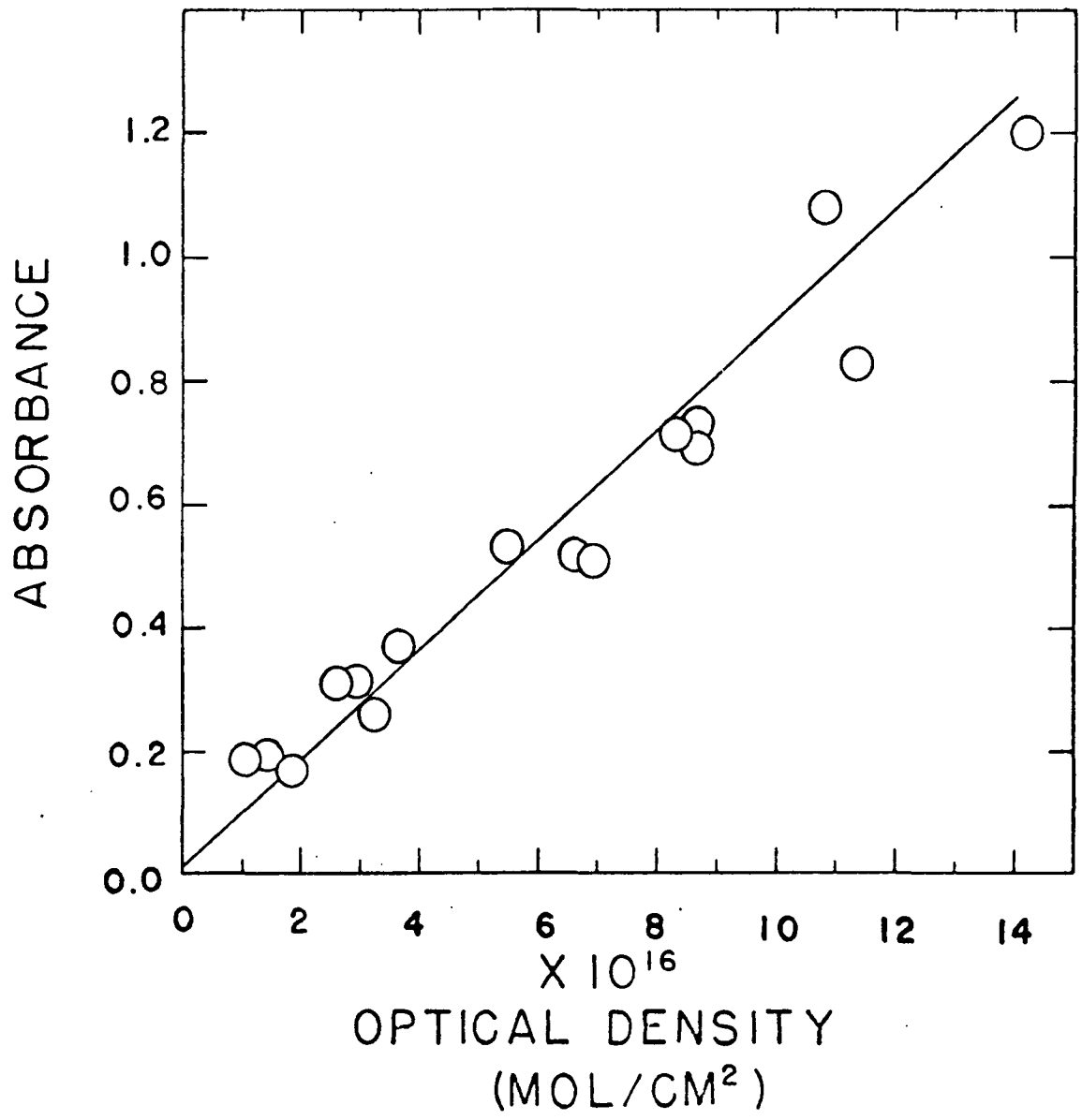

Figure 6. Peak absorbance of FC-12 at 1160.9 cm^{-1} as a function of optical density (pl)

Examination of other solar spectra recorded over this two-month interval shows similar results. Hanst, et al.[6] measured a partial pressure of 2.3×10^{-10} atm for FC-12. Hester et al.[4] used gas chromatography to measure ambient levels of FC-12. Their results show a wide fluctuation in concentration over a period of 14 days, but the average amount of FC-12 appears from their data to be close to 4.0×10^{-10} atm. Thus the quantity of atmospheric FC-12 which is measured from our solar spectra is in agreement with other reported values.

EXPLORATION OF TECHNIQUES FOR SPECTRAL DATA REDUCTION AND ANALYSIS CALCULATION OF SYNTHETIC SPECTRA

The spectrum of molecular absorbers along a given path can be calculated if the amounts of the absorbing gases, the temperature and pressure variations along the path, and the requisite molecular parameters of the absorbing gases are known. McClatchey et al.[8] have compiled the available information on the positions, intensities, and widths (for pressure broadening by air), together with the lower state transition energies for many absorption lines of seven permanent atmospheric gases; i.e., O_2, CO, N_2O, CO_2, CH_4, O_3, and H_2O. This line listing has been used to calculate absorption spectra of horizontal homogeneous paths or slant paths through the atmosphere by a number of workers (see, for example, Refs. 11, 12, 13). We have used this compilation to obtain synthetic spectra for comparison with experimental spectra of ground level air and with solar spectra. Since all these spectra were recorded at ground level we have assumed that the spectral lines are pressure broadened and can be represented by the Lorentz line shape

$$K(\nu) = S\alpha/\pi[(\nu-\nu_0)^2 + \alpha^2], \tag{3}$$

where $K(\nu)$ = absorption coefficient at frequency $\nu(cm^{-1})$ due to a line of intensity $S(cm^{-1}/molecules\ cm^{-2})$ and half width (at half height) $\alpha(cm^{-1})$. This line shape is a good approximation of the shape of most lines of atmospheric gases at pressures greater than about 10 Torr. At lower pressures the Voigt profile should be used.[14] However, with the exception of O_3, the contribution to the absorption in ground level solar spectra by atmospheric molecules at pressures below 10 Torr is small compared with that due to the molecules at higher pressures. The attenuation due to molecular scattering, and to aerosol absorption and scattering, has also been neglected in the computations since these factors are not strongly frequency dependent[8,15] and the experimental data show relative rather than absolute transmittances.

Absorption By A Gas

The monochromatic absorbance of a homogeneous layer of thickness Δl due to a single absorption line with a Lorentz shape is

$$A_0(\nu) = \ln P_0/P = \frac{S}{\pi} \frac{\alpha \circ \Delta l}{(\nu-\nu_0)^2 + \alpha^2}, \tag{4}$$

where P_o = power incident on the layer, and
P = power transmitted by the layer.

Since each gas gives rise to many absorption lines the total absorbance $A_k(\nu)$ at frequency ν due to the kth gas in the layer is found by summing Eq. (4) over the N_k lines which contribute to the absorption at that frequency;

$$A_k(\nu) = \frac{\rho_k}{\pi} \sum_{i=1}^{i=N_k} \frac{S_{ik}\, \alpha_{ik}\, \Delta l}{(\nu-\nu_{oik})^2 + \alpha_{ik}^2}, \tag{5}$$

where i represents the ith line of the kth gas.

The total absorbance due to n different gases is

$$A_n(\nu) = \sum_{k=1}^{k=n} \frac{\rho_k}{\pi} \sum_{i=1}^{i=N_k} \frac{S_{ik}\, \alpha_{ik}\, \Delta l}{(\nu-\nu_{oik})^2 + \alpha_{ik}^2}. \tag{6}$$

If the temperature and pressure or the mixing ratios of the gases vary along the path, the total absorbance can be calculated by dividing the path into M layers, each of which is considered homogeneous and summing over all the layers

$$A_M(\nu) = \sum_{m=1}^{M} \sum_{k=1}^{n} \frac{\rho_{km}}{\pi} \sum_{i=1}^{N_k} \frac{S_{ikm}\, \alpha_{ikm}\, \Delta l_m}{(\nu-\nu_{oik})^2 + \alpha_{ikm}^2}. \tag{7}$$

Although the positions of the lines are essentially independent of the pressure and temperature of the sample, the line intensity S is a function of temperature and the line width α depends on both temperature and pressure[8] such that

$$S = S_o \left(\frac{T_o}{T}\right)^n \exp[E''\ (T_o-T)/0.6946\ T_oT], \tag{8}$$

and

$$\alpha = \alpha_o\ (T_o/T)^{1/2}\ P/P_o, \tag{9}$$

When S_o is the line intensity at temperature T_o, α_o is the half width at temperature T_o and pressure P_o, E" is the energy of the lower state of the transition, and n is a parameter which depends on the molecule.[8] For H_2O, O_3, CH_4, n = 1.5, and for CO, N_2O, CO_2, and O_2, n = 1.

Since most measurements of linear parameters have been made for room temperature and pressure, the AFCRL line compilation has chosen T_o = 296 K and P_o = 1013 mbar.

In our applications the atmospheric paths to be simulated were either homogeneous (M = 1) or slant paths corresponding to solar spectra. Provided the zenith angle z of the sun is less than about 80° the plane parallel approximation can be used to describe the atmosphere and the path length through a given layer can be written as

$$\Delta l_m = \Delta h_m \sec z,$$

when Δh_m is the vertical thickness of the layer. For larger zenith angles the effects of refraction and departures from the plane parallel approximation be- increasingly important and corrections must be obtained from suitable tables.[16] Table I shows equivalent air masses for zenith angles between 0° and 90°.

As indicated by Eq. (3), the absorption coefficient for a Lorentzian line shape is never completely zero. Therefore every line in a spectrum contributes to the absorbance at all frequencies, and these contributions should all be summed to find the total absorbance at a given frequency. However, the amount of computation time to perform this task would be prohibitive. Therefore, several approximations have been incorporated into the programming to reduce the computation time. The first approximation is the elimination of lines which have a negligible contribution to the total absorbance at their center frequencies. This cancellation is performed by calculating the absorbance of a line at center frequency. From Eq. (4) this absorbance is $A(\nu_o) = S \cdot c \cdot l/\alpha\pi$. If this quantity is less than 0.001 the line is ignored.

The second approximation employed to produce synthetic spectra is the elimination of the wings of each absorption line. It was assumed that any absorption line had negligible contribution to the total absorbance at frequencies greater than 20 cm^{-1} away from the center frequency of the line. This is a conservative estimate of the range of influence for many of the absorption lines, and use of this cut-off value has resulted in computed spectra which show good agreement with observed spectra. Thus the summations over the index i over N_k lines in Eq. (5,6,7) are subject to these limitations.

A spectrum with an effective resolution $\delta\nu$ cm^{-1} is obtained by calculating the monochromatic transmittances at frequency intervals $\delta\nu$ cm^{-1}. As $\delta\nu$ goes to zero, the resolution becomes infinite. In order to synthesize a spectrum the size of the interval $\delta\nu$ between calculated data points should be equal to α/m where α is the halfwidth of a computed line and m is an integer greater than 5. For ground level homogeneous path spectra with line halfwidths typically about 0.05 cm^{-1}, a good value of $\delta\nu$ is about 0.01 cm^{-1}. However, in order to obtain a good representation of ozone lines in solar spectra whese halfwidths are less than 0.01 cm^{-1} a better value for $\delta\nu$ is 0.002 cm^{-1} or less.

TABLE I. EQUIVALENT AIR MASSES FOR ZENITH ANGLES 0° to 90° (FROM REF. 16)

	0°	1°	2°	3°	4°	5°	6°	7°	8°	9°
0°	1.00	1.00	1.00	1.00	1.00	1.00	1.01	1.01	1.01	1.01
10°	1.02	1.02	1.02	1.03	1.03	1.04	1.04	1.05	1.05	1.06
20°	1.06	1.07	1.08	1.09	1.09	1.10	1.11	1.12	1.13	1.14
30°	1.15	1.17	1.18	1.19	1.20	1.22	1.24	1.25	1.27	1.28
40°	1.30	1.32	1.34	1.37	1.39	1.41	1.44	1.46	1.49	1.52
50°	1.55	1.59	1.62	1.66	1.70	1.74	1.78	1.83	1.88	1.94
60°	2.00	2.06	2.12	2.20	2.27	2.36	2.45	2.55	2.65	2.77
70°	2.90	3.05	3.21	3.39	3.59	3.82	4.08	4.37	4.72	5.12
80°	5.60	6.18	6.88	7.77	8.90	10.40	12.44	15.36	19.79	26.96

In order to compare synthetic spectra with actual spectra whose spectral resolutions are less than $\delta\nu$ the resolution of the synthetic spectra must be degraded by convolution with an appropriate instrument function. In the work reported here a triangular function was chosen with a halfwidth $a(cm^{-1})$. The transmittance $T(\nu)$ of the degraded spectrum is then obtained from the expression

$$T'(\nu) = \frac{\int \sigma(\nu_1,\nu')\ T(\nu')\ d\nu',}{\int \sigma(\nu_1,\nu')\ d\nu'} \tag{10}$$

where $\sigma(\nu_1,\nu')$ is the instrument response function. This integration is done numerically by the trapezoid rule

$$T'(\nu) = \frac{\delta\nu}{2a^2}\left[2\sum_{i=\nu-a}^{\nu+a}\left\{(a-|\nu_i-\nu|)T(\nu)\right\} - (a-|\nu_{\nu-a}-\nu|)T(\nu_{\nu-a}) - (a-|\nu_{\nu+a}-\nu|)T(\nu_{\nu+a})\right] \tag{11}$$

where the summation extends over all computed frequencies from $\nu - a$ to $\nu + a$. It was found that the accuracy of the convolution was strongly dependent on the precision with which the calculation is performed. For this reason, the convolution was performed in double precision.

The effect of degrading the spectral resolution on the appearance of a spectrum is illustrated in Fig. 7, which shows a spectrum of a 1 km path of air at 296 K and 760 Torr. The spectral resolution increases from the top to the bottom of figure. In the upper curve $a = 0.5\ cm^{-1}$ and then successively changes to 0.3, 0.1, 0.05, and 0.01 cm^{-1} in the lowest curve. In addition to degrading its resolution it is also noticeable that the spectrum approaches a more continuous curve as the value of $a/\Delta\nu$ increases.

Specification of Parameters for Synthetic Spectra

Horizontal Paths--

For homogeneous, horizontal paths it is necessary to specify the temperature, pressure, and path length of the absorbing medium as well as the mixing ratios of the absorbing gases. Values for the number densities of CH_4, O_2, CO_2, CO, and N_2O which were used to compute ground-level spectra at 294 K and 1013 mbar ars shown in Table II. These values are adjusted as described below when spectra at different temperatures and pressures are computed. There is no absorption by oxygen in the spectral region investigated here and the amount of O_3 at ground level is not sufficient to produce significant absorption in this spectral region for the path lengths used.

Local and temporal variations in CO and CO_2 are known to occur and slight changes in the number densities of these molecules were made to obtain the best agreement between observed and computed spectra. The large variability

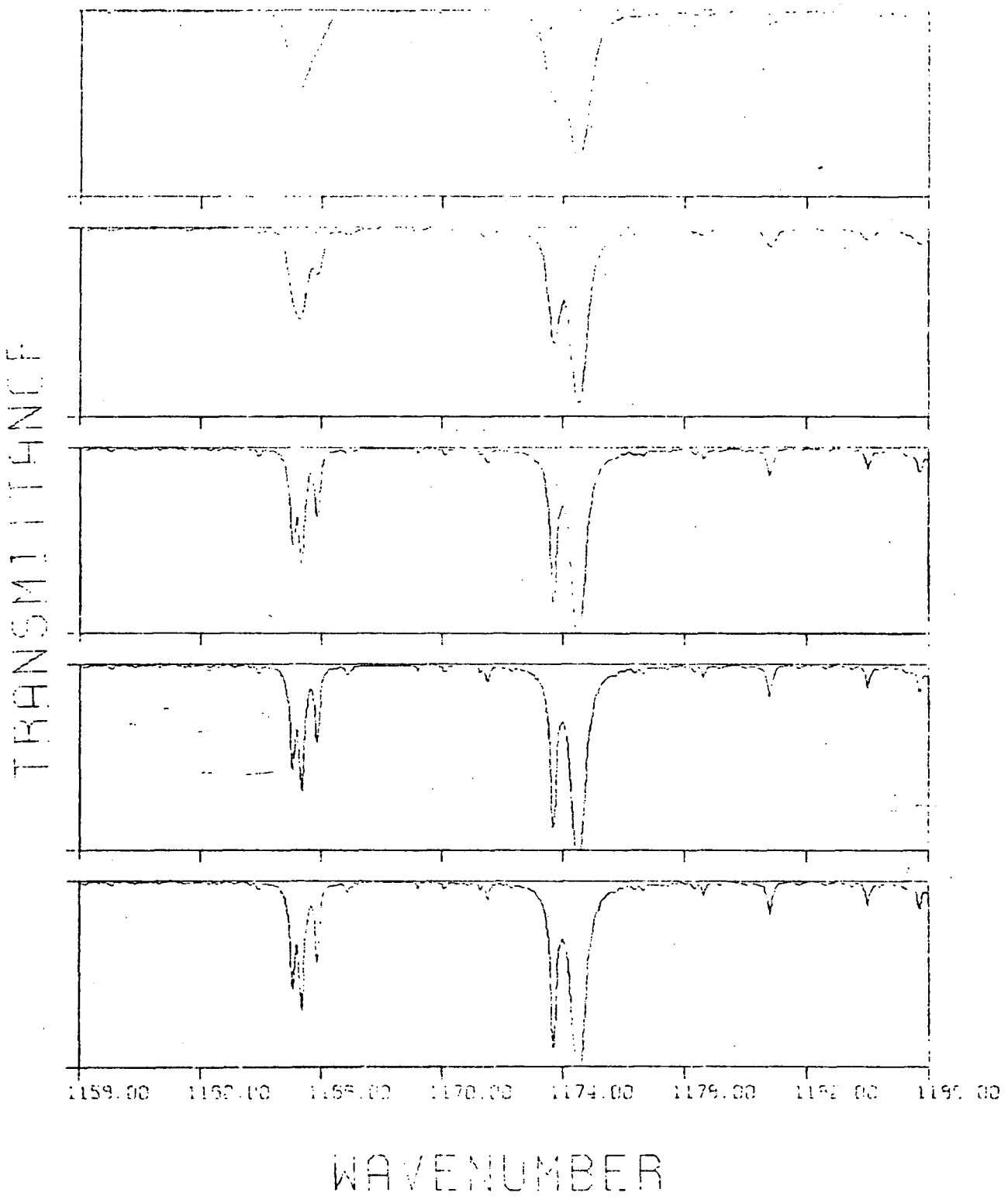

Figure 7. Effect of the width of the instrument function a (cm^{1}) on resolution for values of a of 0.5, 0.3, 0.1, 0.05, and 0.01 cm^{-1}, respectively

TABLE II. SURACE NUMBER DENSITIES AT T = 294 K and P = 1013 MBAR FOR ATMOSPHERIC GASES WITH CONSTANT MIXING RATIOS

Gas	Density (molecules cm^{-3})
CH_4	4.30×10^{13}
O_2	5.63×10^{19}
CO_2	8.87×10^{15}
CO	2.03×10^{12}
N_2O	7.28×10^{12}

of atmospheric water vapor on the other hand, makes its concentration difficult to determine. For a collected air spectrum the water vapor content was estimated from the air temperature and relative humidity. Thus each new synthetic spectrum required a different estimate of the water vapor concentration in order to obtain a good spectral fit.

Slant Path (Solar Spectra)--

In order to calculate the transmittance of a slant path through the atmosphere it is necessary to assume vertical profiles through the atmosphere showing the dependence of temperature, pressure, and mixing ratios of the absorbing gases as functions of height. Since most of the solar spectra were obtained in the summer and autumn of 1975 the midlatitude summer atmospheric model described by McClatchey et al.[8] has been used. This model, which is partially reproduced in Table III shows pressure, temperature, and the mass mixing ratios of water vapor and ozone as functions of height. It was assumed that the other absorbing gases have constant volume mixing ratios as shown in Table II. Thus the number density ρ_k at height h, pressure P, and temperature T, is related to the number density ρ_{ok} at the surface (pressure P_o and temperature T_o) by

$$\rho_k = \rho_{ok} \, P \, T_o/P_o T.$$

The number densities of H_2O and O_3 can be calculated from the mass mixing ratios given in Table III by finding the partial pressures of these gases P_p by

$$P_p = P \, m_r/c,$$

where $c = M_g/M_{air}$ is the ratio of the molecular mass M_g of either H_2O or O_3 to the mean molecular mass of air, M_{air}, and then by using the perfect gas equation

$$P_p = \rho_k \, R \, T$$

to give

$$\rho_k = P \, m_r/c \, R \, T.$$

Synthetic solar spectra such as the one shown in Fig. 8 were calculated by a computer program which divided the atmosphere between 0 and 30 km into the 13 layers shown in Table IV. In each layer the average temperature, pressure, and number density were assumed to be those at the arithmetic mean height of the layer. These values were used to calculate the absorbance of each layer. The total absorbance of the atmosphere is the sum of the individual absorbances and from this total value the atmospheric transmittance was calculated [Eq. (7)]. Then transmittances were convolved with a triangular instrument function by using Eq. (11) to give synthetic spectra.

TABLE III. MIDLATITUDE SUMMER ATMOSPHERIC MODEL (FROM REF. 8)

Height (km)	Pressure (mbar)	Temperature (K)	Mixing Ratio Water (kg/kg)	Mixing Ratio Ozone (kg/kg)
0	1013.00	294	1.2E-2	5.04E-8
1	902.00	290	8.6E-3	5.56E-8
2	802.00	285	6.0E-3	6.15E-8
3	710.00	279	3.7E-3	7.01E-8
4	628.00	273	2.4E-3	8.00E-8
5	554.00	267	1.4E-3	9.15E-8
6	487.00	261	9.4E-4	1.06E-7
7	426.00	255	6.3E-4	1.29E-7
8	372.00	248	4.0E-4	1.52E-7
9	324.00	242	2.6E-4	1.84E-7
10	281.00	235	1.5E-4	2.16E-7
11	243.00	229	5.9E-5	2.98E-7
12	209.00	222	1.8E-5	3.67E-7
13	179.00	216	6.2E-6	5.20E-7
14	153.00	216	4.0E-6	7.31E-7
15	130.00	216	3.6E-6	9.03E-7
16	111.00	216	3.6E-6	1.17E-6
17	95.00	216	3.6E-6	1.56E-6
18	81.20	216	3.8E-6	2.15E-6
19	69.50	217	4.4E-6	2.88E-6
20	59.50	218	4.8E-6	3.60E-6
21	51.00	219	6.3E-6	4.47E-6
22	43.70	220	7.4E-6	5.24E-6
23	37.60	222	9.2E-6	5.80E-6
24	32.20	223	1.2E-5	6.38E-6
25	22.70	224	1.6E-5	7.00E-6
30	13.20	234	2.7E-5	1.51E-5
35	6.52	245	1.7E-5	1.41E-5
40	3.33	258	1.3E-5	1.23E-5

TABLE IV. THICKNESS, MEAN PRESSURE, AND TEMPERATURE OF LAYERS USED IN SLANT PATH COMPUTATION

km	Mean Height (km)	Mean p (mbar)	Mean T (K)
0-1	0.5	957.5	292.0
1-2	1.5	852.0	287.5
2-3	2.5	756.0	282.0
3-4	3.5	669.0	276.0
4-5	4.5	591.0	270.0
5-7	6.0	487.0	261.0
7-9	8.0	372.0	248.0
9-11	10.0	281.0	235.0
11-15	13.0	179.0	216.0
15-19	17.0	95.0	216.0
19-23	21.0	51.0	219.0
23-27	25.0	27.7	224.0
27-31	29.0	16.1	232.0

ATLAS OF GROUND LEVEL AIR SPECTRA AND SOLAR SPECTRA

During the past two years a series of spectra from 400 cm^{-1} to 3500 cm^{-1} of path lengths of approximately 10, 100, and 1000 m of air at ground level temperature and pressure have been obtained by using a 21 m stainless steel multiple traversal cell. The short air path spectra were obtained by observing the absorption due to the approximately 8.5 m air path between the source, interferometer, and detector. Four traversals of the cell, when filled with air, increased the air paths to 92 m and, by using 48 traversals of the cell, a total path length of 993 m was obtained. In addition to these ground level, homogeneous path spectra, solar spectra have been obtained between 400 and 3500 cm^{-1} for solar zenith angles ranging from 40° to more than 87°. The effective atmospheric path length for small zenith angles is equivalent to about 8 km at surface temperature and pressure; this increases to more than 50 km effective path length as the solar zenith angle approaches 90°.

Examples of these spectra are shown in Figs. 8-11, each of which covers a 28 cm^{-1} interval. Tables V and VI give some information for these figures. The upper three curves are spectra of 8.5 m, 92 m, and 993 m of air at ambient temperature and pressure obtained using the 21 m multiple traversal cell. The two lower curves are solar spectra recorded for solar zenith distance of approximately 40° and 85°. At the present time we are compiling an abbreviated atlas of spectra which will cover the region from 700 cm^{-1} to 1500 cm^{-1}, each page of which will be similar to these figures.

The principal atmospheric absorption features in this spectral region are bands of H_2O, CO_2, O_3, CH_4, and N_2O. These figures show how individual absorption features increase in intensity as the absorbing path is increased. They also show that even for the longest atmospheric paths, taken with low sun, there are spectral regions with high transmittance in which features of other absorbing gases can be sought.

We have made comparisons of the appearances of the several thousand features in the spectral regions investigated, between different spectra. The spectra obtained for a given path length with our instrument on different days and at different seasons are very similar. There are differences in the intensities of O_3 lines (in solar spectra) and H_2O lines on spectra taken on different days and at different seasons because of the variabilities in the abundances of these gases.

One of the reasons for undertaking this study was to search for absorption features of atmospheric pollutants. This can be done by comparing spectra of a suspected pollutant with the atmospheric spectra and searching for characteristic absorption features as described earlier in this chapter. It is often found that the spectral regions when the strongest and most characteristic features occur also contain absorption lines of other gases. These must be identified if the existence or otherwise of the pollutant is to be verified.

These identifications can be carried out in a number of ways. For example, we have compared our spectra with atmospheric spectra of similar resolution obtained by other workers.[17,18,19] The agreement in general is good although some differences have been noted. We have also attempted to compare the

TABLE V. INFORMATION CONCERNING SPECTRA SHOWN IN FIGURES 8-11

	Path Length (m)	Solar Zenith Angle (°)	Date (1975)
a	8.5		Nov 14
b	92.0		Nov 13
c	993.0		Nov 6
d		45	Sept 30
e		87	Oct 3

TABLE VI. PARAMETERS FOR SYNTHETIC SPECTRA IN FIGURES 8A-11A

	Molecular Number Density (No./cm^3)								
	H_2O ($\times 10^{17}$)	CO_2 ($\times 10^{15}$)	CO ($\times 10^{12}$)	N_2O ($\times 10^{12}$)	CH_4 ($\times 10^{13}$)	O_3 ($\times 10^{11}$)	Halfwidth of Triangular Convolution Function a(cm^{-1})	T (K)	P (mbar)
a	3.85	8.87	2.03	7.28	4.30	6.70	.025	293	1013
b	3.85	8.87	2.03	7.28	4.30	6.70	.025	293	1013
c	3.85	8.87	2.03	7.28	4.30	6.70	.025	293	1013
		Surface Molecular Number Density (No./cm^3)							
d	See Table III	8.87	2.03	7.28	4.30	See Table III	.060		
c		8.87	2.03	7.28	4.30		.120		

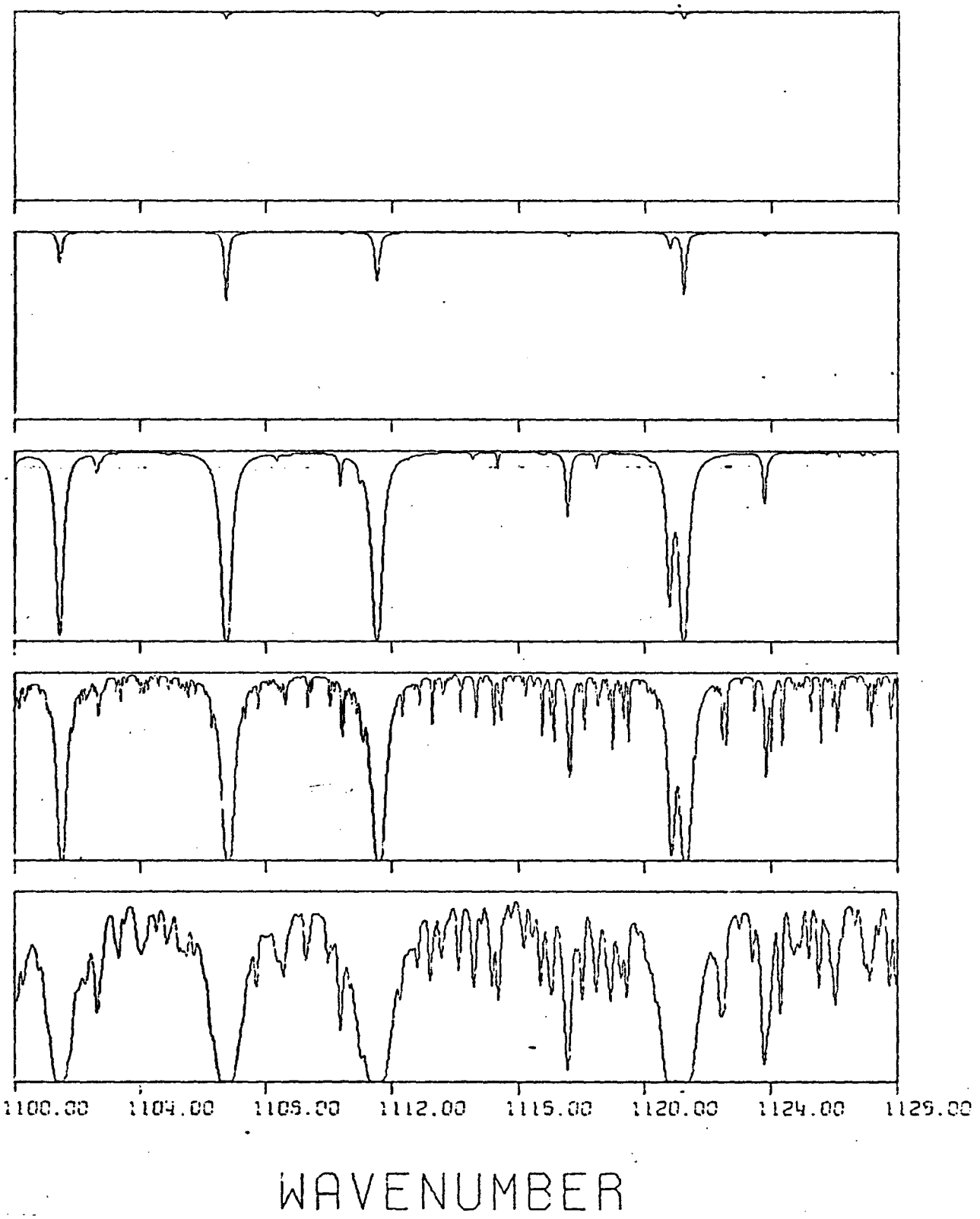

Figure 8a. Synthetic atmospheric spectra between 1100 and 1128 cm^{-1} (see Table VI)

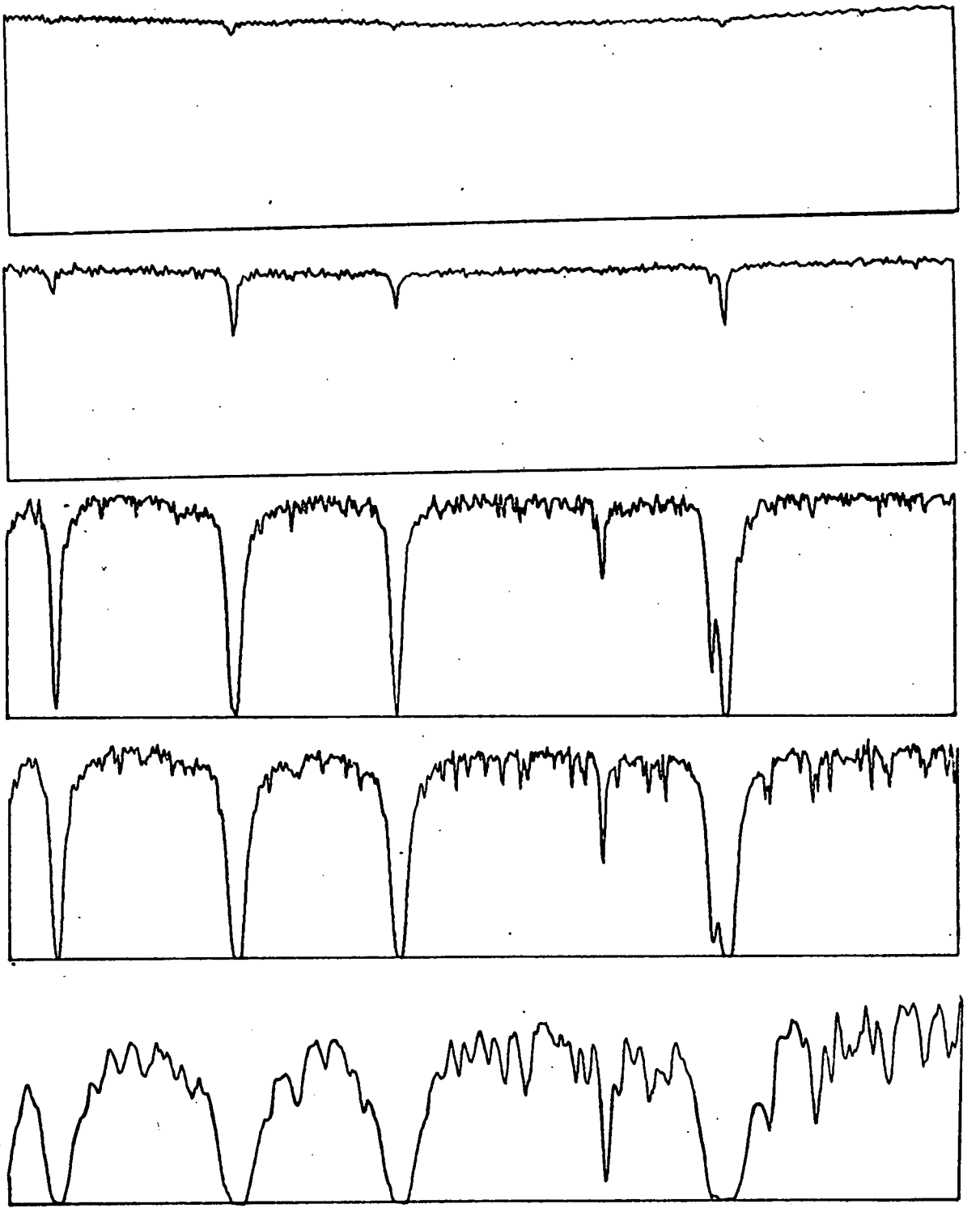

Figure 8. Atmospheric spectra between 1100 and 1128 cm^{-1} (see Table V)

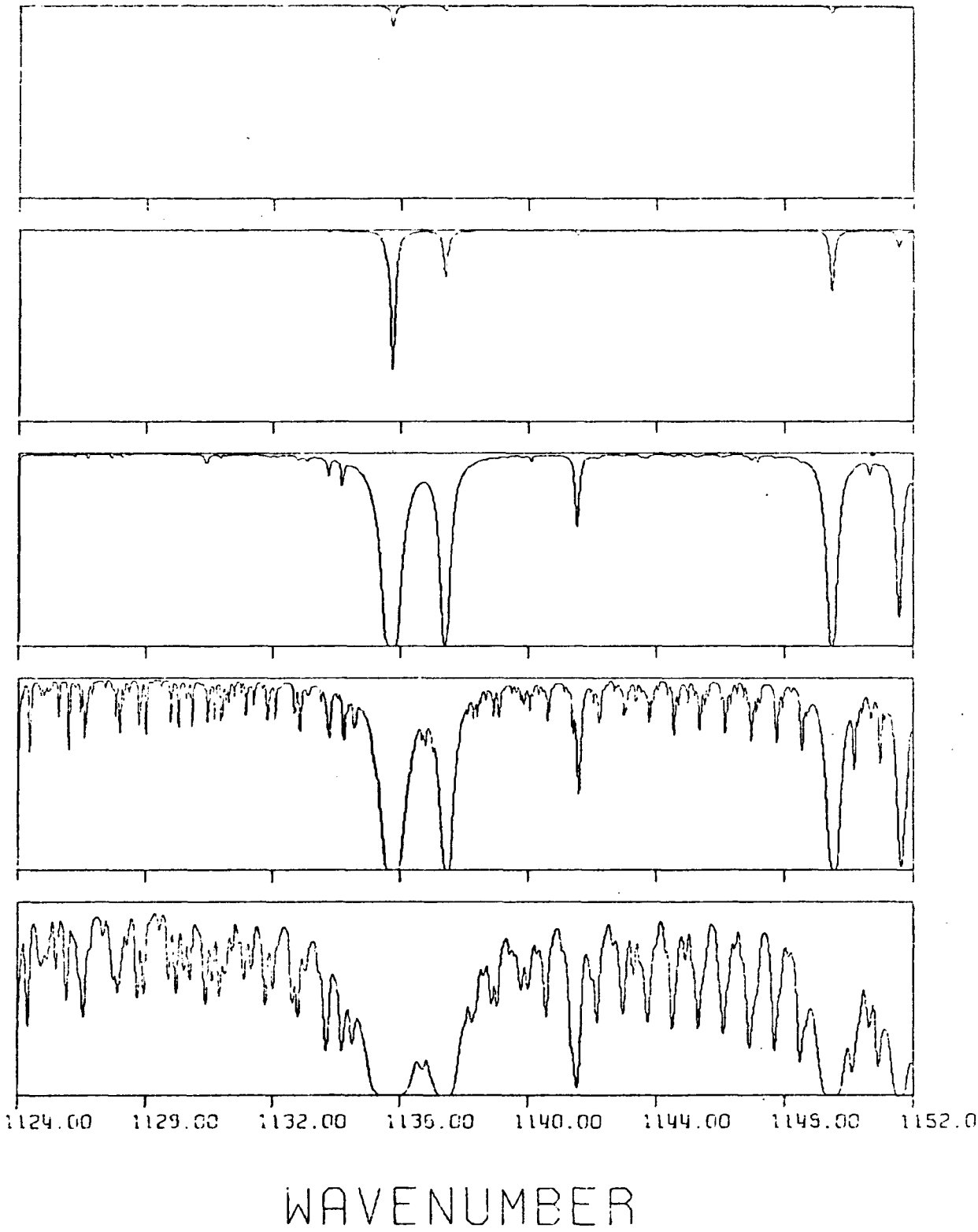

Figure 9a. Synthetic spectra between 1124 and 1152 cm^{-1}

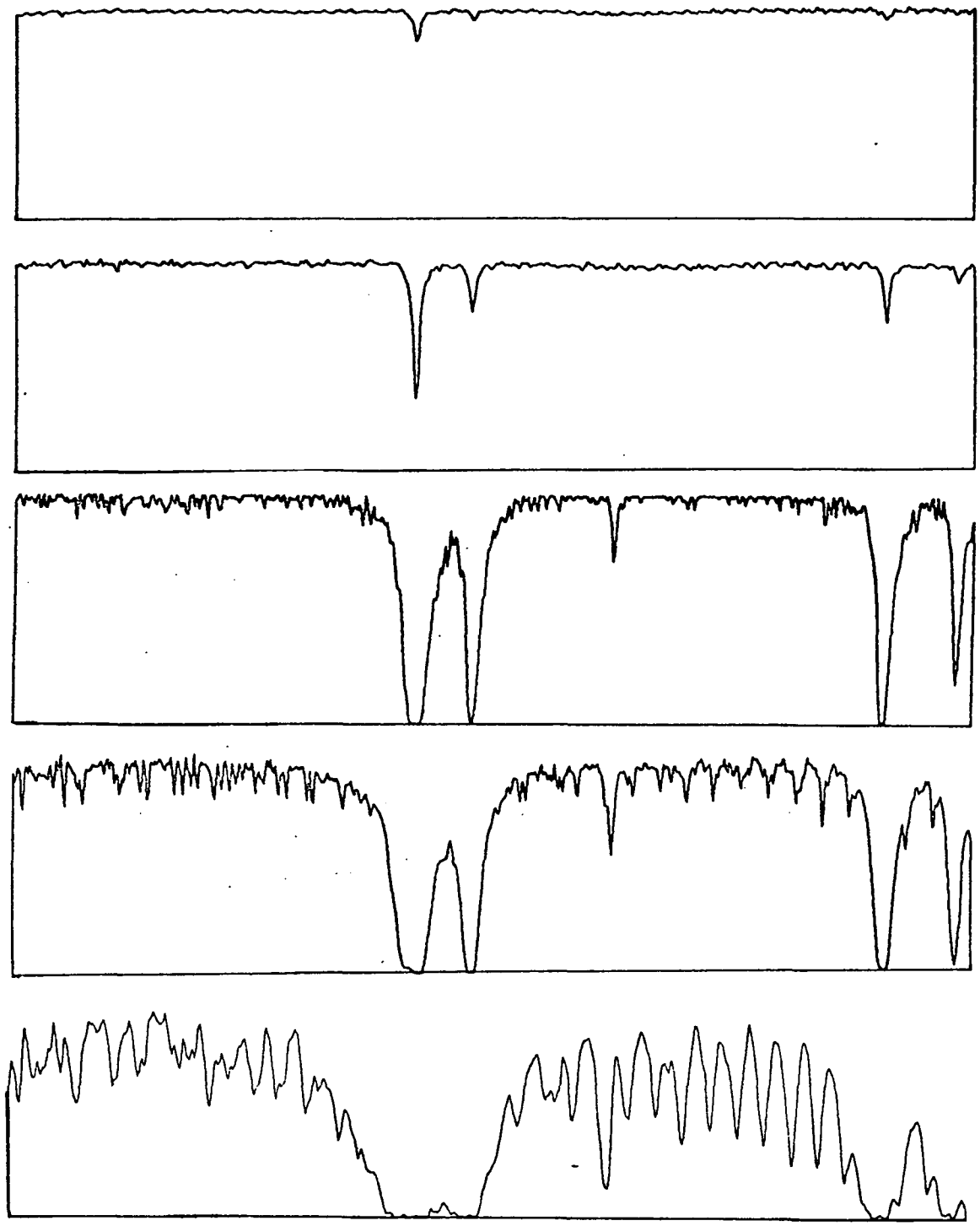

Figure 9. Atmospheric spectra between 1124 and 1152 cm^{-1}

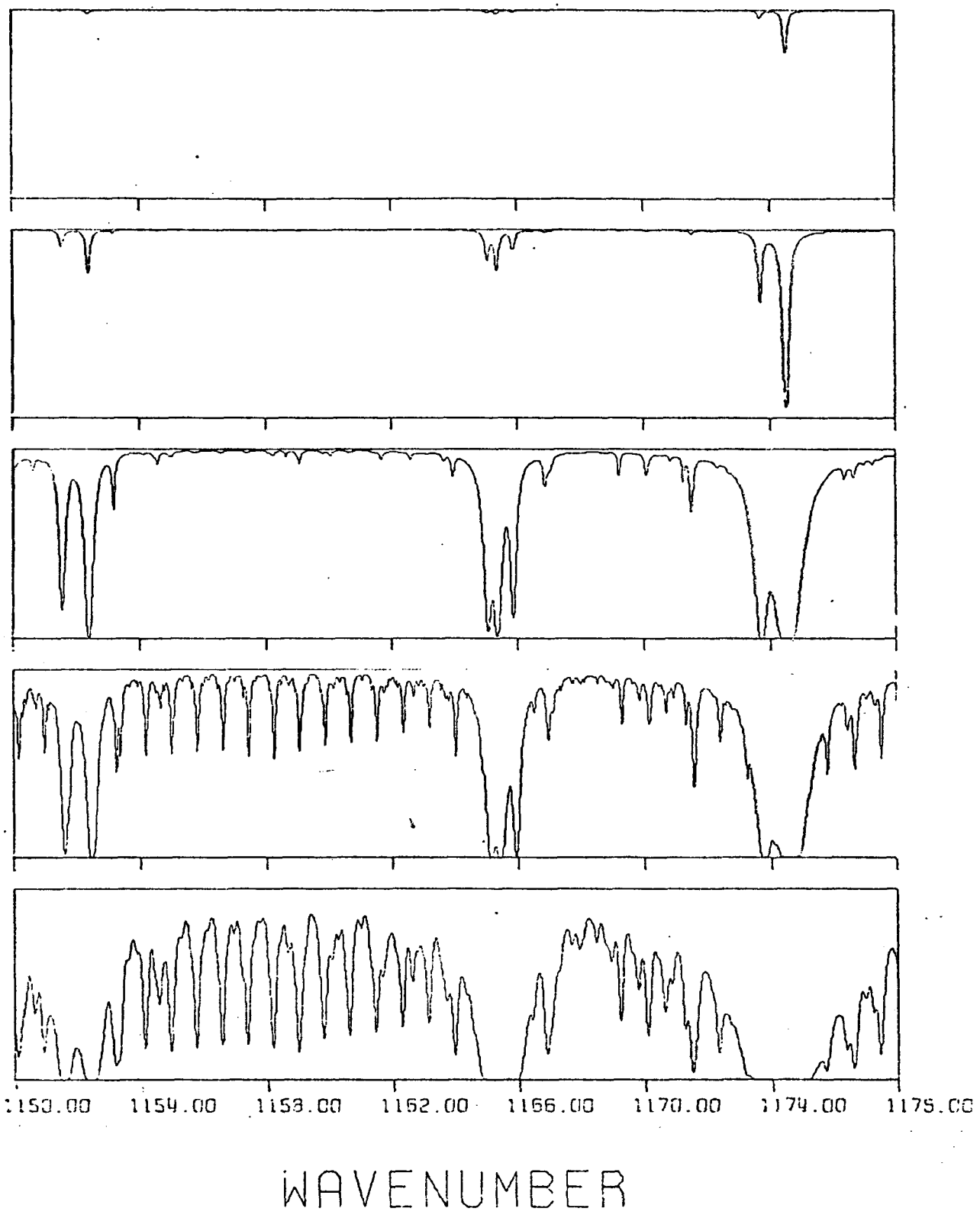

Figure 10a. Synthetic spectra between 1150 and 1178 cm^{-1}

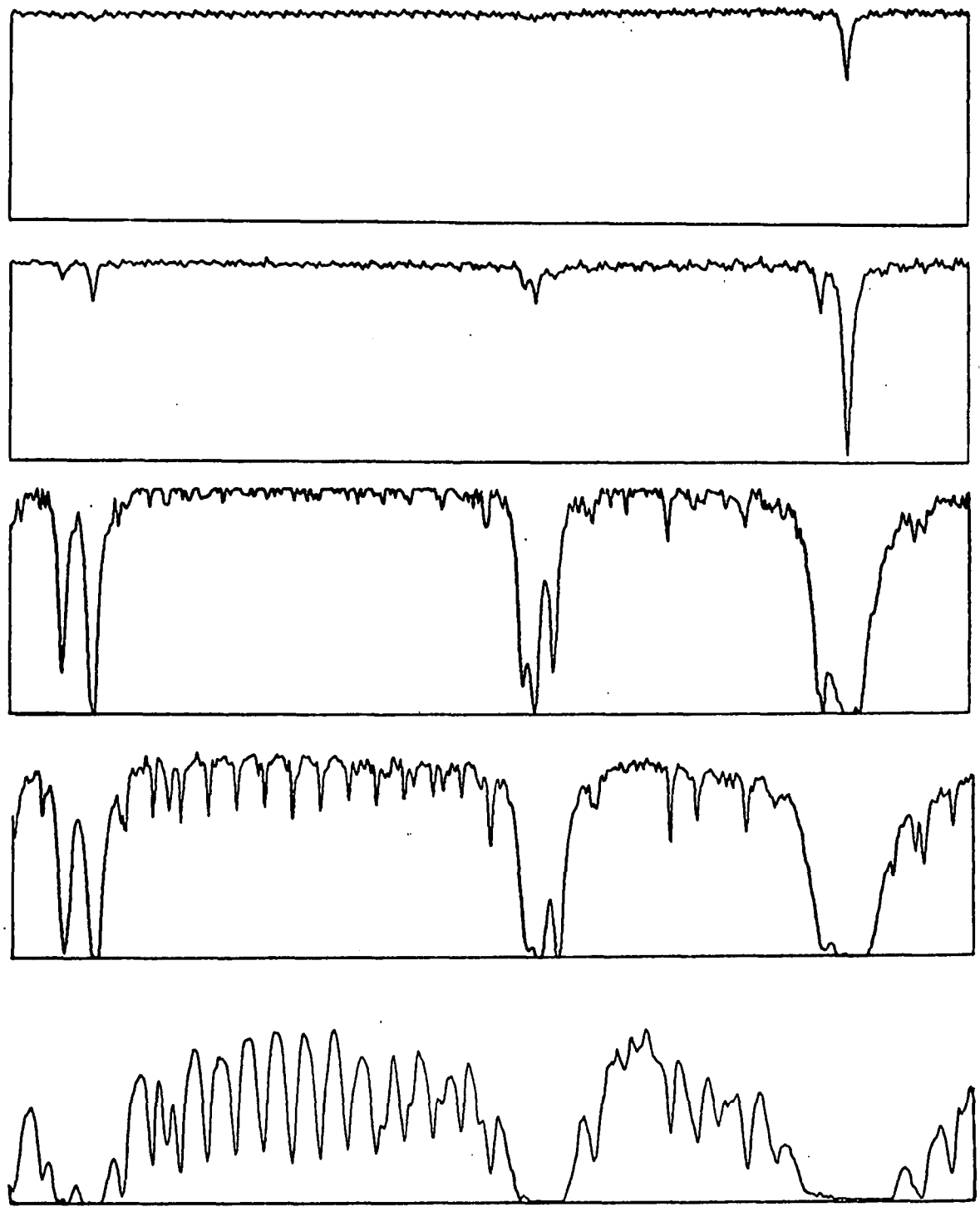

Figure 10. Atmospheric spectra between 1150 and 1178 cm^{-1}

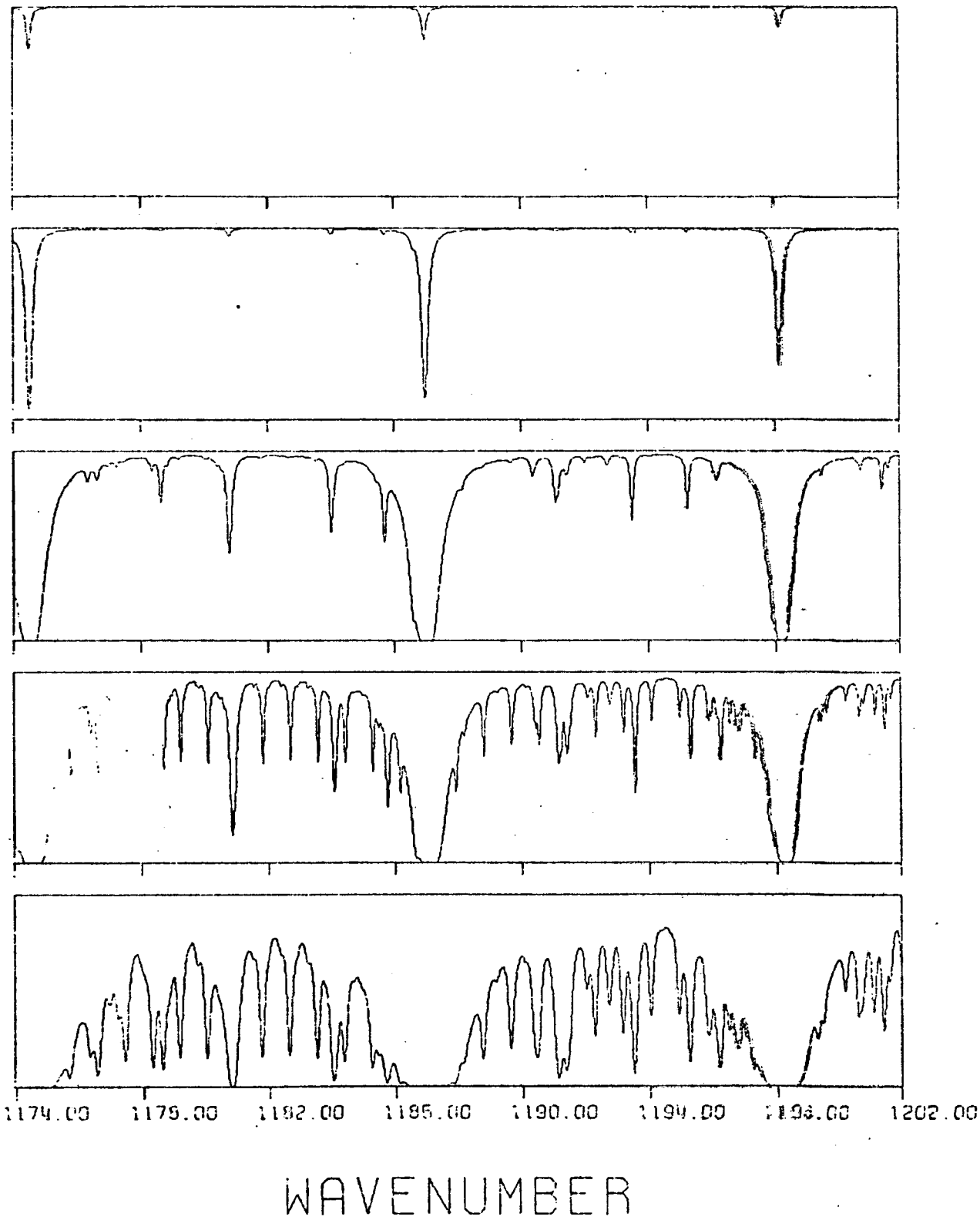

Figure 11a. Synthetic spectra between 1174 and 1202 cm^{-1}

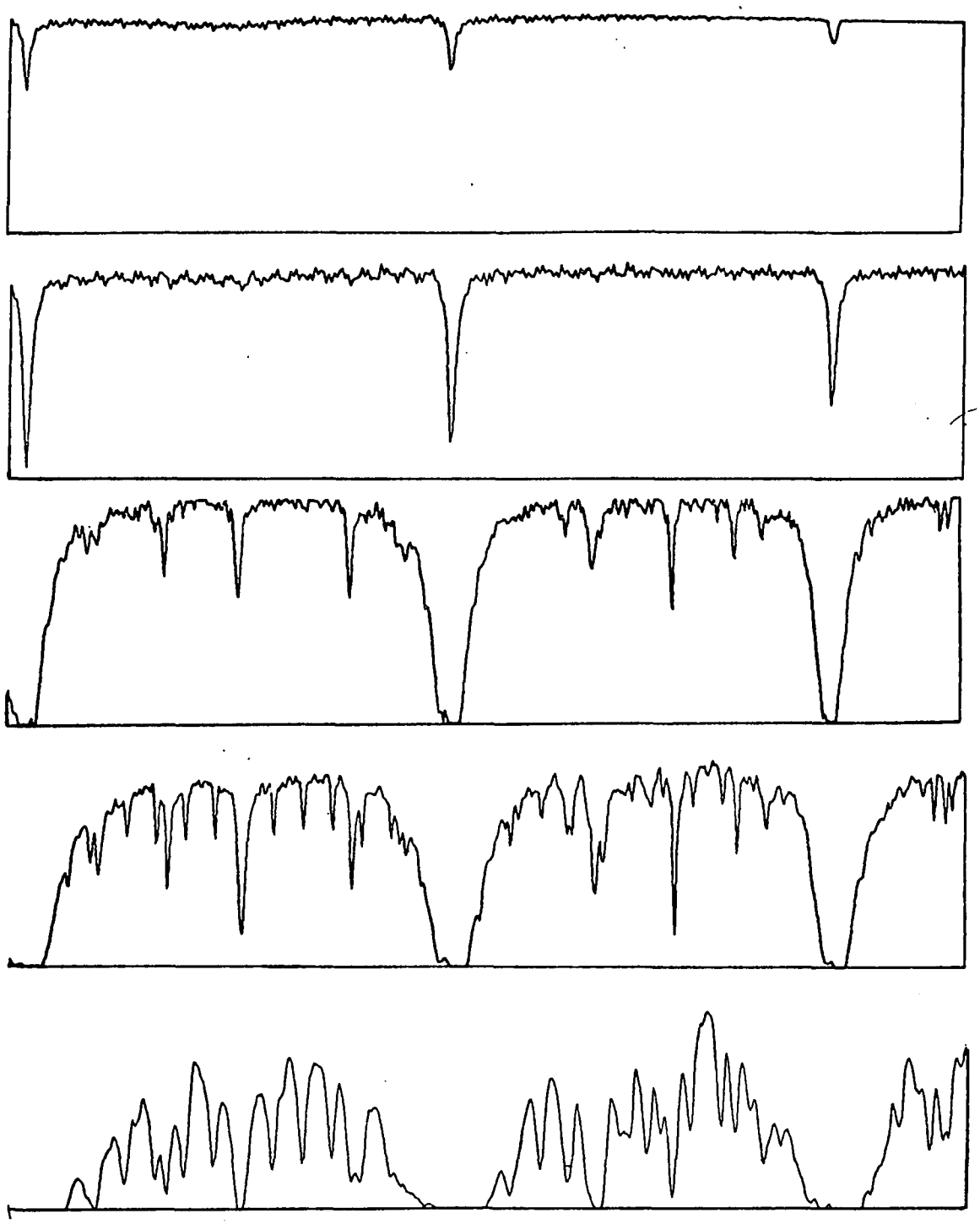

Figure 11. Atmospheric spectra between 1174 and 1202 cm^{-1}.

atmospheric spectra with spectra of individual gases obtained with our instrument. These comparisons have confirmed that essentially all the features in the atmospheric spectra are due to known permanent atmospheric constituents. However, such direct comparisons cannot be made to identify water vapor absorption features in low sun solar spectra because the amount of water vapor in the path traversed by solar radiation is much greater than can be obtained in laboratory spectra. Although some of the H_2O lines have been identified in spectra taken by other observers[20] and most can be predicted from the actual models[21] of water vapor molecular parameters such methods of identification of absorption features in our spectra can be ambiguous and other methods of identification such as those described below must be used.

Each atmospheric gas gives rise to absorption features characterized by their spectral positions and intensity. The intensity in a spectrum depends on the path length-mixing ratio product. For the ground-level atmospheric spectra, when the sample is at a uniform temperature and pressure it is possible to estimate the abundance of a given constituent by comparing the intensities of its bands with other laboratory spectra of the gas when the path length and concentration are known.

The abundances of CO_2, CO, N_2O, CH_4, and H_2O in the ground-level air samples whose spectra were recorded can be obtained in this way. However, it is not possible to estimate the abundances of these gases by comparing the intensities of these bands in solar spectra with laboratory spectra because of the varying temperature and pressure along the path traversed by solar radiation. More sophisticated techniques are required to estimate abundances of atmospheric gases from these spectra, such as the calculation of synthetic spectra as described earlier in this chapter.

Spectra similar to those shown in Figs. 8-11 can be analyzed to search for the appearance of features of suspected trace gases. We have analyzed these spectra for evidence of various contaminants such as HNO_2, HNO_3, HCOOH, fluorocarbon-11, fluorocarbon-12, and fluorocarbon-22. At this time only fluorocarbon-12 (CCl_2F_2) has definitely been identified. While it is possible to set upper limits on the amounts of these gases in ground-level air by direct comparison of such spectra with laboratory spectra, it is not possible to use such direct comparisons to set upper limits to the concentrations of undetected gases in solar spectra since the atmospheric profiles of pressure and temperature are not reproducible in laboratory spectra.

Although the spectra shown in Figs. 8-11 are for a limited number of path lengths and spectral resolutions they were recorded digitally on magnetic tape. Such spectra can be manipulated with a digital computer to produce spectra with degraded resolution or with different apparent absorber concentrations. These artifical spectra can be used to predict the transmittance of atmospheric paths of different lengths and at the same or lower spectral resolutions than those originally recorded. These manipulations do not allow improved resolution to be obtained, neither can the absorptance of a slant path through the atmosphere be simulated.

However, if the line parameters are available as in the AFCRL line listing,[8] synthetic spectra which simulate the actual transmittance can be calculated,

as described earlier. We have used these techniques to calculate synthetic spectra of both homogeneous ground-level atmospheric paths and also slant paths through the atmosphere. Examples of these synthetic spectra are shown in the overlays to Figs. 8-11 which are labelled Figs. 8a-11a, respectively. These synthetic spectra have a spectral resolution similar to the actual spectra and the amounts of the absorbing gases have been chosen to give an absorptance similar to that observed. It is seen that the general agreement between the two sets of spectra for all five spectra on each page, including the solar spectra, is excellent. This range of path lengths is from 10 m to the equivalent of 10^5 m, a ratio of 10^4. One set of line parameters was used for all the calculations. It is also seen that there are some disagreements, of which some must be attributed to inaccurate line parameters. Improved line parameters can be obtained from the experimental measurements.

Thus an important use of the air atlas is to allow improved line parameters to be obtained. Once accurate line parameters an available it is possible to calculate synthetic spectra for any type of path and for any spectral resolution. These synthetic spectra can then be used for comparison with actual spectra to estimate abundances of any atmospheric constituent from any spectrum, including low sun spectra. Such synthetic spectra will allow unpredicted features to be easily identified.

The experience gained so far in comparing synthetic and actual spectra indicates that some adjustments to the AFCRL compilation are required to obtain better agreement with experimental data. It has also been found that the compilation contains only information about seven permanent gases. No line parameters for possible pollutant gases are included. Our investigations into the identification of halocarbon and other features in solar spectra have shown the urgent need to be able to create synthetic spectra of these gases. This information is not at present available and must be collected.

DESIGN OF ABSORPTION CELL TO SIMULATE THE ENVIRONMENT OF THE STRATOSPHERE

Another objective proposed for this work is to test the chemistry of the Freon-O_3 - air system under conditions which simulate as many features of the stratosphere as possible. This involves four basic components; i.e., temperature, pressure, gas composition, and radiation field. Since our laboratory does not now possess a chamber or source suitable for these studies, it has been necessary to design a new photochemical reaction chamber and short wavelength source with which to observe the direct photolysis of the Freons in air at stratospheric temperatures and pressures.

During the initial phases of the cell design, it was found that Professor R. K. Long, in the Department of Electrical Engineering at The Ohio State University, was interested in building a cell with characteristics similar to those required in this study since he wished to measure the transmittance of infrared laser radiation through ozone under simulated stratospheric conditions. It was therefore decided to build a single cell which can be used for both investigations.

Although both groups are interested in obtaining long path lengths by using multiple traversal optics it was recognized that the problems associated with cooling the system increased rapidly as the size of the system increased. An initial decision was therefore made to use a set of White[22] multiple traversal system mirrors with a 2 m radius of curvature which was already available in the laboratory. With these mirrors path lengths in excess of 100 m can easily be obtained in a cell approximately 2 m long and 0.5 m in diameter. This fixed the rough dimensions of the cell.

The corrosive properties of many of the reactant gases and their expected products fixed the allowable construction materials. The only material with excellent resistance to O_3, HF, Cl_2, CF_2O, etc. is iridium. Unfortunately the high cost and extreme difficulty of working with this material necessitated a compromise. Stainless steel was determined to be the best substitute material for the main body of the chamber and the mirror mounts and other structures inside the chamber. Many of the experimenters who have worked with ozone have reported the formation of CO and CO_2 inside their cells as the ozone decays.[23,24,25] In hopes of reducing the sources of carbon inside our cell and for improved weld quality, an extra-low-carbon composition, type 316 stainless steel, was finally chosen.

There are two main approaches to controlling the temperature of a cell. One is to wrap coils around the cell and circulate a coolant through the coils. The coolant is then passed through heat exchangers to control the temperature. This method uses a relatively small mass of coolant to control the temperature of the much larger cell mass. The cost and ease of operation of such systems are relatively independent of the size of the cell to be cooled. Consequently this approach has been used to cool large cells such as the 10 m multiple traversal cell designed by Horn and Pimentel.[26] For this cell a temperature uniformity of 0.3°C over the length of the cell was reported although temperatures were measured several degrees higher at the end plates. This temperature difference could be reduced by installing additional cooling coils at the end plates.

The second approach is to place the cell in a bath of coolant which can be stirred. This approach requires a larger mass of coolant than the first approach and, since the cell is immersed in the coolant, severe sealing problems may be encountered. On the other hand, a temperature bath is better suited to phase change cooling than the first approach. In this process the energy removed by the coolant produces a phase change (e.g., the melting of ice or the sublimation of CO_2) without a corresponding temperature change. This is to be contrasted with kinetic cooling in which the removed energy increases the kinetic energy of the coolant molecules and hence its temperature. The bath approach has been used, for example, by Burch, Gryvnak, and Patty[27] to cool a 1 m cell and by Blickensderfer, Ewing, and Leonard[28] for a liquid nitrogen cooled 3.8 m cell.

The need for precise temperature control in chemical reaction studies has long been recognized. Indeed in a recent study[29] of the reaction

$$H_2O + NO + NO_2 \rightleftarrows 2\,HONO$$

conducted in this laboratory it was found that a 60% change in the equilibrium concentration of HONO occurred for a change in temperature from 23° to 30°C.

Although both cooling approaches have merits and disadvantages, it has been decided to adopt the cooling bath approach in this application. We concluded that, although this approach was more bulky, it was simpler to operate and would cause less vibration (which could affect the mirror stability) than a flowing coolant system. It also appeared that a uniform temperature could be maintained throughout the chamber more cheaply than with a flowing coolant system.

A diagram of the proposed photochemical cell and cooling bath is shown in Fig. 12. The cell will be made from 4.76 mm (3/16") thick plate rolled into a tube. One elliptical shaped end cap will be welded onto one end and another will be bolted onto the other end through the flanges shown. One of the flanges has three concentric grooves cut in it. It is planned that the inner groove will contain a silicone O-ring with good resistance to ozone at low temperatures and that the outer groove will contain a spring-loaded Teflon O-ring with excellent resistance to the coolant and the ability to seal at temperatures up to 260°C and down to cryogenic temperatures. The middle groove will be continuously pumped to prevent mixing of a sufficient quantity of O_3 and coolant vapor to produce an explosion. Infrared radiation will be introduced into the cell through windows at the right end (Fig. 12A). These windows are shown in Fig. 12B. Ultraviolet radiation will be introduced through the windows shown in the middle of Fig. 12A.

The cell will be mounted inside the bath shown in Fig. 12C. This is constructed of 6.35 mm (1/4") thick steel plate. Ports at the end and in the middle of the bath will connect to the cell through the stainless steel bellows and teflon O-ring seals shown in Fig. 13. These are designed to be leak free as far as the coolant is concerned and flexible enough to allow for misalignment between cell and bath as well as temperature-induced structural deformation. The bath will be covered with 12.7 mm (1/2") thick plate glass resting on teflon seals

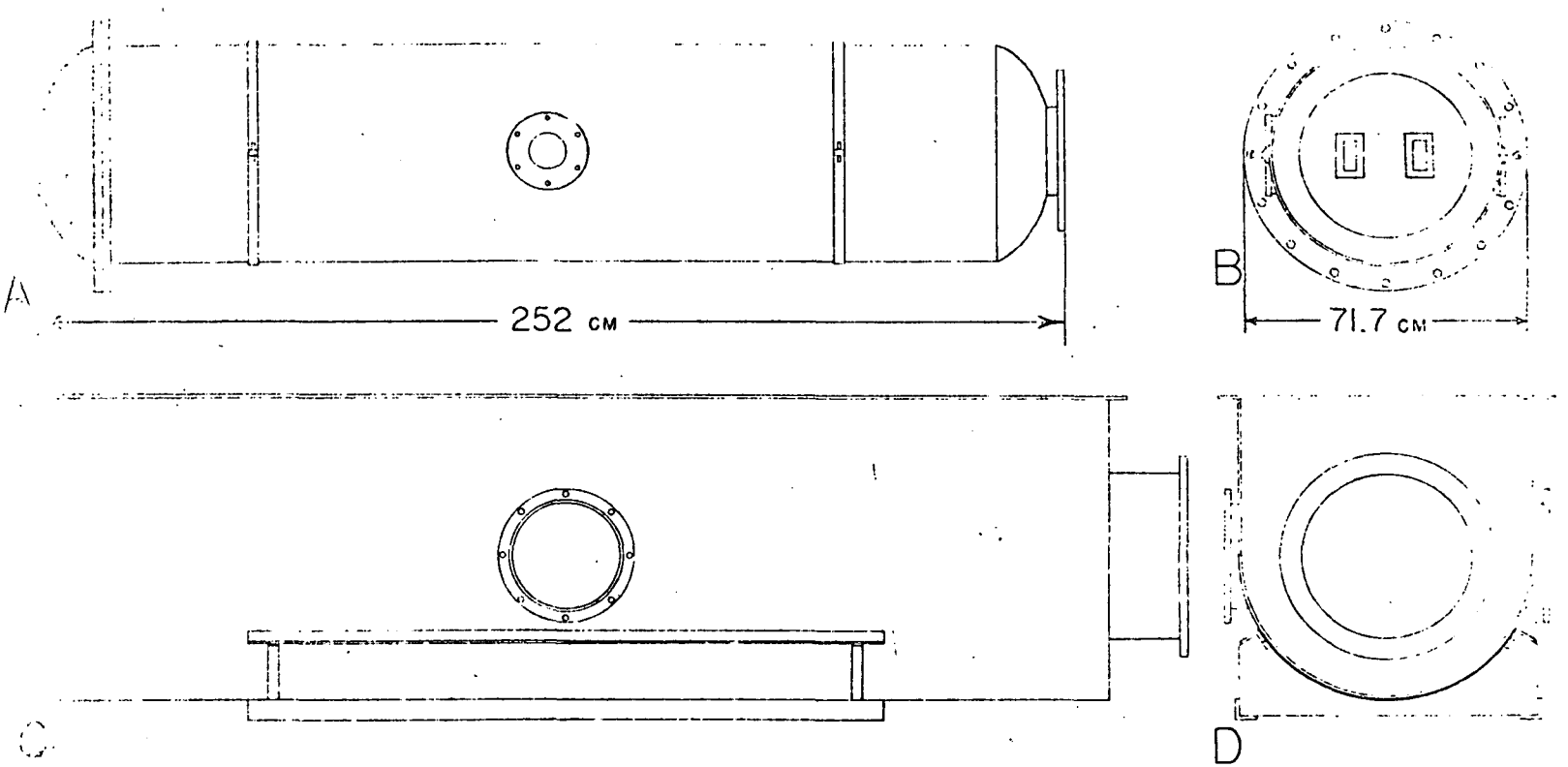

Figure 12. Schematic diagrams of the cell and bath. (A) sideview of cell showing window for ultraviolet radiation, (B) end view of cell showing windows for infrared radiation, (C) side view of bath, (D) end view of bath. Bath is shown without insulation.

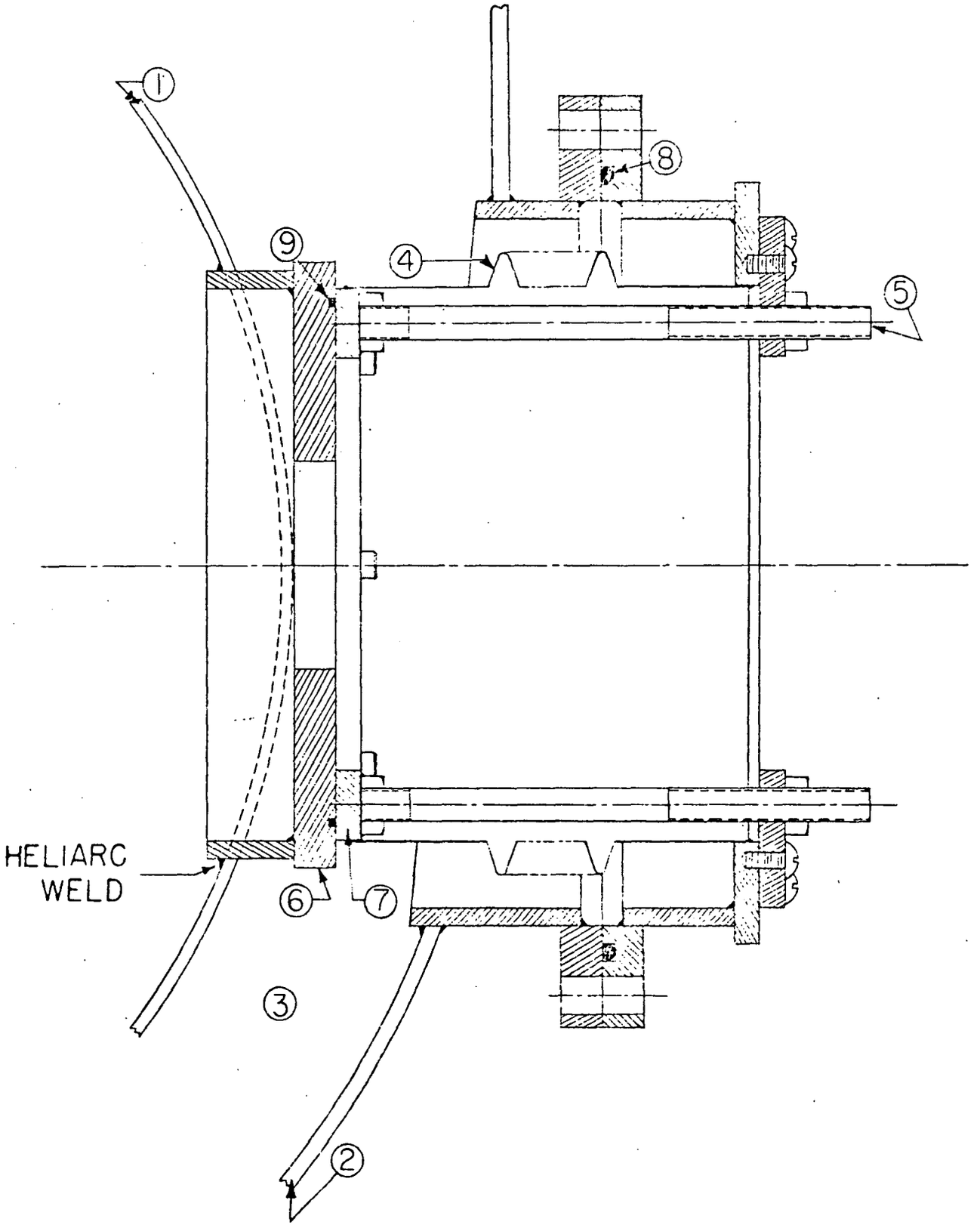

Figure 13. Schematic diagram of typical bellows connection from cell to bath. (1) cell wall, (2) bath wall, (3) coolant space, (4) bellows, (5) bellows length-adjustment rod, (6) window mounting plate, (7) mating flanges for port (6), (8) and (9), teflon O-rings

to contain the coolant vapors and prevent leakage of warm room air into the bath. Styrofoam insulation 15.24 cm (6 inches) thick will cover the bath on all sides.

The bath-cell arrangement is estimated to weigh 653.12 kg (1751 lb) dry and 1137.65 kg (3050 lb) when full of ethanol. It is estimated that it will require about 1.12 kg (3 lb) of dry ice per 0.56 K (°F) of temperature change and about 1.12 kg (3 lb) per hour to maintain a temperature of 188 K (-85°C). Different operating temperatures may be selected by using different coolants (e.g., H_2O) at their ice points or sublimation boiling points (e.g., CO_2). It is planned to obtain intermediate temperatures by dripping liquid nitrogen into the coolant and stirring with several motor-driven propellers immersed in the liquid. It is hoped that an overall temperature uniformity of 1 K or better can be achieved.

Since the stainless steel cell has a different coefficient of thermal expansion than that of the glass mirrors a temperature change will tend to change the optical alignment. A temperature change of 85 K (85°C) should produce a contraction of 3 mm of the cell with respect to the radius of curvature of the mirrors. Some provision must then be made to realign the mirrors after the cell has cooled down. This will be accomplished by feedthroughs built from Veeco style bellows seal valve assemblies. These are similar to the design of Blickensdeifer et al., (Ref. 28). These feedthroughs will also enable the mirror system to be realigned without opening the cell. In order to prevent condensation on the windows, the boil-off from LN_2 will flow over the windows and flush any moisture from the bellows connection areas.

The optical path of the infrared radiation inside a White multiple traversal system is well known.[22] In the three-mirror system shown in Fig. 14 the beam enters the cell through window W_1 and forms an image of the source at M_1. After multiple reflections inside the cell the beam emerges through window W_2. In a conventional system, the mirrors M_2 and M_3 are placed close together. However, in order to introduce the ultraviolet radiation into the cell, we propose to spread these two mirrors apart as shown. The ultraviolet radiation from a microwave-excited high-pressure xenon lamp[30] (which has a continuum from 150-210 nm[31]) emerges through a CaF_2 window and is introduced into the chamber through a window in the middle of the cell. The beam is focused on a beam divider which reflects part of the energy to M_1 and part to M_2 and M_3. Since the beam divider is at the focal point of all three mirrors, after reflection from the White mirrors, a parallel beam is produced which travels down to flat mirrors at the ends of the cell. These reflect the radiation back down the cell to the White mirrors. By spreading the White mirrors apart, the infrared path is completely isolated from the ultraviolet optics and no shadows are formed.

At the present time two-thirds of the purchases of material for the cell have been made. The stainless steel chamber and mirror mounts are about 60% completed and the steel bath and connecting bellows are nearly 80% completed. Most of the components for the ultraviolet radiation system have been purchased.

It is estimated that the system will be ready for preliminary testing by the end of April.

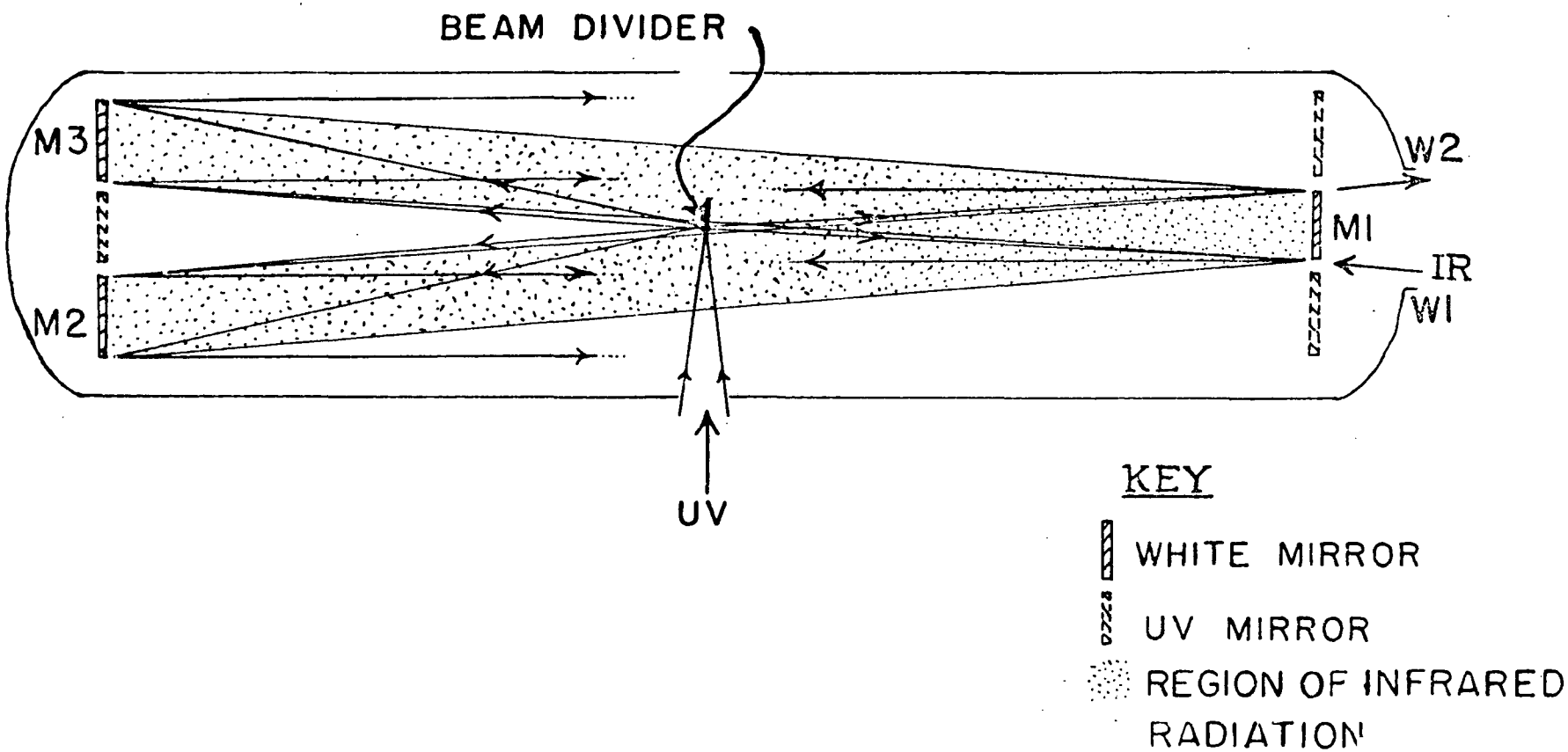

Figure 14. Radiation field inside cell (note IR clearance of beam divider)

STUDY OF SOME KEY REACTIONS OF PROBABLE IMPORTANCE IN PHOTOCHEMICAL SMOG FORMATION

CONSTRUCTION AND PERFORMANCE OF PHOTOCHEMICAL CELL

The major details of the 6 m photochemical cell have been described in the Final Report under EPA Grant No. R-803075.[32] This cell has been completed, tested, and is now being used to study a variety of photochemical reactions.

The cell is constructed of four 1.5 m lengths of Corning low-expansion borosilicate glass tubing giving an overall length of 6 m and an internal diameter of 30 cm. Surrounding this cell are four banks of black light fluorescent tubes which emit energy in the UV region (3000Å - 4700Å). The multiple traversal optical system inside the cell has been described by Hanst.[33] It consists of four rectangular-shaped mirrors and four quadrant-shaped mirrors, each of which has a radius of curvature of 5.31 m. When photolysis experiments are being performed, the cell is covered with aluminum foil reflectors. The photochemical cell is fitted with NaCl windows. When the cell is evacuated, an ultimate pressure of 10^{-3} Torr can be attained. The leak rate is ~ 0.8 Torr/day. Additional details of the cell are given below.

Transfer Optics to the Photochemical Cell

A schematic of the optical arrangements used in this work is given in Fig. 15.

Radiation from a Nernst glower (N) is reflected by the spherical mirror M_1 ($f_1 = 15$ cm) to an off-axis paraboloid M_2 ($f_2 = 27$ cm) which results in parallel radiation on the beam splitter (B.S.) inside the interferometer. This beam splitter is made of germanium on a KBr substrate. The collimated beam is amplitude-divided at the beam splitter; half of it is reflected to the movable mirror M_4 and half of it is transmitted to a stationary mirror M_5. These two beams then combine at the beam splitter and exit the interferometer. The energy, after being reflected by two plane mirrors (M_6 and M_8) and two spherical mirrors (M_7, $f_7 = 60$ cm; M_9, $f_9 = 45$ cm), is directed into the long-path absorption cell and an image is formed at N_3 in the plane of the field mirror and an image of the beam splitter is formed on the top left quadrant at the other end of the cell. Intermediate images of the Nernst and the beam splitter are also formed at positions N_1 and N_2; and at B_1, respectively. If high spectral resolution is required, most of the energy from the elongated image of the source cannot be usefully collected. An aperture should be placed at either position N_1 or N_2 to reduce the beam-spreading effect.

When the beam exits the absorption cell, it is focused on the Cu:Ge detector which is operated at liquid helium temperature.

The entire optical system external to the cell is mounted on a slab of aluminum and enclosed in a transparent plastic box sealed to be essentially air tight. The box is purged with dry N_2 gas during operation and residual CO_2 and H_2O in the gas are removed by placing traps of KOH and NaOH on the floor of the box.

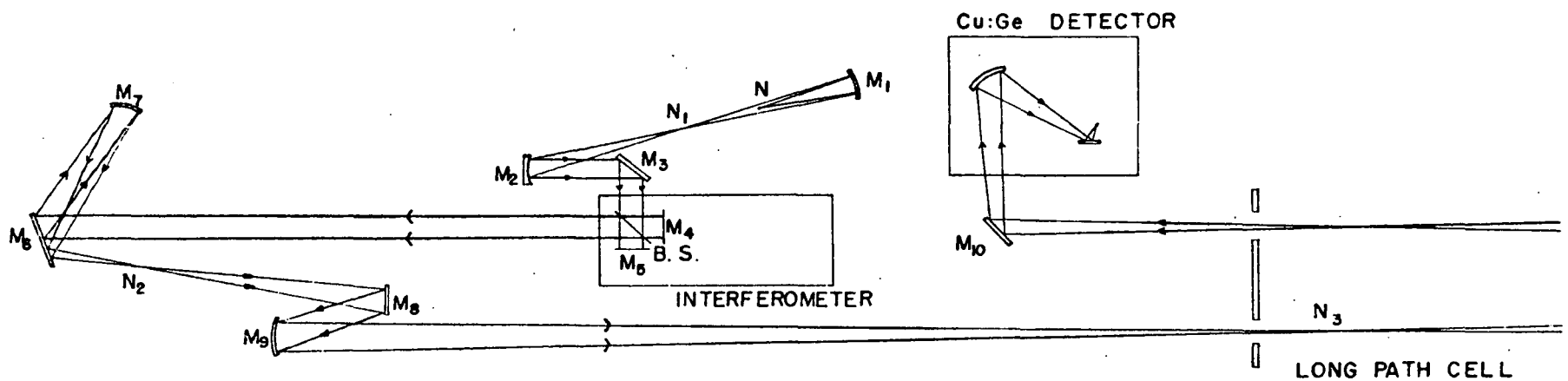

Figure 15. Optical transfer system from interferometer to photochemical cell

Path Length Stability and Signal-to-Noise Ratio

The base path of the photochemical cell is 5.31 m. It has been found that the highest number of traversals to be used without a significant loss of signal-to-noise ratio is 48 passes. This gives a total path length of 255 m. The fluorescent lamps cause the temperature of the cell to rise about 10 K (10°C) in 1/2 hour above ambient temperature. This results in a shift of the optical alignment, which in turn affects the signal-to-noise ratio. All the photolysis experiments reported here were carried out with room air forced into the channel between the glass surface and the reflectors by a fan. This ensures cool air circulation and maximum change of temperature of less than 2-3 K (2-3°C) during the run. A temperature gradient of about 2 K (2°C) is found at the ends of the cell during photolysis experiments. Under favorable conditions, a signal-to-noise ratio greater than 100 is usually obtained. Except for the NO_2 photolysis experiments in which only one scan is collected for the interferogram, all other experiments involved five scan-averages per interferogram. At a resolution of 1 cm^{-1}, the minimum time needed for one scan and storage of the data is 23 seconds.

Gas Handling and Injection System

The gases are injected into the cell through a stainless steel [6.35 mm (1/4") O.D.] injection manifold at five inlets (one at each spacer and one at each endplate (see Fig. 16). The stainless steel bellows values are mounted close to the inlets in order to keep reactive gases out of the high surface-to-volume ratio injection manifold.

The grease and mercury free gas handling system is all glass with teflon valves (see Fig. 17). Connections are made with stainless steel Cajon unions employing Viton O-rings. Low background pressures are achieved by a single stage oil diffusion pump which is separated from the system by a liquid nitrogen trap. Pressures are read on a glass spiral gauge which is calibrated with one of two Wallace and Tiernan absolute pressure gauges (0-20 mm and 0-800 mm).

The gas handling manifold was designed to have small dead volumes and to allow positive injections of samples with N_2 gas; positive injection capability is essential for forming multicomponent mixtures in the photolysis cell.

The eight volumes built into the vacuum system (2.7 to 92.4 ml) allow injection of samples of less than 0.01 ppm (0.5 mm in 2.7 ml, cell volume 445 liters). The volumes were designed for making samples in the low ppm range. For injecting very large concentrations or for samples with low working pressures (e.g., H_2CO), larger volumes can be connected to the system. These add-on volumes are constructed with two valves to allow positive injection.

Ultraviolet Intensity and Distribution Measurements

The 6.3 m long photolysis cell (30.5 cm interval diameter pyrex tubing) is surrounded by eight rows of black light fluorescent lamps (G.E. F72T12/BL/HO, 85 watts) for 5.3 m and ten rows of less powerful black lights (G.E. F40BL, 40 watts) for the remaining one meter. These lamps are approximately 7 cm from

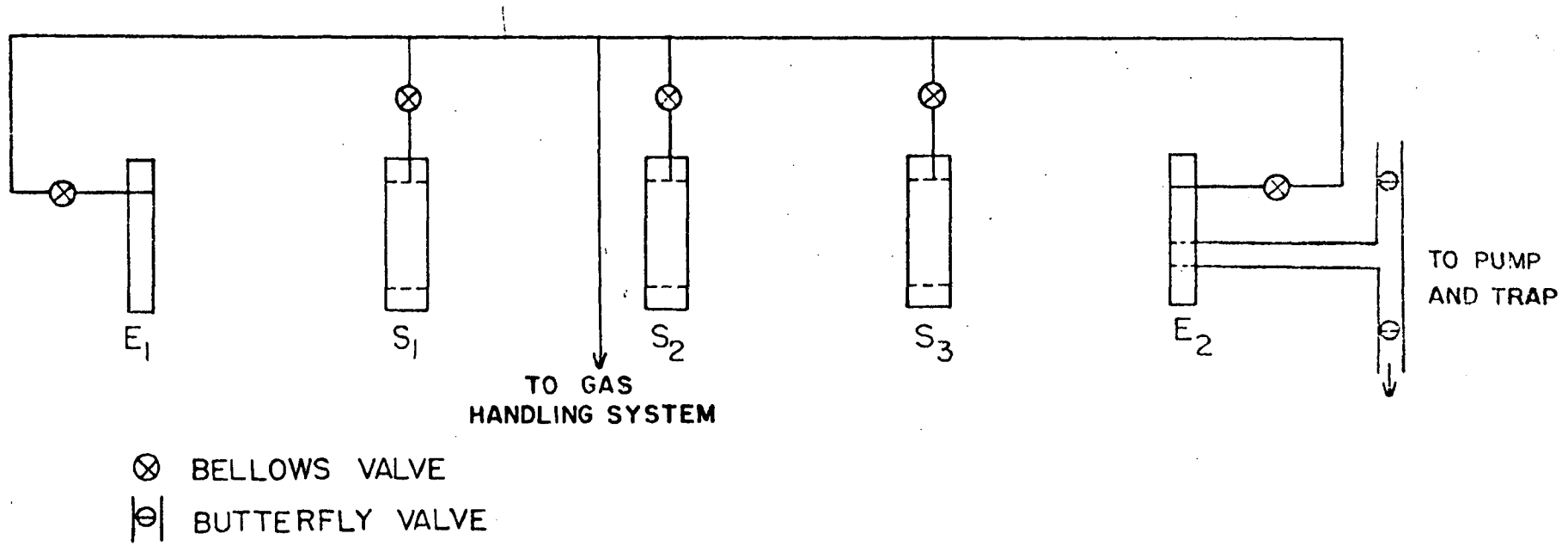

Figure 16. Gas inlet system to 6 m cell

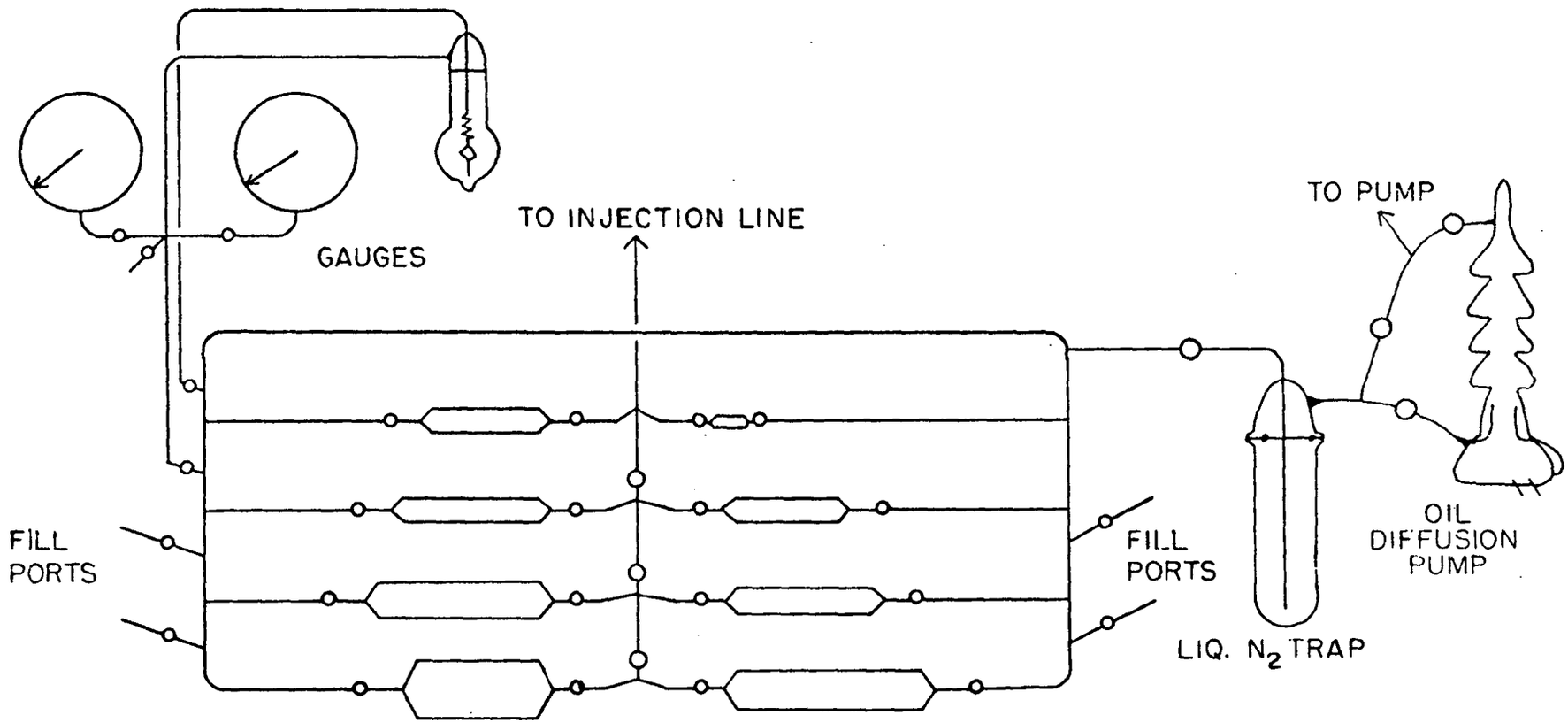

Figure 17. Gas handling system for 6 m cell

the outer cell wall. The cell and lights are surrounded by an external concentric shell of aluminum foil approximately 23 cm from the cell wall to increase the intensity and improve the distribution uniformity.

The number and types of lamps were chosen to mimic the solar intensity and distribution in the photochemically interesting region from 300 to 400 nm. In Fig. 18 the lamp distribution through the cell pyrex wall is compared with the solar distribution in the region of interest.

In order to get some feel for the radiant energy intensity within the cell and the intensity uniformity at various positions within the cell a Hewlett-Packard Radiant Flux Detector (model 8334A) was used. This thermopile detector measures the incident power in absolute units (W/cm^2) and has a flat spectral response from 300 to 3000 nm (a 1 mm thick Infrasil quartz window covers the thermopile detector). The detector has an effective field of view of 0.1 sr (20.5° conical angle) and a detector area of 0.184 cm^2.

When the detector is centered in the cell it measured radiance values between 1.0 and 3.5 $mW \cdot cm^{-2} \cdot sr^{-1}$ (over all wavelengths) depending on what it sees in its field of view. A polar plot of detector readings is presented in Fig. 19. For these readings the detector was mounted on the axis of the cell (0.76 m from one end) and rotated in a plane containing the axis of the cell (they are an average of the values for a plane along a row of lights and a plane between two rows of lights). A similar measurement was performed at the other end of the cell and gave a very similar profile indicating uniformity of intensity for these two positions.

When a Corning 7-54 UV pass filter (2.5 mm thick which transmits from less than 300 to 400 nm) was placed over the detector the radiant intensity was reduced to about 40% of the original reading. We thus conclude that approximately 50% of the total radiant energy within the cell is in the 300 to 410 nm region of interest.

It was observed that the radiant energy did not drop significantly (in the 300 to 400 nm range) as the lights warmed up 10 K (10°C) over a half-hour time range [the average amount of temperature change we observed with the cooling we use is 2-3 K (2-3°C) over two hours].

The solar spectral irradiance at the Earth's surface in the wavelength range 290 to 390 nm is about 3.6 mW/cm^2 (50° Zenith angle).[34] Above the Earth's surface reflection from the surface would increase this value. At one position in the cell we calculate the irradiance (from 300 to 410 nm) to be 9.4 mW/cm^2. This value is for a planar element along the cell axis and includes contributions from both above and below the plane. This irradiance corresponds to a photon flux irradiance of 1.7×10^{16} $photons \cdot cm^{-2} \cdot s^{-1}$ for 360 nm photons. This value will allow us to calculate a rate constant for the photodecomposition of NO_2 to compare with the experimentally observed rate of 0.52 min^{-1} (see the following section). The general expression for the rate constant is

$$k = (2.303)\ (I_o)\ (\alpha)\ (\phi).$$

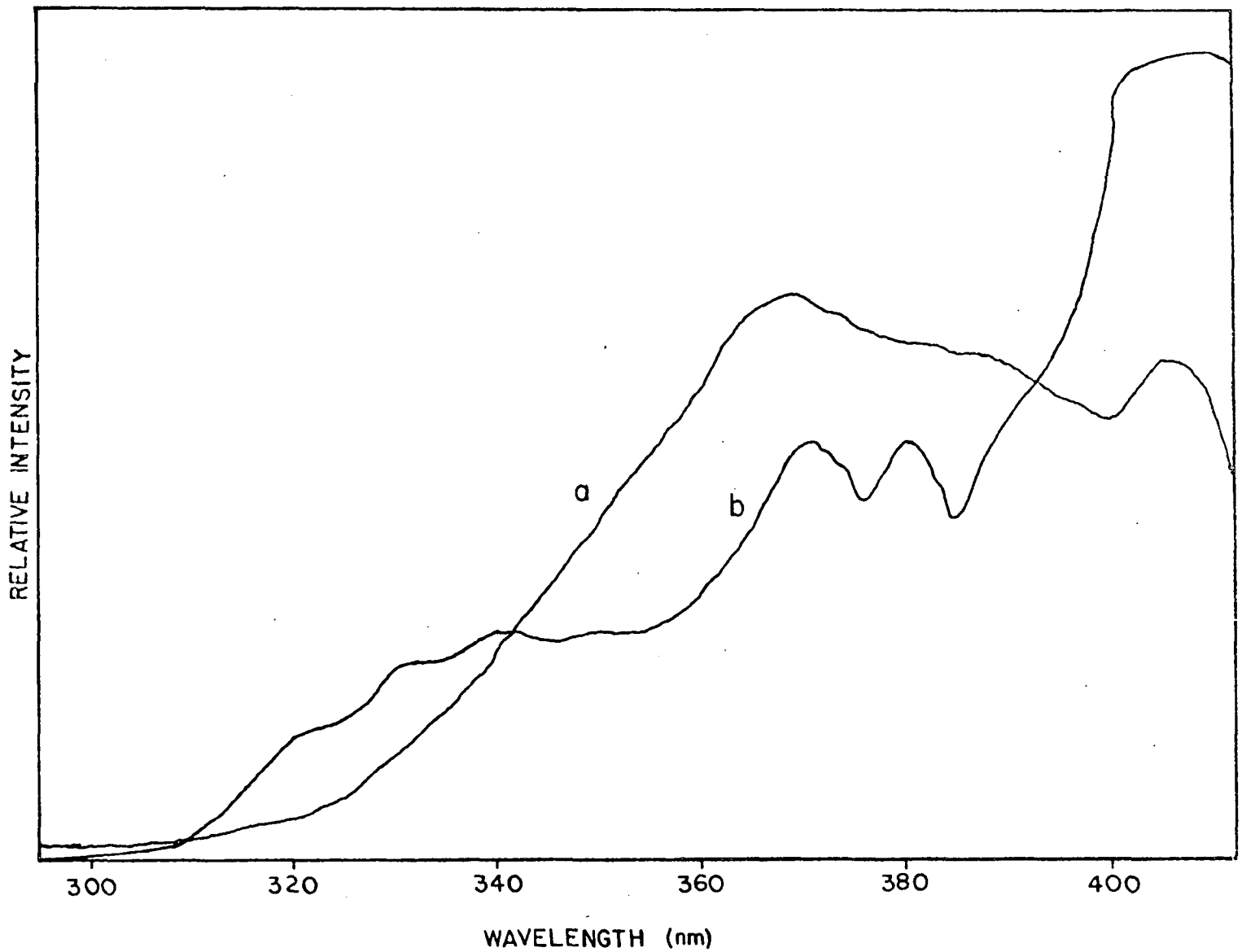

Figure 18. (a) Spectral distribution of fluorescent lamp output after passing through the glass walls of the cell; (b) relative spectral distribution of solar energy at ground level

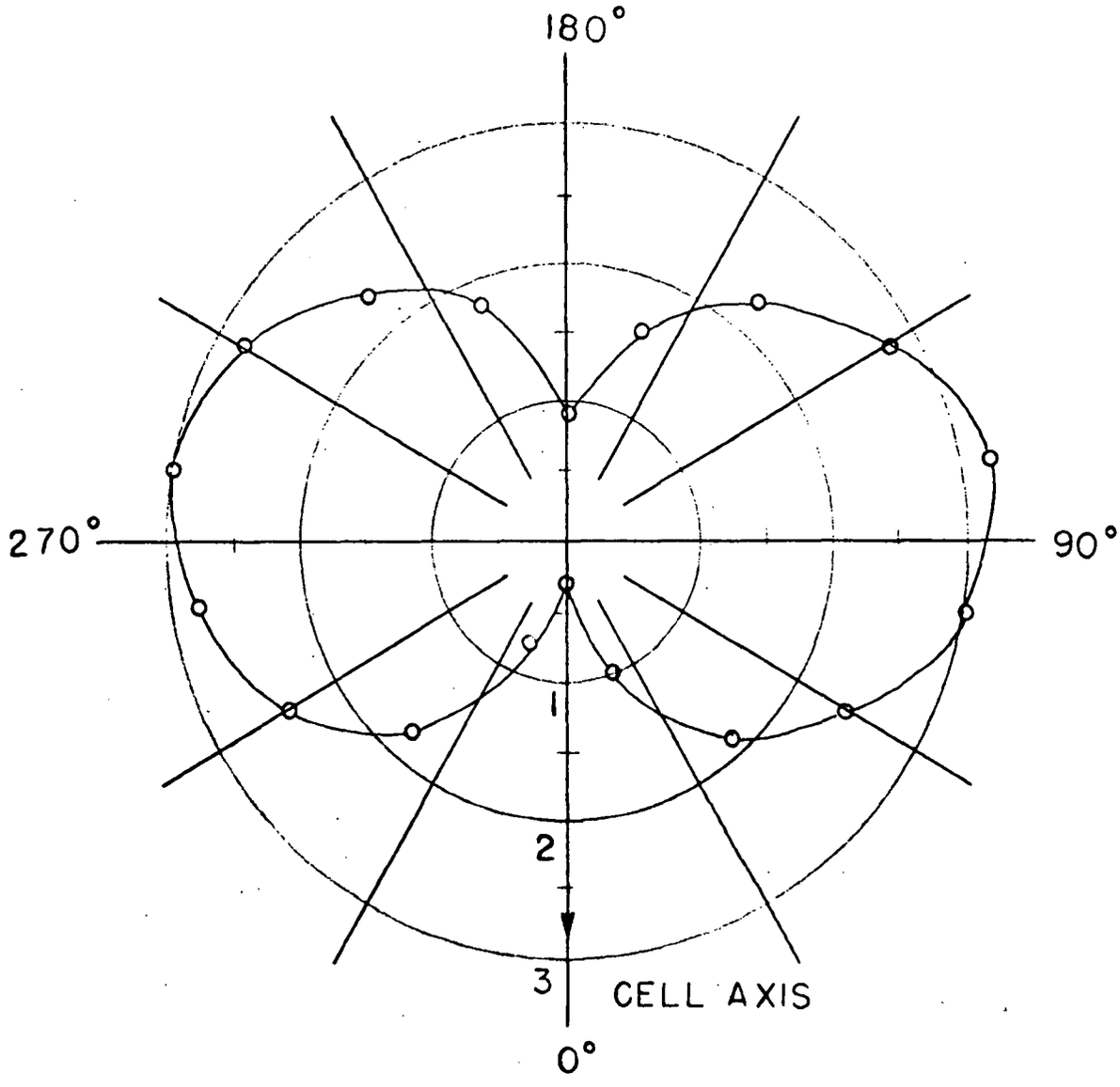

Figure 19. Radiant flux detector readings (in $mW/cm^2 \cdot sr$) measured in a plane containing the cell axis. This average curve is the mean of the readings obtained when a row of lights is in or out of the field of view

A weighted average of the absorption coefficient (α) and quantum yield (ϕ) for NO_2 over the light output distribution curve within the cell (see Fig. 18) gives a value of 127 ℓ mole^{-1} cm^{-1}. This gives a value of 0.50 min^{-1} for an irradiance of 1.7 x 10^{16} photons cm$^{-2}\cdot s^{-1}$ which agrees favorably with the experimentally rate constant of 0.52 min^{-1}. It should also be mentioned that this value is typical for that found in sunlight (see the following section).

Estimation of UV Cell Radiant Intensity from Measurements of the Rate of NO_2 Photolysis[35,36,37]

The photolysis of nitrogen dioxide in the NO_x-polluted atmospheres is the major source of O-atoms and its occurrence results in the generation of O_3 through the following reactions:

$$NO_2 + h\nu(\lambda < 4300\text{Å}) \rightarrow O + NO \tag{12}$$

$$O + O_2 + M \rightarrow O_3 + M \tag{13}$$

$$O_3 + NO \rightarrow NO_2 + O_2 \tag{14}$$

In air at the usual ambient levels of the common pollutants, the above reactions are largely responsible for establishing the ozone concentration. To a first approximation, relation 15 applies;

$$[O_3] \cong \frac{[NO_2]k_{12}}{[NO]k_{14}} \tag{15}$$

Thus the apparent first-order rate constant k_{12} is a very important parameter in smog chemistry. It is a function of the intensity of ultraviolet light present in the lower atmosphere which is within the NO_2 absorption region and which is sufficiently energetic to result in the dissociation of NO_2. A recent theoretical determination of the constant k_{12} for the lower atmosphere near sea level is shown in Fig. 20 as a function of solar zenith angle.[34]

It has become general practice to determine the experimental value of k_{12} in smog chambers to compare the degree of correspondence of the chamber intensity with that of the solar intensity within the atmosphere. We have carried out this determination in two types of experiments. The first and the most direct method involved the photolysis of pure NO_2 gas at low pressures within the reaction chamber. For those conditions only the following reactions are important:

$$NO_2 + h\nu \rightarrow O + NO \tag{12}$$

and

$$O + NO_2 \rightarrow NO + O_2. \tag{16}$$

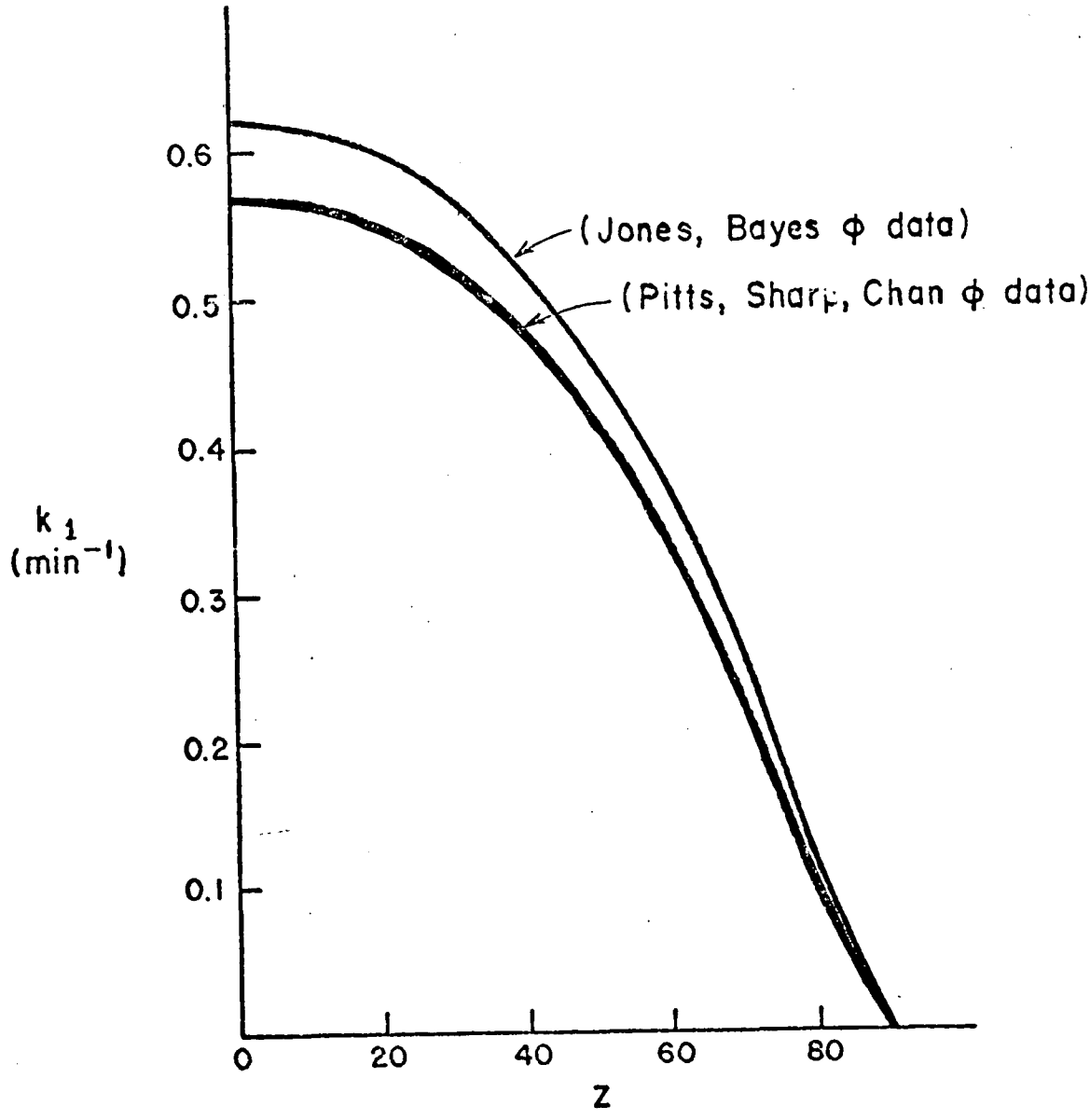

Figure 20. The theoretical magnitude of the rate constant k, for the formation of $O(^3p)$ atoms through NO_2 photolysis at different solar zenith angles as estimated for the atmosphere of Los Angeles; values are calculated for the conditions of no attenuation of the ultraviolet within the polluted layer and no reflection from the surface of Los Angeles

The reaction of O-atoms with NO_2 is the only fate of O for these conditions, so relation (17) follows:

$$-d[NO_2]/dt = 2k_{12}[NO_2] \tag{17}$$

and

$$-d[NO_2]/[NO_2] = 2k_{12}dt. \tag{18}$$

Upon integration of (18) between initial $[NO_2]_o$ and $[NO_2]_t$ at time t, Eq. 19 results;

$$\ln([NO_2]_o/[NO_2]_t) = 2k_{12}t = \ln(A_o/A_t). \tag{19}$$

If we restrict our measurement to that range of $[NO_2]$ for which the Beer-Lambert relation applies, then the absorbance (A) is proportional to concentration, and a linear relation between $\ln(A_o/A_t)$ and time is expected with a slope equal to $2k_{12}$.

Absorbance data for NO_2 as a function of time were determined in a series of experiments in this work. The data from one such experiment are shown in Fig. 21. It can be seen that the plot is linear within the experimental error. Values of k_{12} derived from this and similar experiments are shown in Table VII. From these data we conclude that $k_{12} = 0.515 \pm 0.07\ min^{-1}$.

It could be argued that the photolysis of NO_2 at low pressures may not reflect accurately the rate of O-atom production from reaction (12) in air at 1 atm. pressure. It is possible that collisional deactivation of NO_2 excited at the lower wavelengths, near the dissociation limit of NO_2, may occur, and hence the use of k_{12} derived from low-pressure experiments may be unjustified.[38] To test this hypothesis and to derive a meaningful value for k_{12} applicable to the system of greatest interest in our work, air at atmospheric pressure, additional experiments were carried out photolyzing small amounts of NO_2 in a synthetic air mixture containing 140 Torr of O_2 and 560 Torr of N_2. The results of two such experiments are shown in Figs. 22 and 23. In this case there are a number of reactions which occur and the treatment of the results to derive values for k_{12} is considerably more complicated. The following reactions must be considered:

$$NO_2 + h\nu \rightarrow O + NO \tag{12}$$

$$O + O_2 + M \rightarrow O_3 + M \tag{13}$$

$$O_3 + NO \rightarrow NO_2 + O_2 \tag{14}$$

$$O_3 + NO_2 \rightarrow NO_3 + O_2 \tag{20}$$

$$NO_3 + NO \rightarrow 2NO_2 \tag{21}$$

$$NO_3 + NO_2 \rightarrow N_2O_5 \tag{22}$$

$$N_2O_5 \rightarrow NO_2 + NO_3 \tag{23}$$

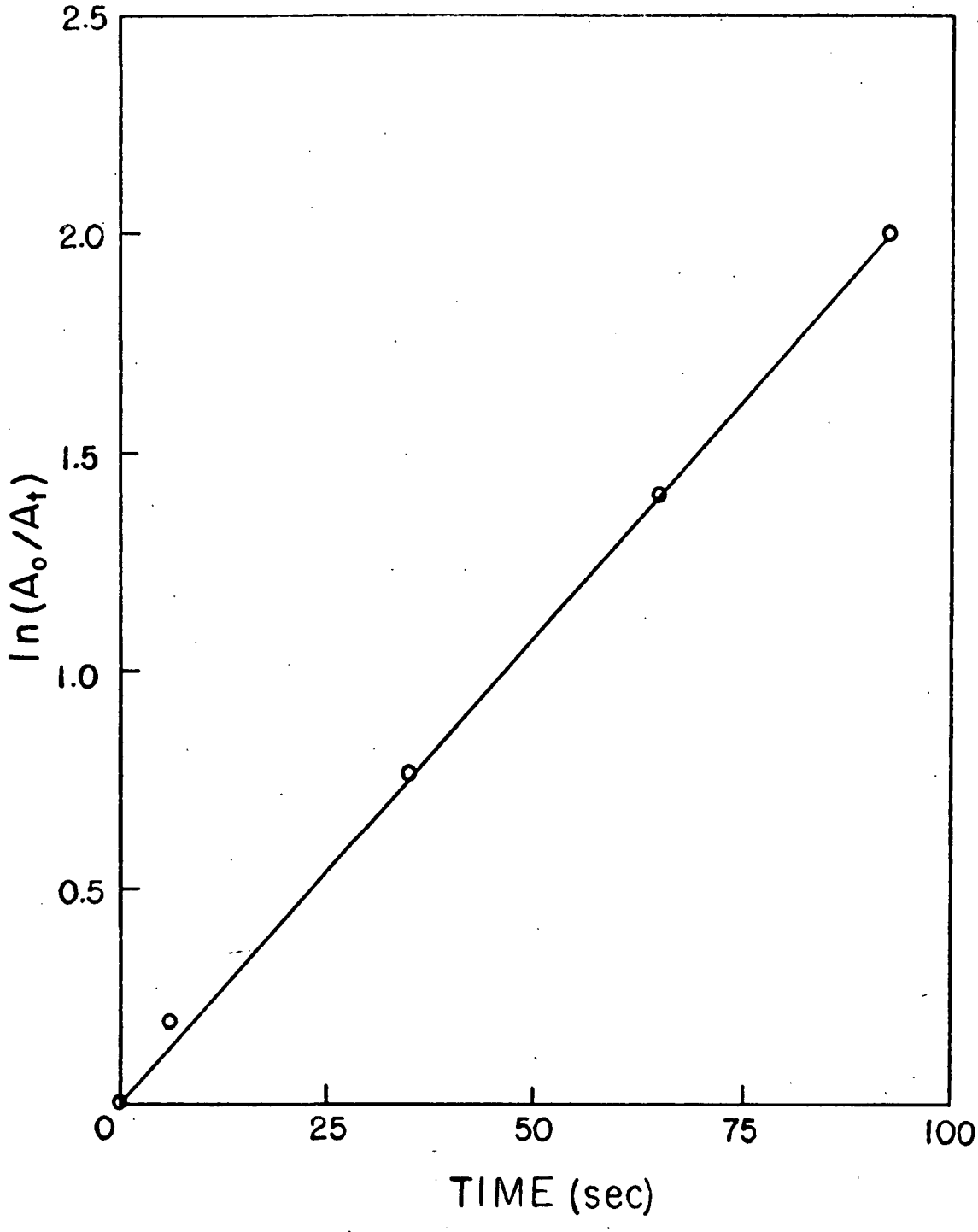

Figure 21. A plot of $\ln[A_o/A_t]$ vs time for NO_2 photolysis at low pressure $[NO_2]_o$ = 30.4 ppm

TABLE VII. RATE DATA ON THE PHOTOLYSIS OF NO_2 AT LOW PRESSURE

$[NO_2]_o$ (ppm)	$2k_{12}$ (min^{-1})	% linear correlation
13.41	1.16	99.2
17.74	0.913	92.0
24.54	0.882	98.0
28.70	0.923	97.7
30.45	1.264	100
30.45	1.065	99.3
36.85	1.113	100
44.77	0.919	98.0

Best Estimate: $2k_{12} = 1.03 + 0.14\ min^{-1}$

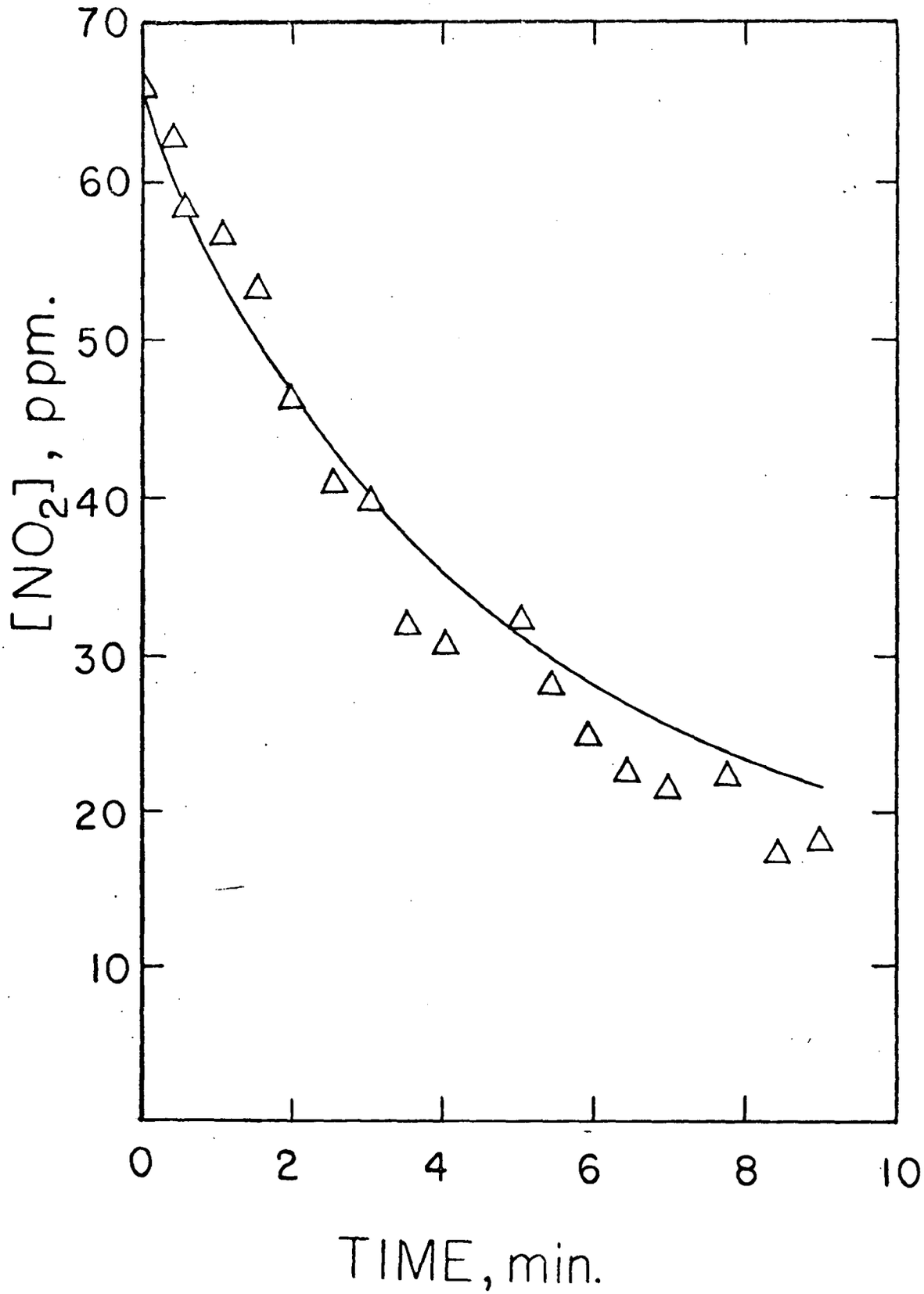

Figure 22. Plot of $[NO_2]$ versus time of irradiation in the photochemical cell; $[NO_2]_0$ = 66.0 ppm, P_{O_2} = 140 Torr, P_{N_2} = 560 Torr; solid line is computer simulation of the NO_2 - time dependence using $k_{12} = 0.51_5$ min^{-1}

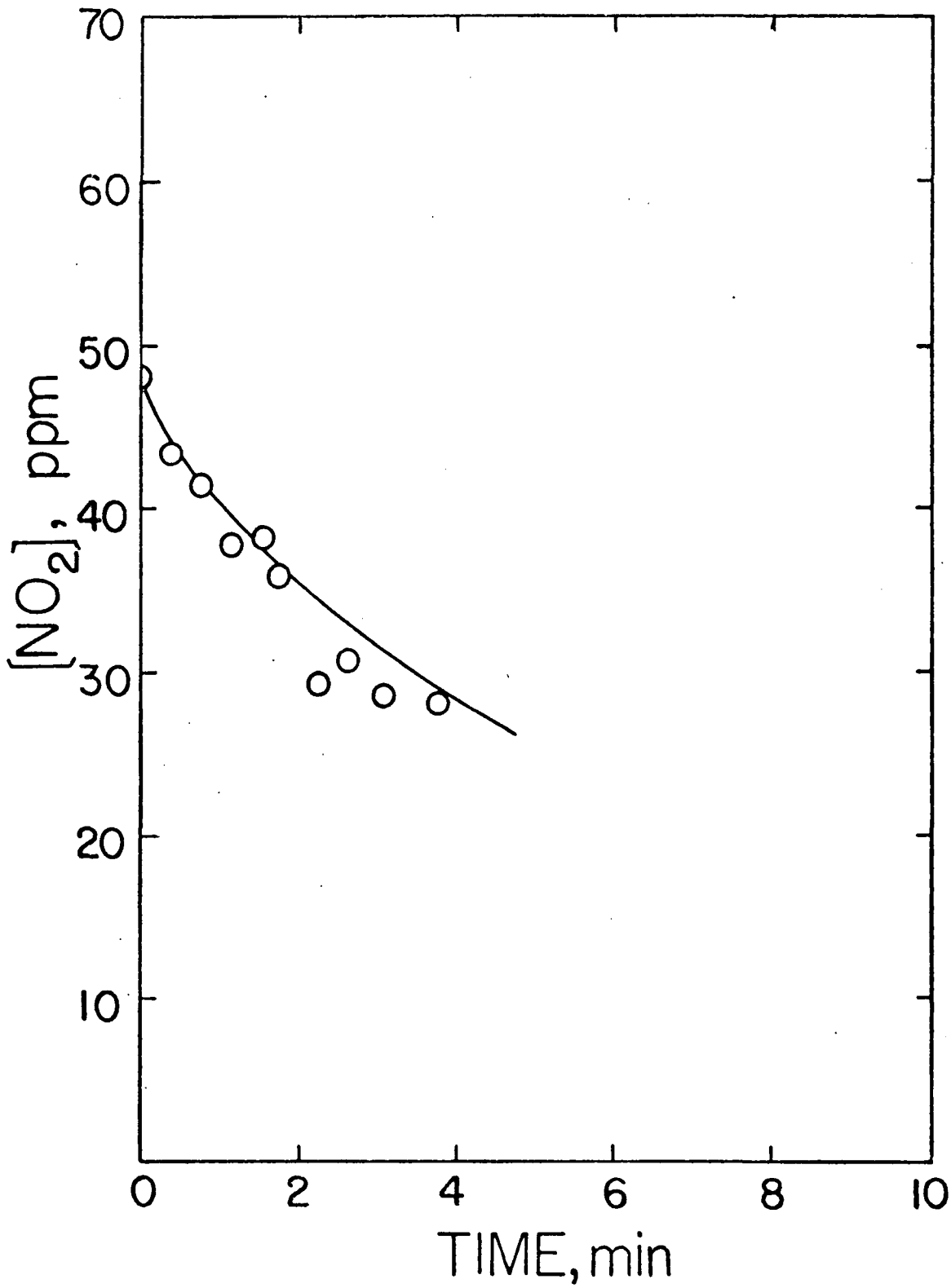

Figure 23. Plot of $[NO_2]$ versus time of irradiation in the photochemical cell; $[NO_2]_0$ = 48.1 ppm, P_{O_2} = 140 Torr, P_{N_2} = 560 Torr; solid line is computer simulation of the $[NO_2]$ time dependence using $k_{12} = 0.51_5$ min^{-1}

$$NO_3 + NO_2 \rightarrow O_2 + NO_2 + NO \quad (24)$$

$$NO_3 + NO_3 \rightarrow O_2 + NO_2\ NO_2 \quad (25)$$

$$N_2O_5 + H_2O \rightarrow HONO_2 + HONO_2 \quad (26)$$

$$O + NO_2 \rightarrow NO + O_2 \quad (27)$$

$$O + NO_2 + M \rightarrow NO_3 + M \quad (28)$$

$$NO + NO + O_2 \rightarrow NO_2 + NO_2 \quad (29)$$

All of the rate constants for the reactions in the above sequence are reasonably well known[39] and a computer simulation of the experimental systems can be made using these constants and the value of $k_{12} = 0.515\ min^{-1}$, derived directly from the low-pressure experiments.

The results of such calculations are shown in Figs. 22 and 23 as the solid lines. The computer-generated variation of $[NO_2]$ with time fits the data well within the uncertainty of these experiments.

Thus we conclude that the value of $k_{12} = 0.515 \pm 0.02\ min^{-1}$ is a reliable estimate of the NO_2 photolysis rate constant in the reaction vessel for our usual conditions (700 Torr air, 23 $\pm$ 2°C). This estimate is gratifying in that it compares well with the theoretical value for k_{12} in sunlight at z = 40° (see Fig. 20). The intensity of ultraviolet light within the photochemical cell designed in this work is very similar to that of the sunlight within the lower atmosphere and both are significantly higher than that found in most of the other smog chambers constructed in recent years. In these cases k_{12} values vary from about 0.22 to 0.40 min^{-1}.

PHOTOLYSIS EXPERIMENTS

Theoretical Estimation of Photochemical Decomposition Rates from Existing Absorption and Quantum Yield Data

In the variety of experiments which are planned for this work a number of light-sensitive compounds will be employed. Estimates of the apparent first-order rate constants have been made for several of these species utilizing published extinction data, quantum yield data, and relative intensity versus wavelength measurements made utilizing our cells and lamps (see Fig. 18). The theoretical first-order decomposition rate constants, k_i, for all systems were compared with that for NO_2 taking our measured value of $k_{12} = 0.51\ min^{-1}$ and the ratios of the integrals $F_i = \int_{\lambda_1}^{\lambda_2} \epsilon(\lambda)\ \phi(\lambda)\ I^\circ(\lambda)d\lambda$ over the entire non-zero range of values for the ith species and for NO_2;

$$k_i = k_{12}(F_i/F_{NO_2}).$$

These data are given in Table VIII with the corresponding reaction to which they apply.

These data are useful in experiment planning and selection of reactant concentration necessary for optimum rate measurements in our system. In those cases where experimental direct measurements of these quantities have been made they appear to be in reasonable accord with the theoretical estimates of Table VIII. However, the one case of nitrous acid appears to be significantly different from that anticipated from the existing absorption data as derived in Table VIII (see the following section).

Nitrous Acid Photolysis

Nitrous acid has been chosen as the most convenient source of HO radicals to be employed in the various phases of this work which are planned. As a consequence we have photolyzed HONO mixtures in an attempt to establish the first-order rate constant for reaction 30 in our photochemical system;

$$HONO + h\nu \rightleftarrows HO + NO \qquad (30)$$

Mixtures of HONO (and necessary small impurity levels of NO_2, NO, and H_2O introduced in the HONO preparation) with varied amounts of CO in N_2 at 700 Torr were photolyzed to determine k_{30}. The results for four experiments at different CO levels are shown in Figs. 24-27. The characteristic frequencies and the absorption coefficients determined for the various reactants and products are summarized in Table IX. (Here base e lagarithms are employed in defining the absorption coefficients.) The experimentally measured points of nitrous acid loss and carbon dioxide formation can be observed from these data. The solid lines drawn represent the computer-simulated rates of HONO loss and CO_2 formation using $k_{30} = 0.070\ min^{-1}$ and the reaction scheme (12) - (30) together with the following additional reactions which are required for this more complicated system:

$$HO + NO + M \rightarrow HONO + M \qquad (31)$$

$$HO + NO_2 + M \rightarrow HONO_2 + M \qquad (32)$$

$$HO + HONO \rightarrow H_2O + NO_2 \qquad (33)$$

$$HO + CO \rightarrow H + CO_2 \qquad (34)$$

$$H + O_2 + M \rightarrow HO_2 + M \qquad (35)$$

$$HO_2 + NO \rightarrow HO + NO_2 \qquad (36)$$

$$HO_2 + NO_2 \rightarrow HONO + O_2 \qquad (37)$$

$$2HO_2 \rightarrow H_2O_2 + O_2 \qquad (38)$$

TABLE VIII. THEORETICAL ESTIMATES OF FIRST-ORDER DECAY CONSTANTS FOR THE PHOTODECOMPOSITION OF SOME LIGHT-SENSITIVE COMPOUNDS OF INTEREST IN THIS WORK (PHOTOCHEMICAL CHAMBER)

Compound	Reaction	$F_i = \int_{\lambda_1}^{\lambda_2} \epsilon(\lambda)\ \phi(\lambda)\ I^\circ(\lambda) d\lambda$ (arbitrary units)	k (min^{-1})
NO_2	$NO_2 + h\nu \rightarrow O + NO$	51693	0.51
HONO	$HONO + h\nu \rightarrow HO + NO$	3418	0.034
$(CH_3)_2N_2$	$CH_3N_2CH_3 + h\nu \rightarrow 2CH_3 + N_2$	897	0.0088
CH_2O	$CH_2O + h\nu \rightarrow H + CHO$	111.9	0.0011
CH_2O	$CH_2O + h\nu \rightarrow H_2 + CO$	290.9	0.0029
CH_3ONO	$CH_3ONO + h\nu \rightarrow CH_3O + NO$	8007	0.079
H_2O_2	$H_2O_2 + h\nu \rightarrow 2HO$	86.7	0.00086

TABLE IX. ABSORPTION COEFFICIENTS DETERMINED IN THIS WORK (PRESSURE N_2 700 TORR; TEMPERATURE, 23 ± 2°; RESOLUTION, 1 CM^{-1}

Compound	Peak Location (cm^{-1})	Absorption Coefficient ($ppm^{-1}\ m^{-1}$)
CO_2	720	1.70×10^{-4}
NO	1876	2.74×10^{-4}
NO_2	826	3.40×10^{-5}
HONO(cis)	853	6.07×10^{-3}
HONO(trans)	1264	3.84×10^{-3}

TABLE X. INITIAL CONCENTRATIONS OF THE HONO PHOTOLYSIS EXPERIMENTS

Initial Concentration (ppm)

[CO]	[HONO]	[NO]	[NO_2]	[O_2]*	[N_2]
520	3.26	7.11	10.78	300	9.21×10^5
1039	3.02	2.32	5.63	300	9.21×10^5
1559	1.81	4.43	6.68	225	9.21×10^5
2078	3.70	2.45	4.18	700	9.21×10^5

*estimated

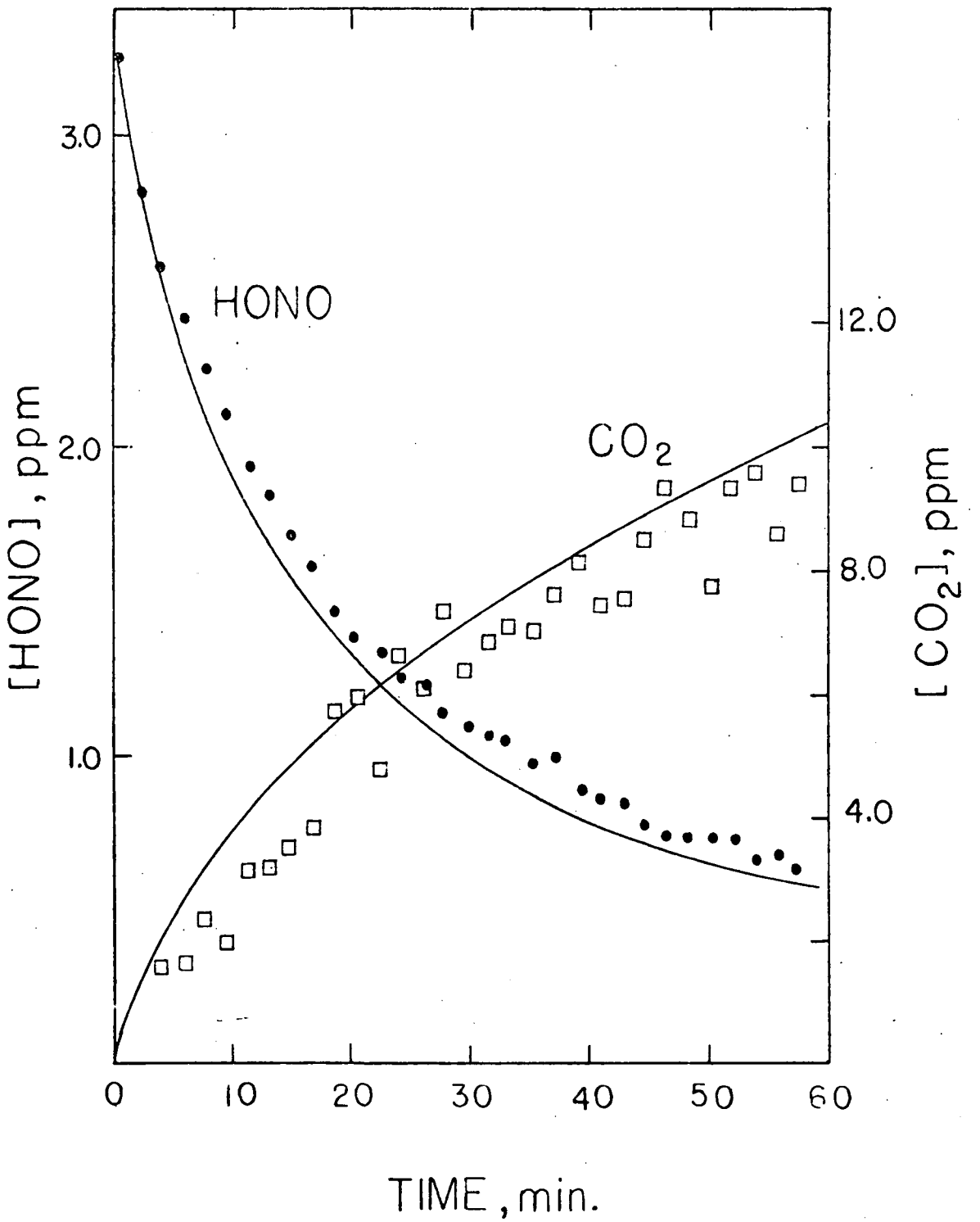

Figure 24. The time dependence of [HONO] and [CO_2] in the photolysis of an HONO-NO_x-CO mixture; $[CO]_o$ = 520 ppm and other reactants are given in Table X

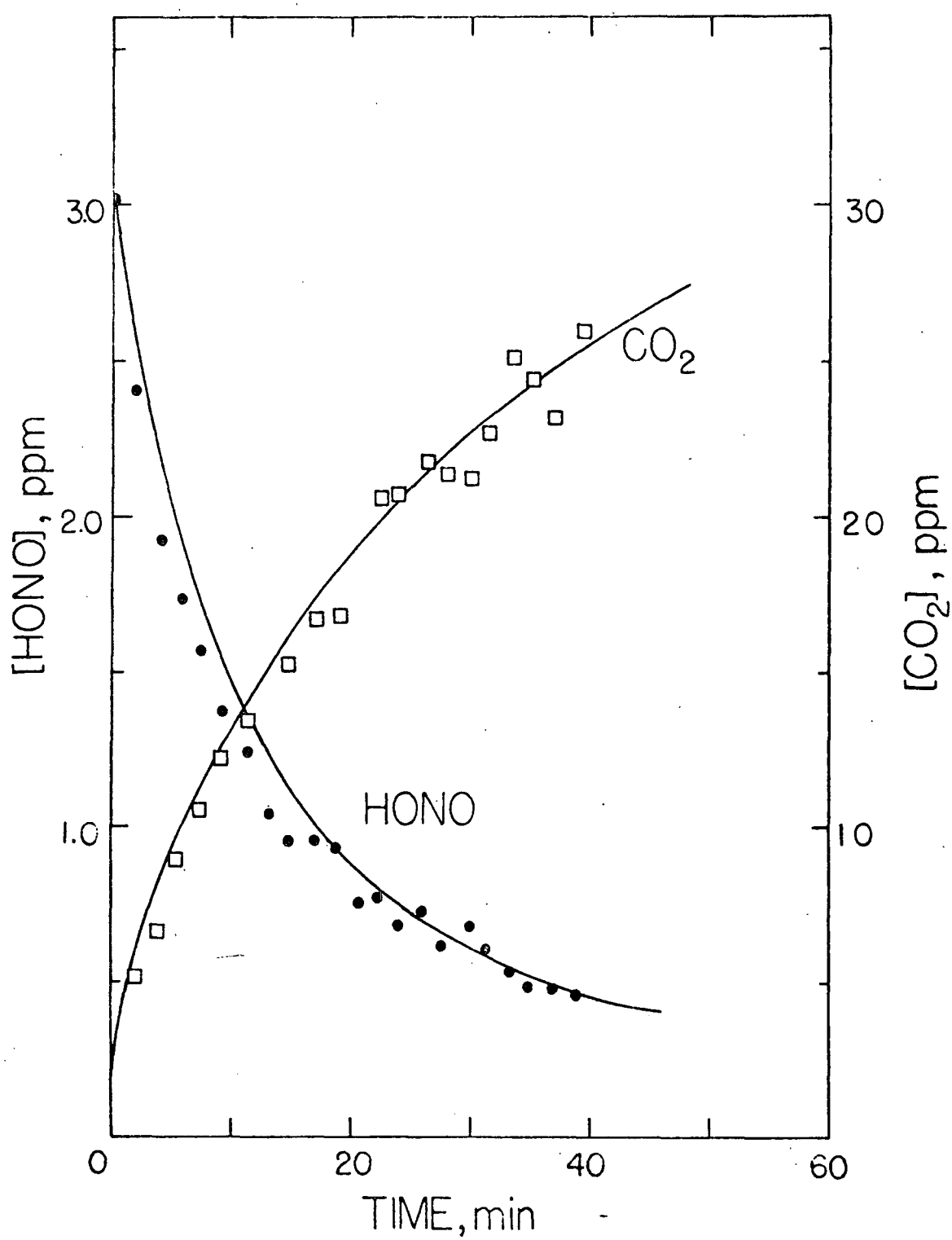

Figure 25. The time dependence of [HONO] and $[CO_2]$ in the photolysis of an HONO-NO_x-CO mixture; $[CO]_o$ = 1039 ppm and other reactants are given in Table X

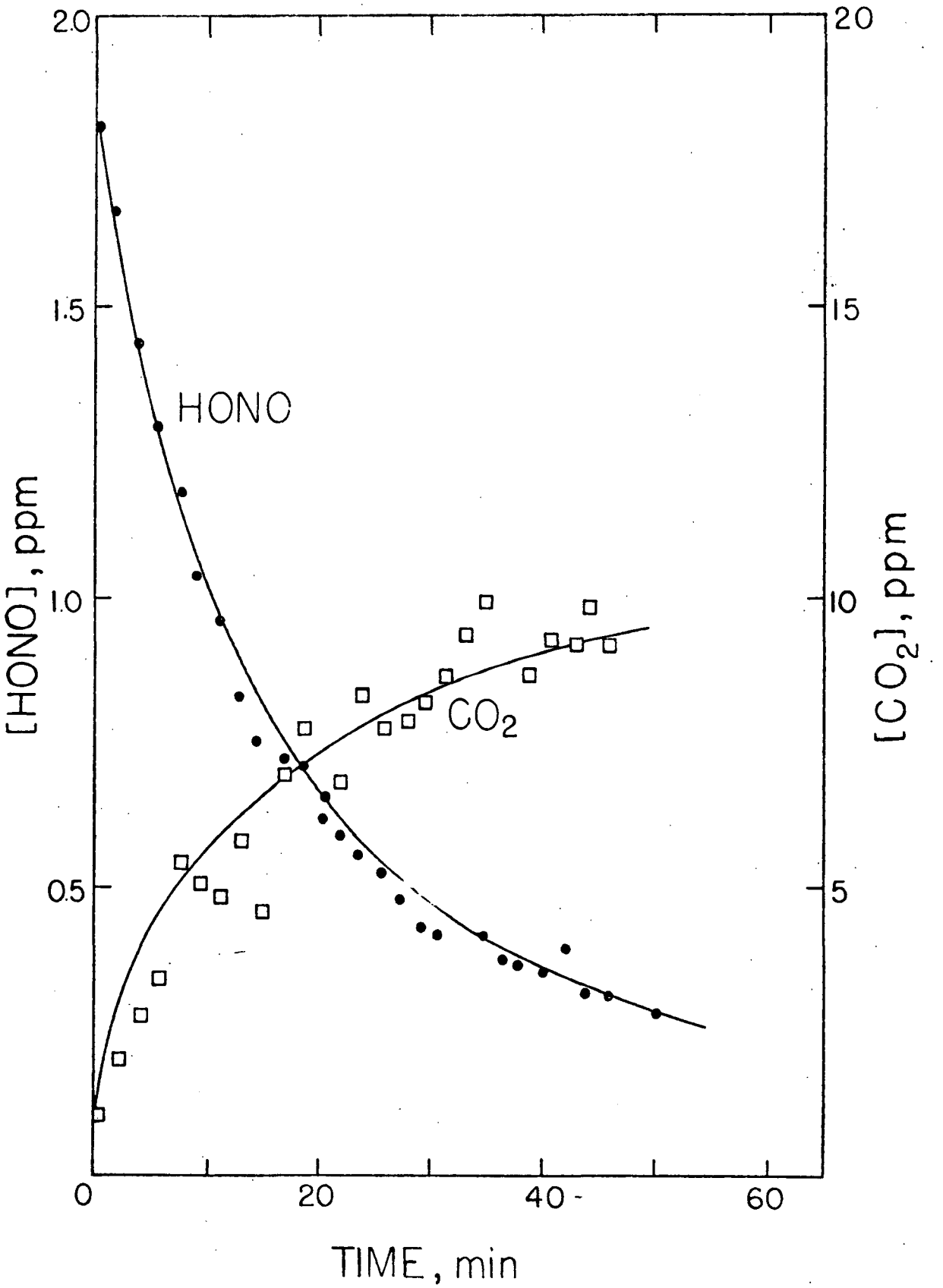

Figure 26. The time dependence of [HONO] and $[CO_2]$ in the photolysis of an HONO-NO_x-CO mixture; $[CO]_o$ = 1559 ppm and other reactants are given in Table X

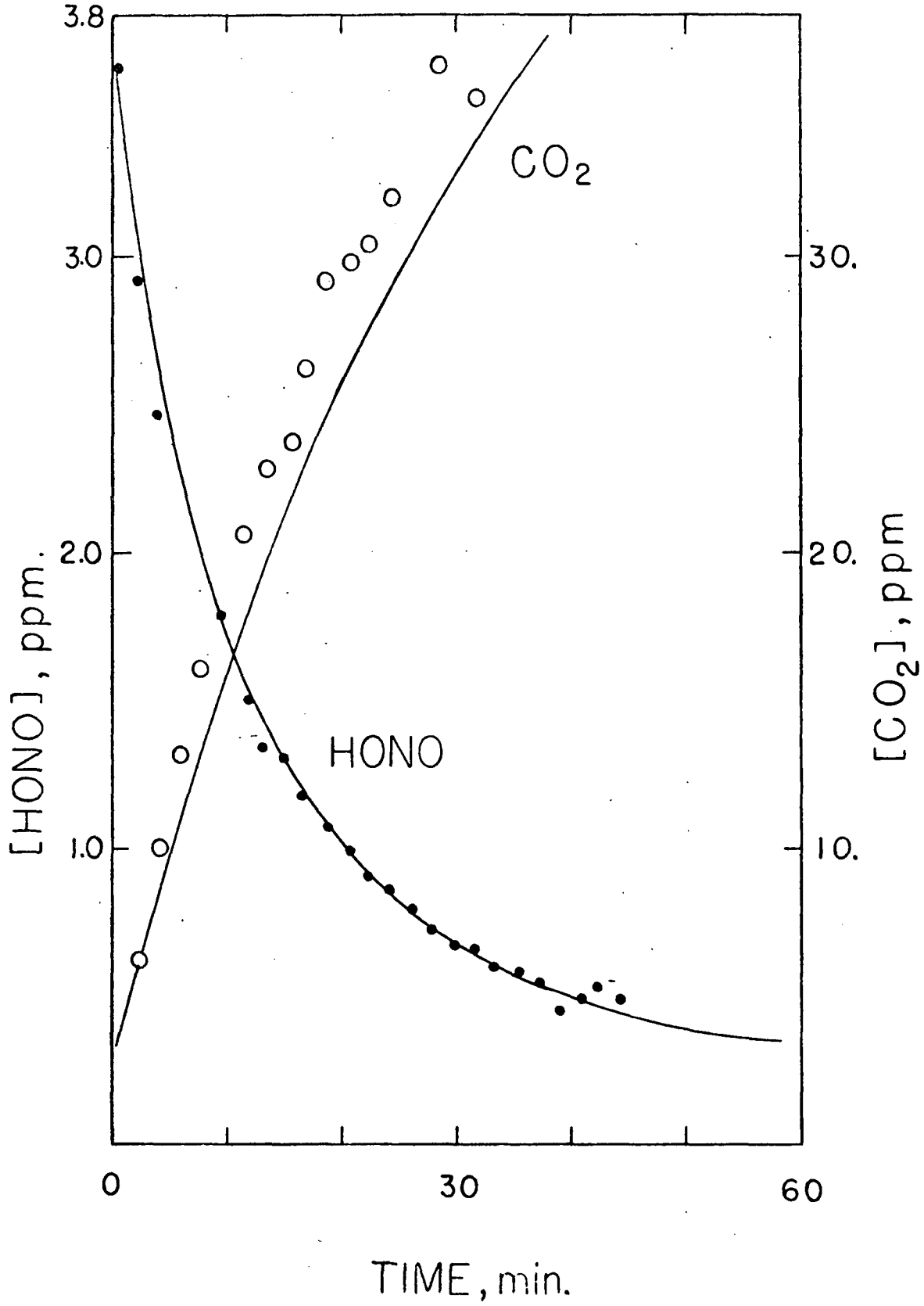

Figure 27. The time dependence of [HONO] and $[CO_2]$ in the photolysis of an HONO-NO_x-H_2O mixture; $[CO]_o$ = 2078 ppm and other reactants are given in Table X

$$H + CO + M \rightarrow HCO + M \quad (39)$$

$$HONO + O \rightarrow HO + NO_2 \quad (40)$$

$$H_2O_2 + h\nu \rightarrow 2HO \quad (41)$$

$$HCO + O_2 \rightarrow HO_2 + CO \quad (42)$$

$$H + NO + M \rightarrow HNO + M \quad (43)$$

$$HNO + O_2 \rightarrow HO_2 + NO \quad (44)$$

$$H + NO_2 \rightarrow HO + NO_2 \quad (45)$$

$$HNO + h\nu \rightarrow H + NO \quad (46)$$

$$O + CO + M \rightarrow CO_2 + M \quad (47)$$

$$O + NO + M \rightarrow NO_2 + M \quad (48)$$

$$HNO + HNO \rightarrow N_2O + H_2O \quad (49)$$

$$HCO + O_2 + M \rightarrow HCOO_2 + M \quad (50)$$

$$HCOO_2 + NO \rightarrow HCO_2 + NO_2 \quad (51)$$

$$HCO_2 + O_2 \rightarrow HO_2 + CO_2 \quad (52)$$

$$HCO_2 \rightarrow H + CO_2 \quad (53)$$

$$H + HONO \rightarrow H_2 + NO_2 \quad (54)$$

It can be seen from the data of Figs. 24-27 that the rate of CO_2 formation in these systems is much greater than the primary rate of HO formation from HONO decay. It became evident to us that small amounts of O_2 are inadvertently added in preparing the mixtures for photolysis and reactions of H-atoms formed in (34) with O_2, NO, NO_2, and CO must occur to generate ultimately more HO radicals through (36), (45), and the other reactions shown. The amount of O_2 assumed to be present affected the R_{CO_2} estimated rather strongly, while it had little effect in the HONO decomposition reaction rate for (30). By curve matching of the CO_2 formed we could estimate the amount of impurity O_2 present at the start of each run. These data are summarized in Table X which also gives the initial concentration measured for each of the other reactants.

The value of k_{30} which was necessary to match the HONO loss rate was not very sensitive to the O_2 level chosen or the fit of the CO_2 rate data. The number which is derived from the best fit of all the data was $k_{30} = 0.070 \pm 0.004$ min^{-1}. It can be seen that this is a factor of two bigger than the value anticipated from the theoretical treatment of the extinction data described earlier and summarized in Table VIII. It is somewhat surprising that the new extinction data for HONO presented by Johnston and Graham[40] show an integrated absorption for HONO which is a factor of two lower than that observed for CH_3ONO, the next

higher homolog in the series. It is possible that the absolute value of the extinctions for HONO are in error by a factor of two. Note our measured k_{30} is about equal to that expected for CH_3ONO photolysis (see Table VIII). In any case our experimental estimate of k_{30} is considered reliable for our conditions and will be employed in several phases of our studies of the following years.

Preliminary Photochemical Studies of Special Interest in The Formulation of Smog Mechanisms

The photodecomposition of CH_2O-air mixtures, CH_2O-HONO-NO-NO_2-air mixtures, $(CH_3)_2N_2$-NO-NO_2-air mixtures $[(CH_3)_3O)_2N_2$-NO-NO_2-air mixtures, and HONO, H_2O_2, NO-air mixtures were carried out to test the feasibility of several experiments which are planned in this continuing study. In those cases we searched the products for evidence of metastable transients, peroxyformylnitrate, $CH_3O_2NO_2$, $(CH_3)_3CO_2NO_2$, and HO_2NO_2 which are postulated as possible products of the reactions of NO_2 with $HCOO_2$, CH_3O_2, $(CH_3)_3CO_2$, and HO_2 radicals (see Ref. 38). Transient absorptions which may correspond to some of those species have been seen to decay in the dark, but the conclusions which can be formed concerning the nature of these species remains uncertain now. Further analysis of those spectra through peak ratioing and subtraction of known compound spectra are in progress.

LIBRARY OF SPECTRA

One of the objectives of this program has been the collection of a library of spectra of molecules of importance in atmospheric processes. Although spectra of most of the gases investigated have been reported elsewhere the results have been of limited value to this investigation because the spectral resolution is usually less than employed here and because quantitative information concerning the physical conditions of the sample were not given. We have attempted to collect spectra which can be used to give quantitative estimates of the amount of gas in other samples. Most of the spectra reported here were obtained with a spectral resolution of 1.0 cm^{-1}, since this has proved most useful in the photochemical studies. We plan to repeat the measurements at higher resolution when necessary. Two spectra are shown for each gas so that estimates of the growth of features with increasing gas concentration can be obtained. Most of the spectra cover the region from about 700 to 1500 cm^{-1}. The increase in the noise level near 700 cm^{-1} and between 1400 and 1800 cm^{-1} is caused by absorption by residual CO_2 and H_2O in the path.

Some of these spectra have been used to obtain quantitative estimates of the amounts of gas in other mixtures. These estimates were made by measuring the transmittances of particularly sharp features in the spectra. The corresponding absorbance is then plotted against the amount of gas in the path to give a curve of growth.

These curves of growth are dependent on the spectral resolution of the spectra and cannot be used directly by other observers. We have attempted to measure the integrated band absorptance of some features by using the arithmetic package associated with the IFTS system. The integrated band absorption is independent of the spectral resolution but uncertainties in estimating the zero absorptance line and overlapping of other bands was often found to limit the usefulness of this method.

Most of the spectra are for samples pressure broadened with N_2 to 700 Torr. For most infrared bands the integrated band absorptance and the spectral absorptance at a particular frequency both increase as the total pressure increases. Some of the halocarbon spectra appear to show very little pressure broadening. However, care must be taken when using the data presented to estimate the amounts of a given gas in a sample at a temperature or pressure different to that measured. A series of spectra of halogenated methanes has been collected. Fig 28 shows a chart of progressive chlorination and fluorination of methane.

Spectra have been recorded for most of the compounds on this chart and are shown in Figs. 29-39. At the time that these spectra were collected, the gas-handling system was not yet operational and the amount of gas injected into the glass cell was unknown. These spectra are useful as a survey of band positions and relative intensities. Spectral resolution for the chloro-

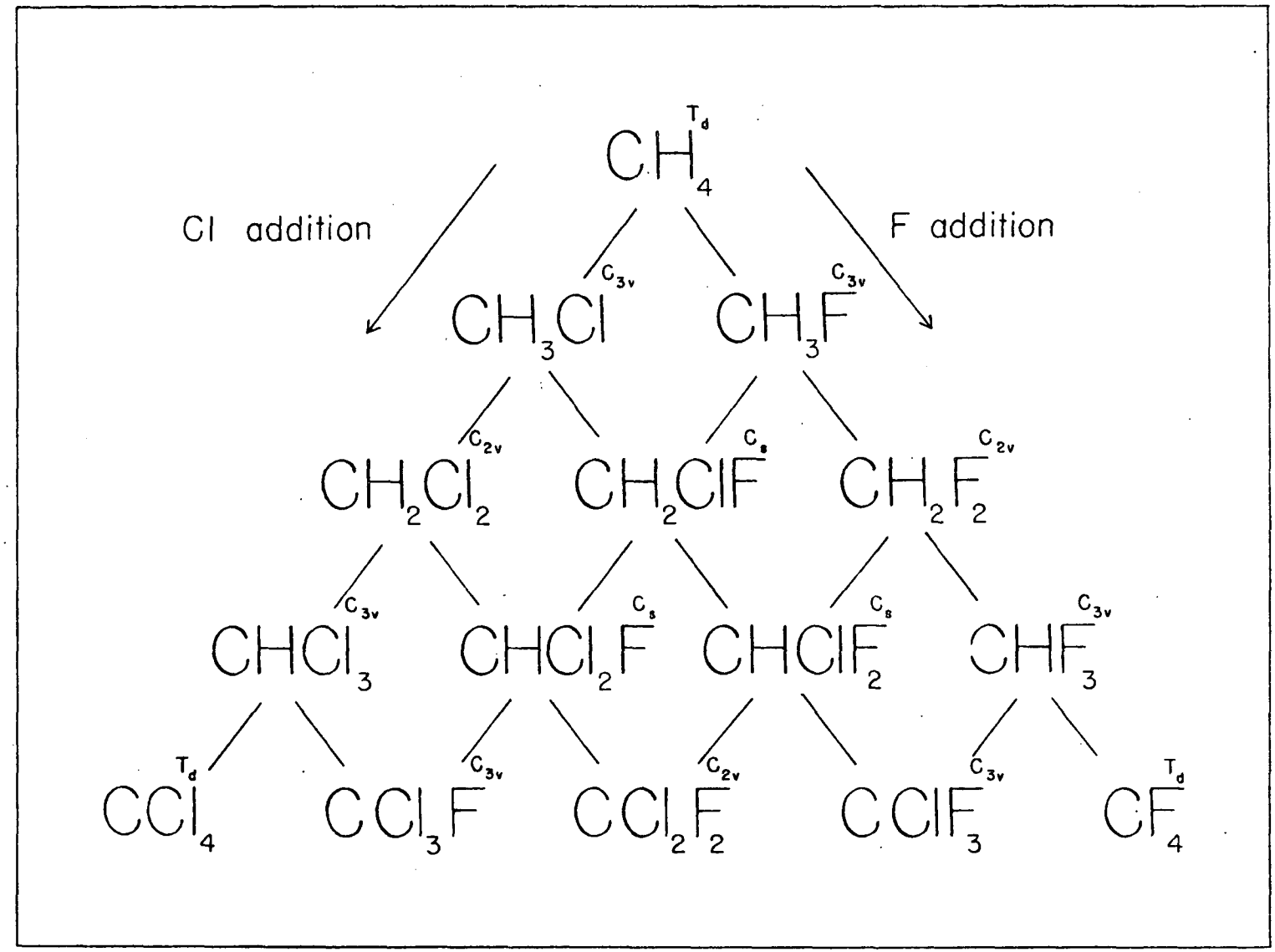

Figure 28. Chart of chlorine and fluorine addition to methane

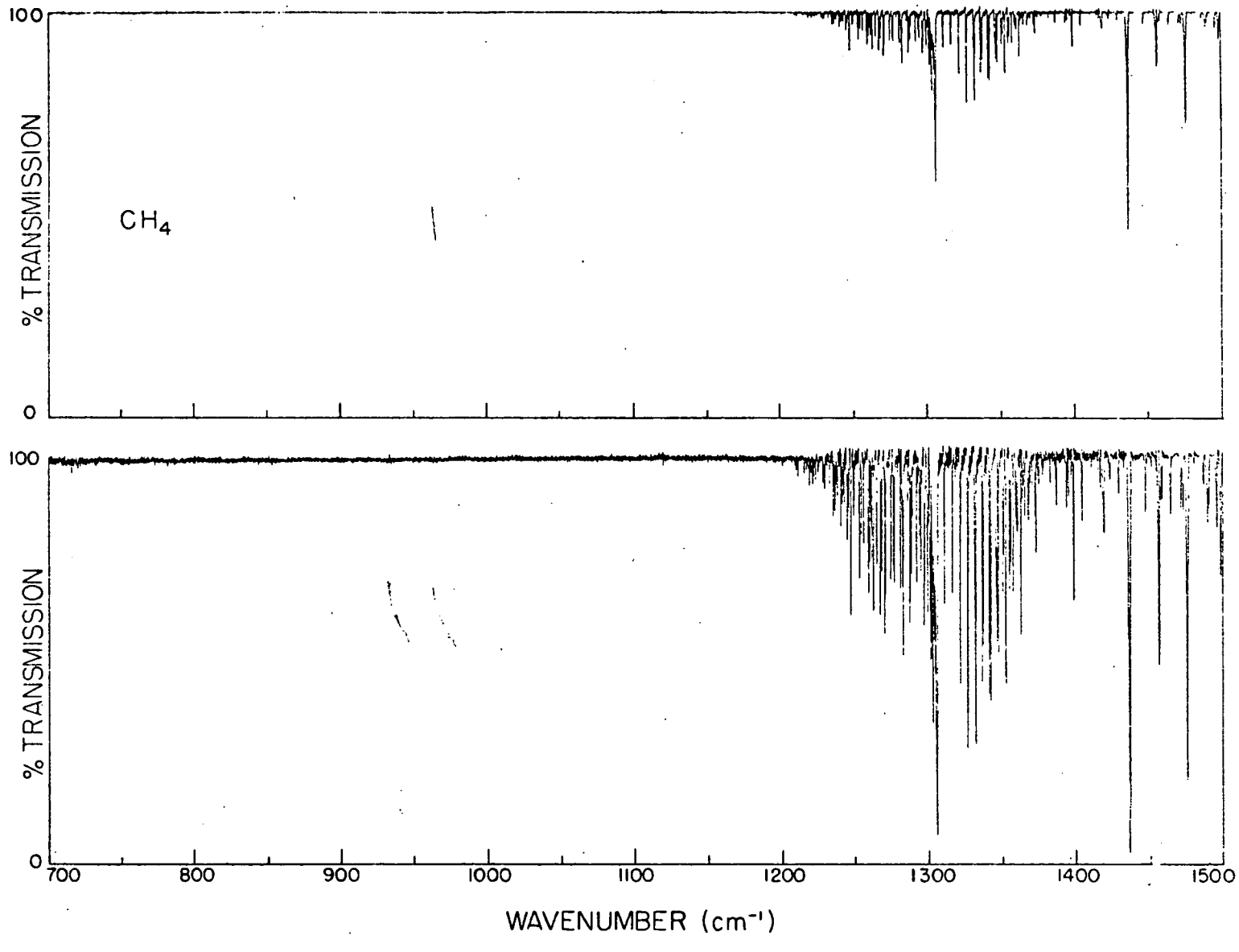

Figure 29. High-resolution spectra of methane

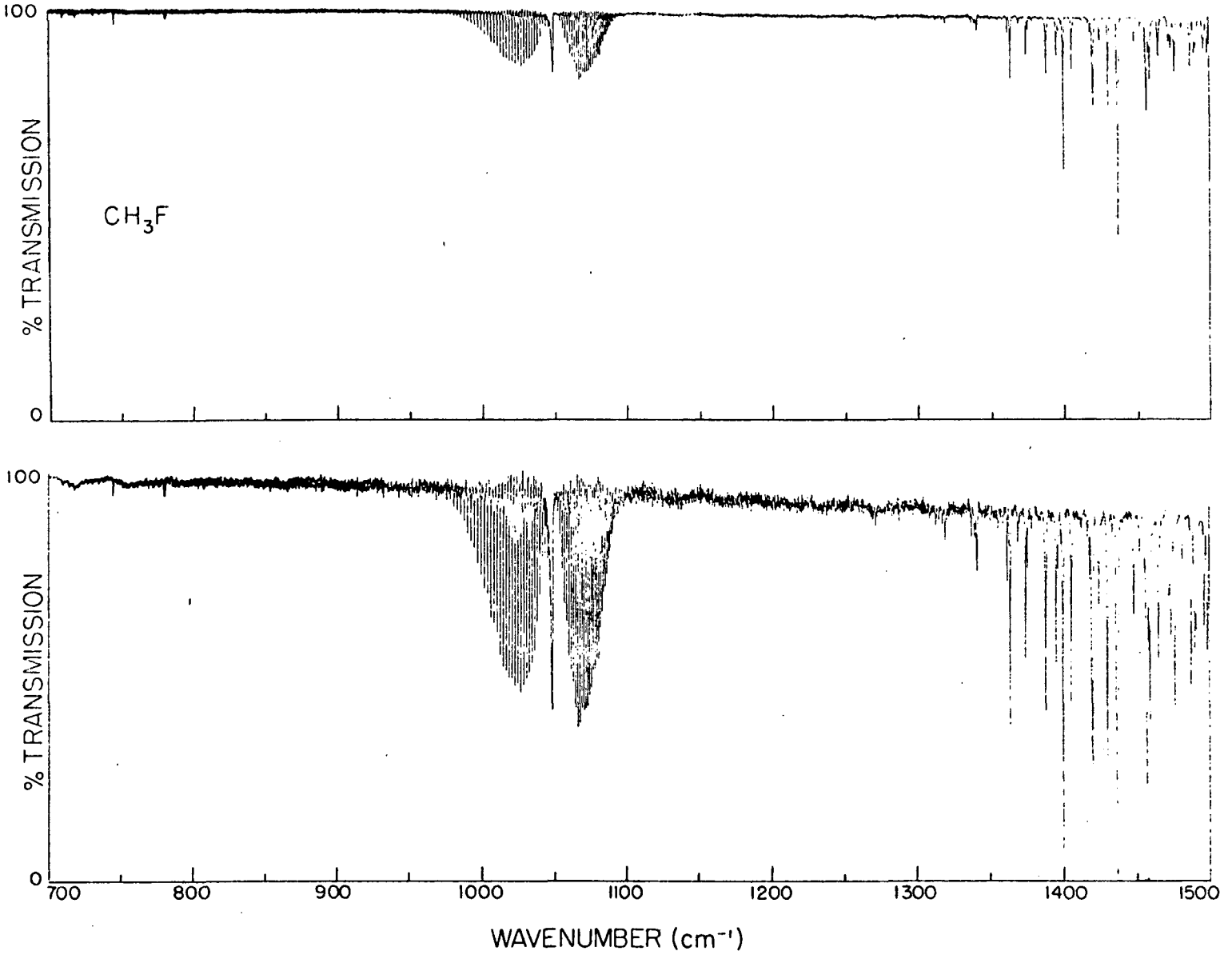

Figure 30. High-resolution spectra of methyl-fluoride

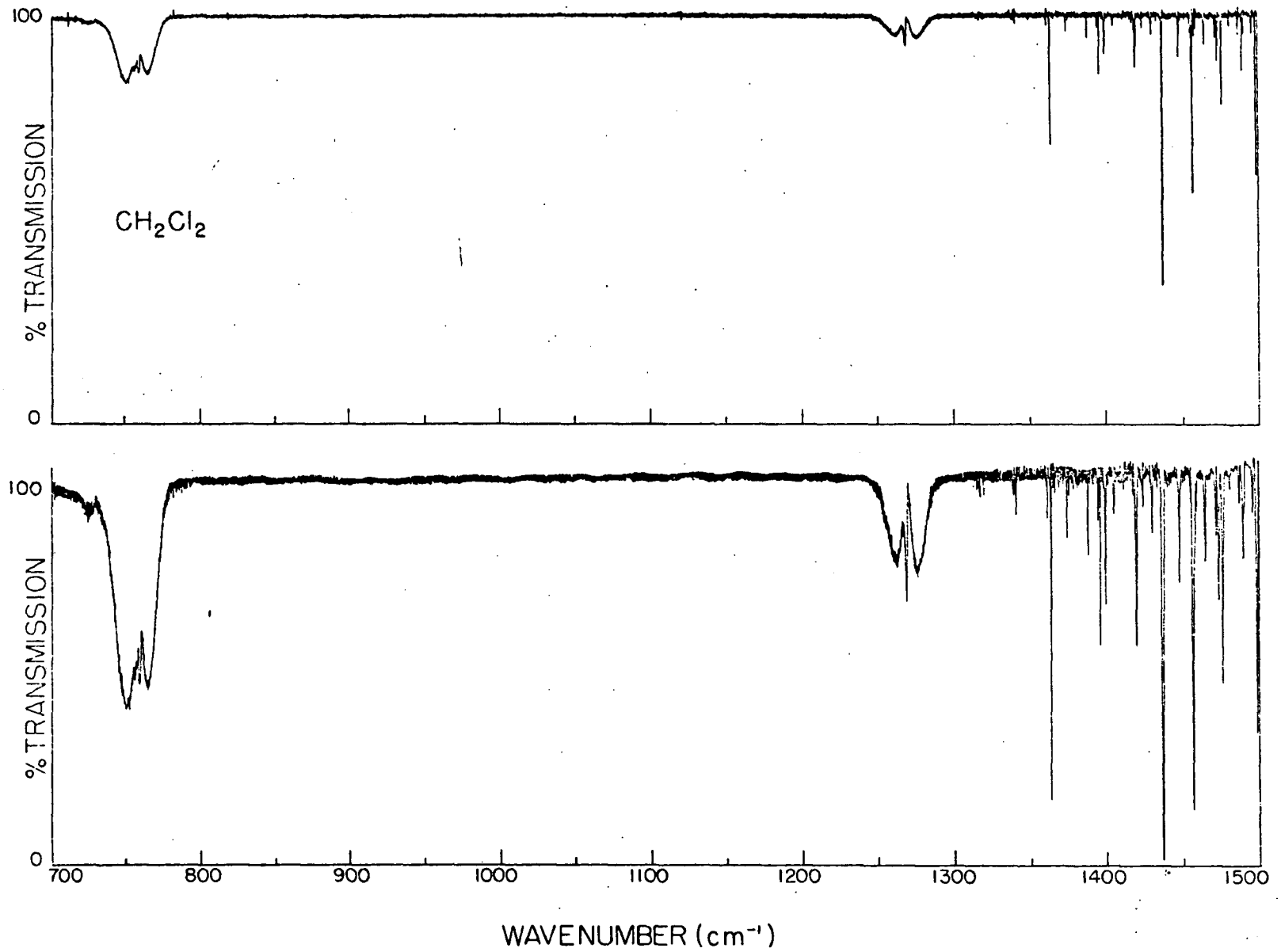

Figure 31. High-resolution spectra of dichloro-methane

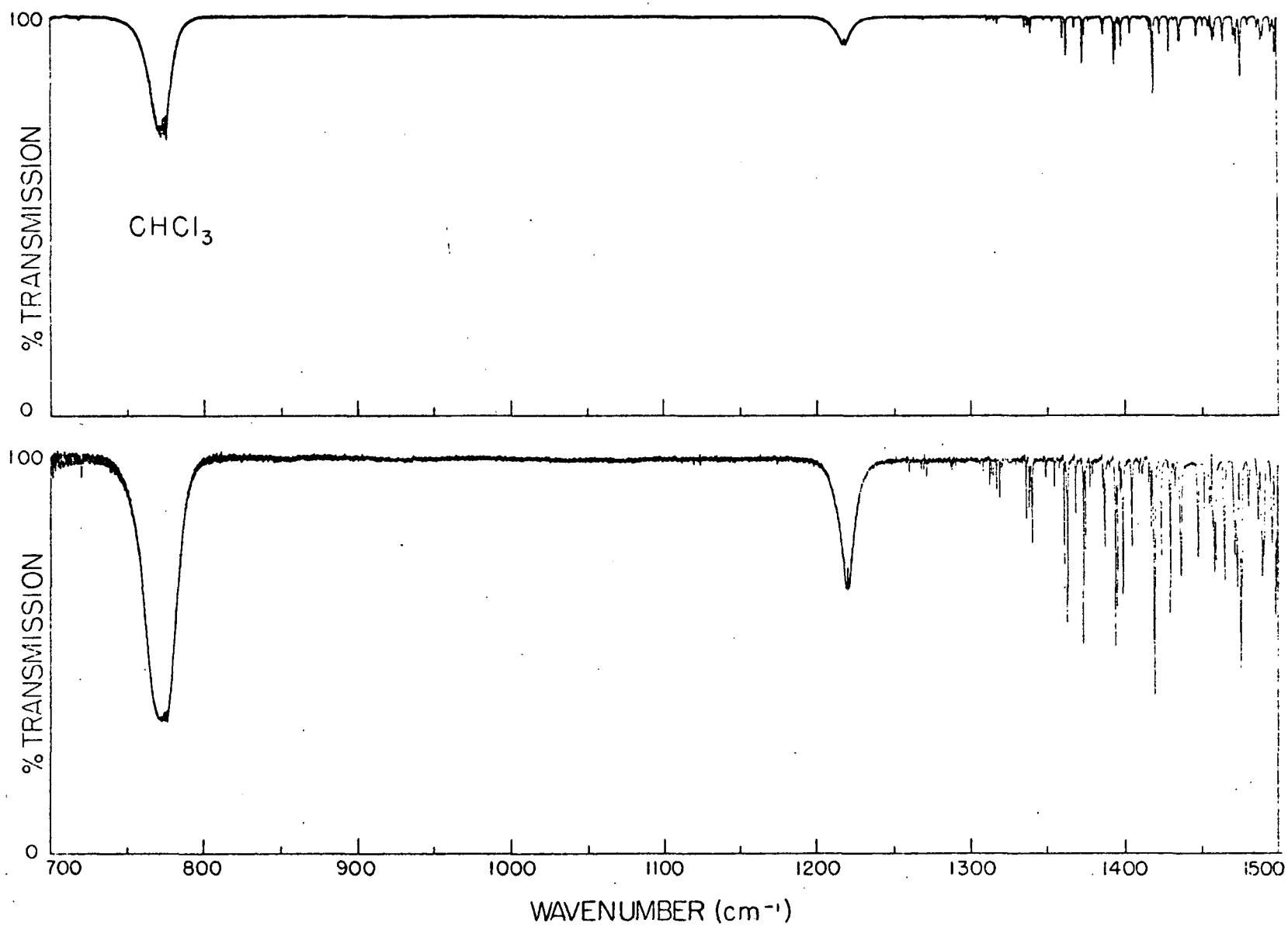

Figure 32. High-resolution spectra of chloroform

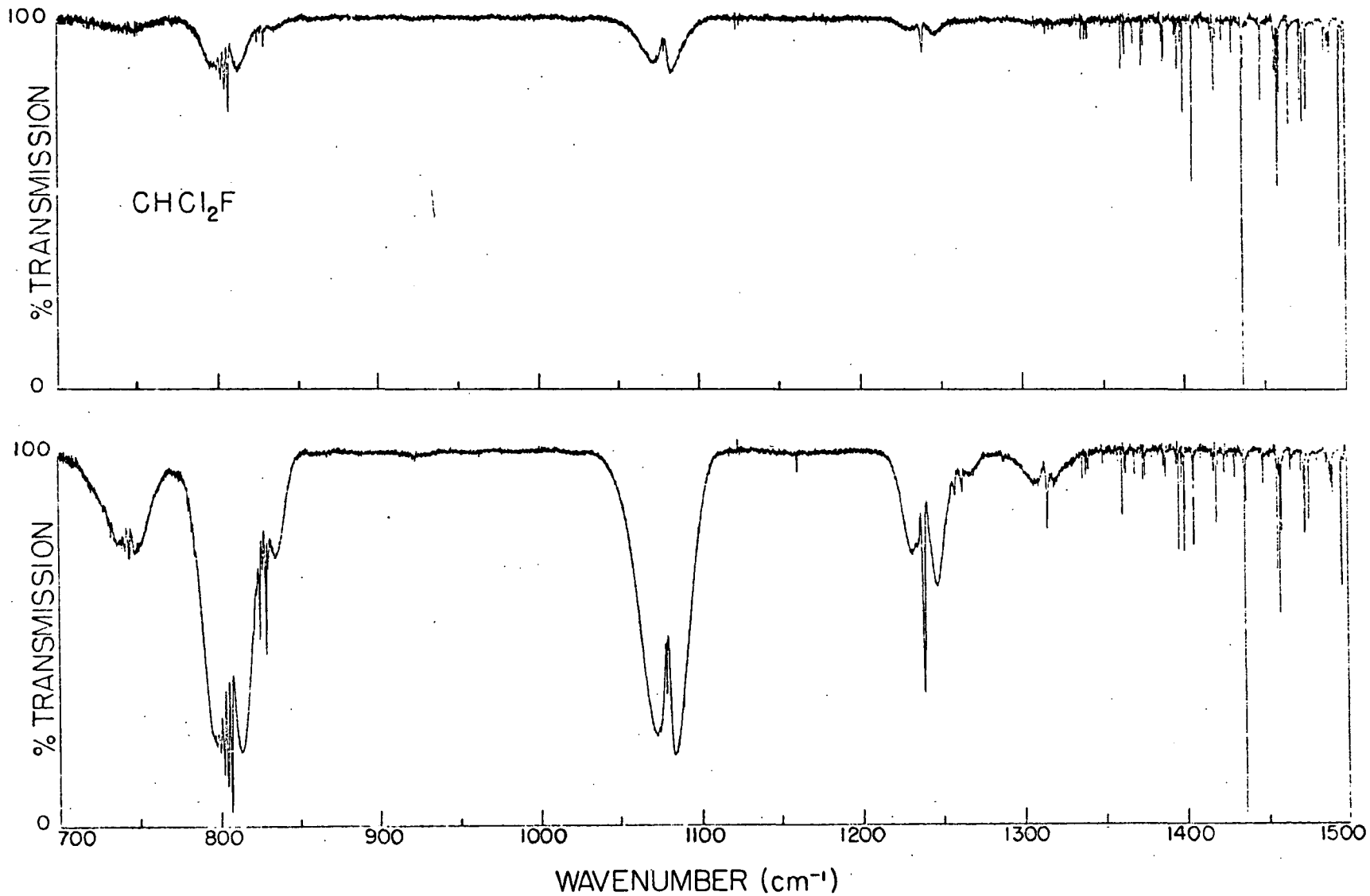

Figure 33. High-resolution spectra of fluorocarbon-21

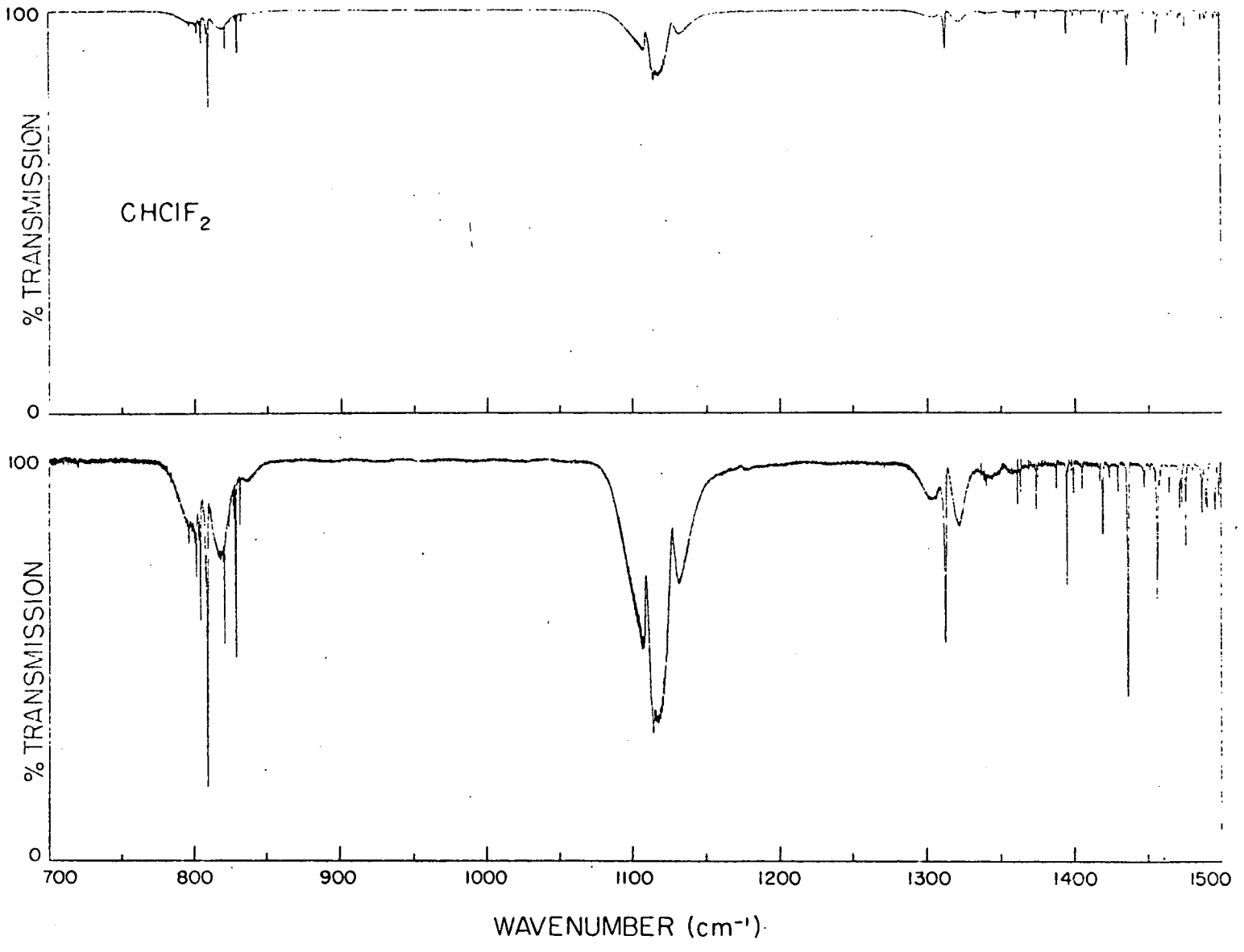

Figure 34. High-resolution spectra of fluorocarbon-22

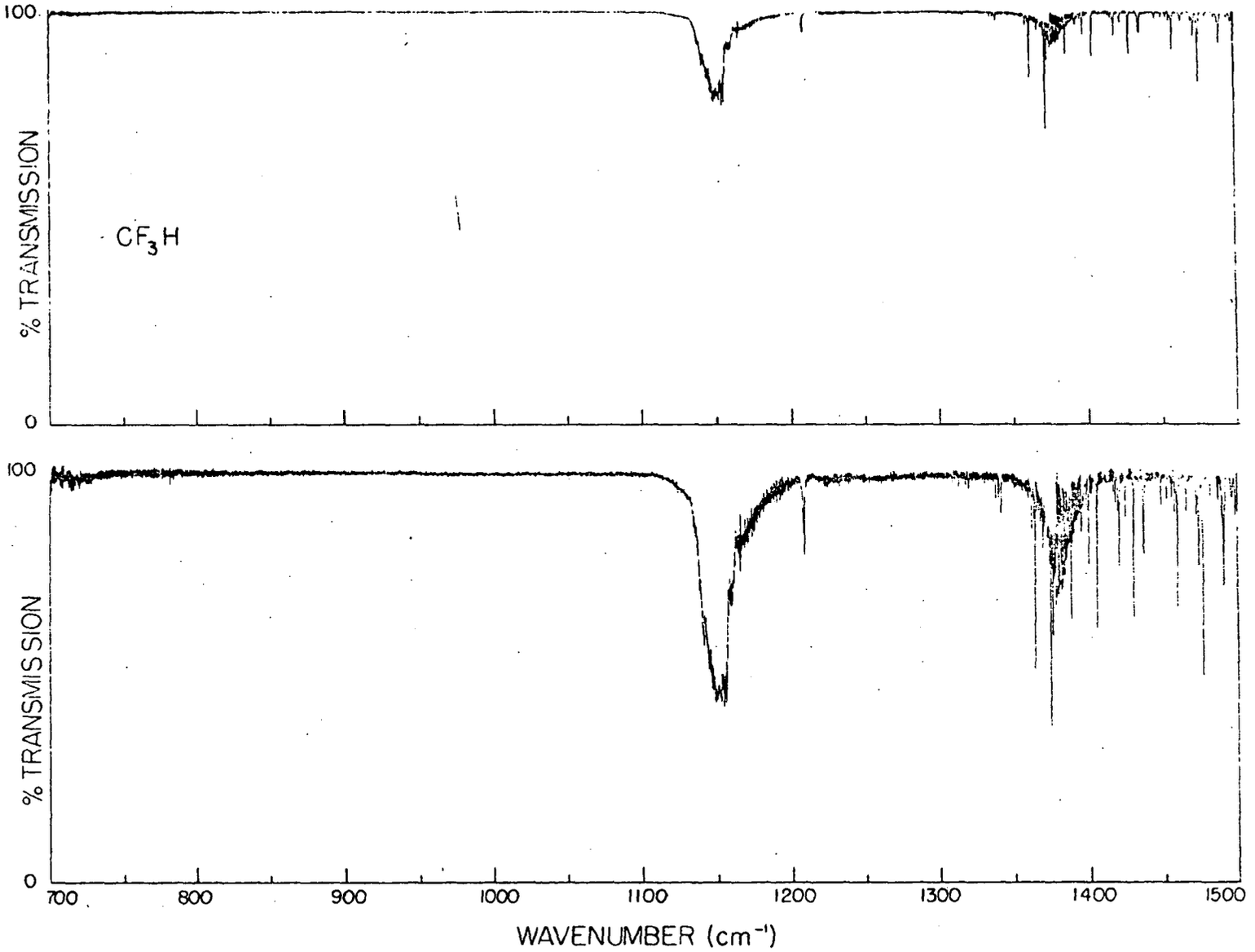

Figure 35. High-resolution spectra of fluoroform

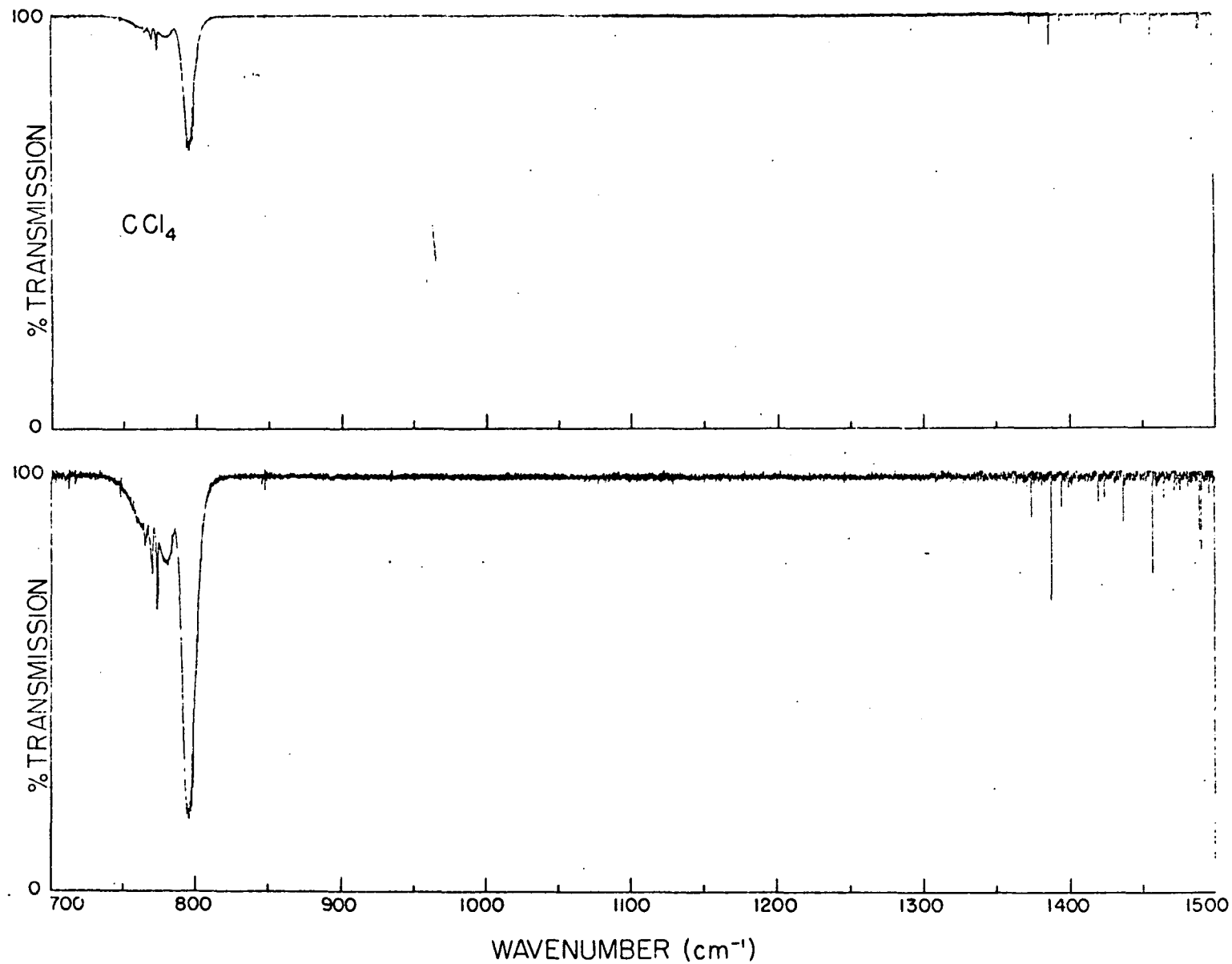

Figure 36. High-resolution spectra of carbon tetrachloride

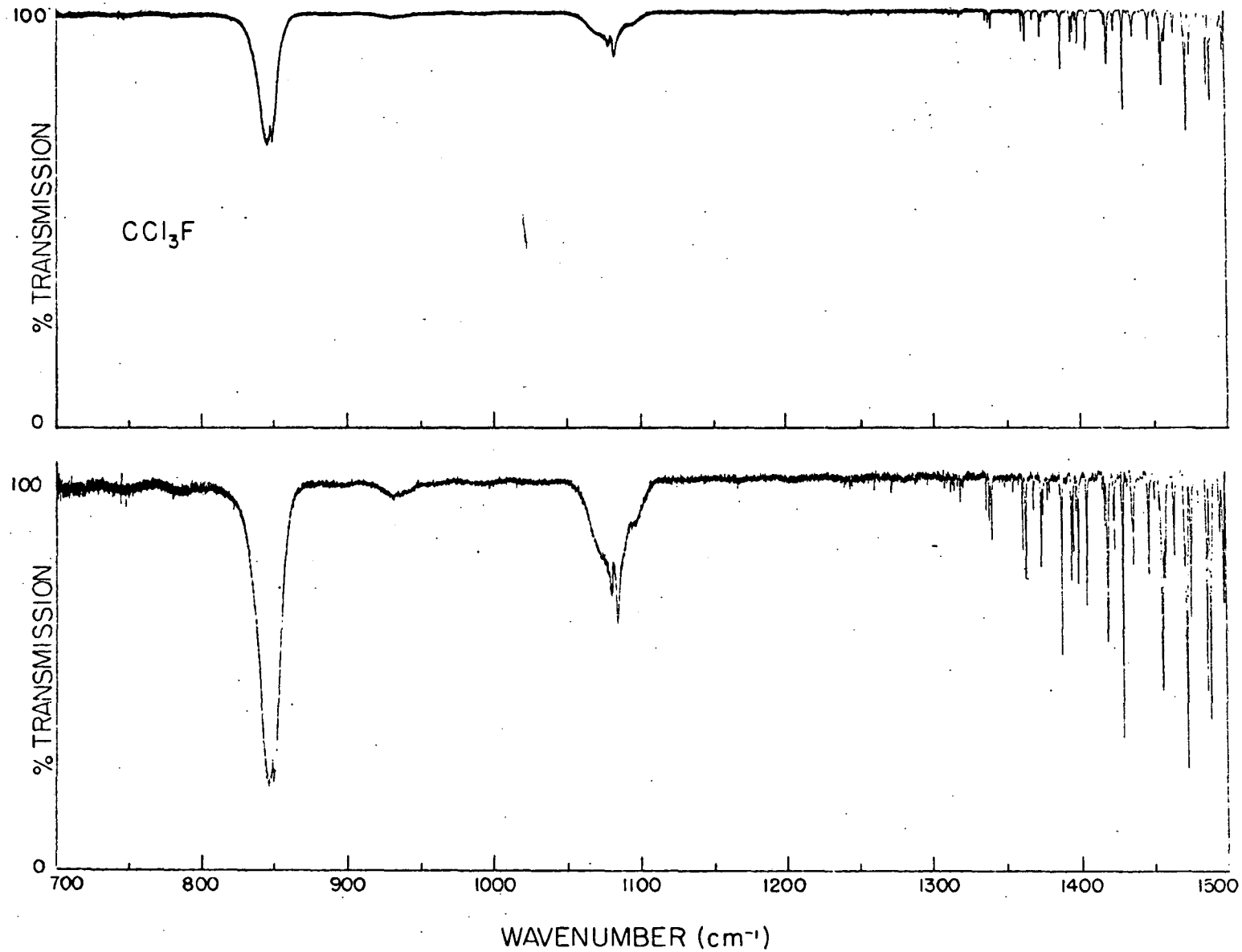

Figure 37. High-resolution spectra of fluorocarbon-11

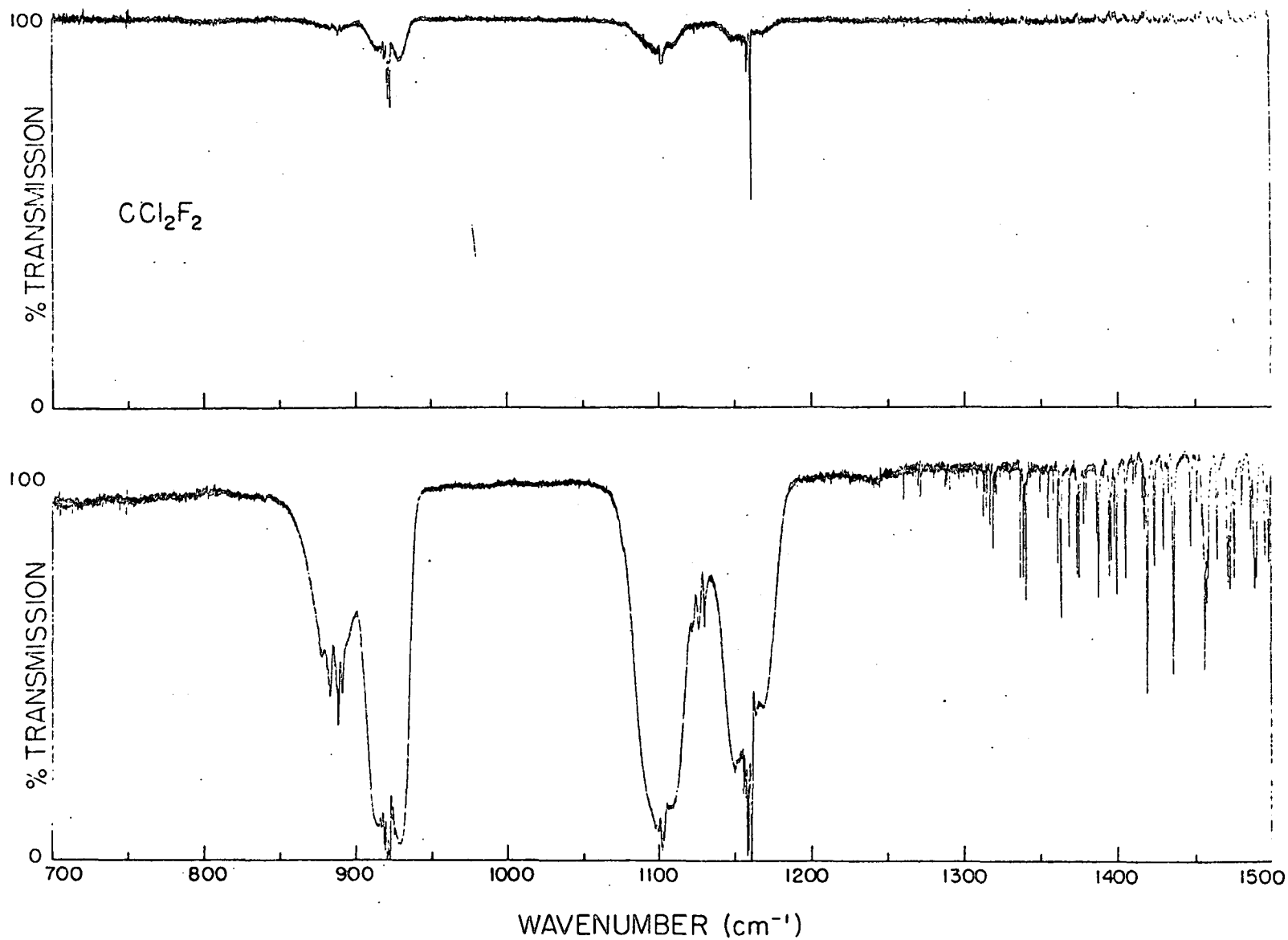

Figure 38. High-resolution spectra of fluorocarbon-12

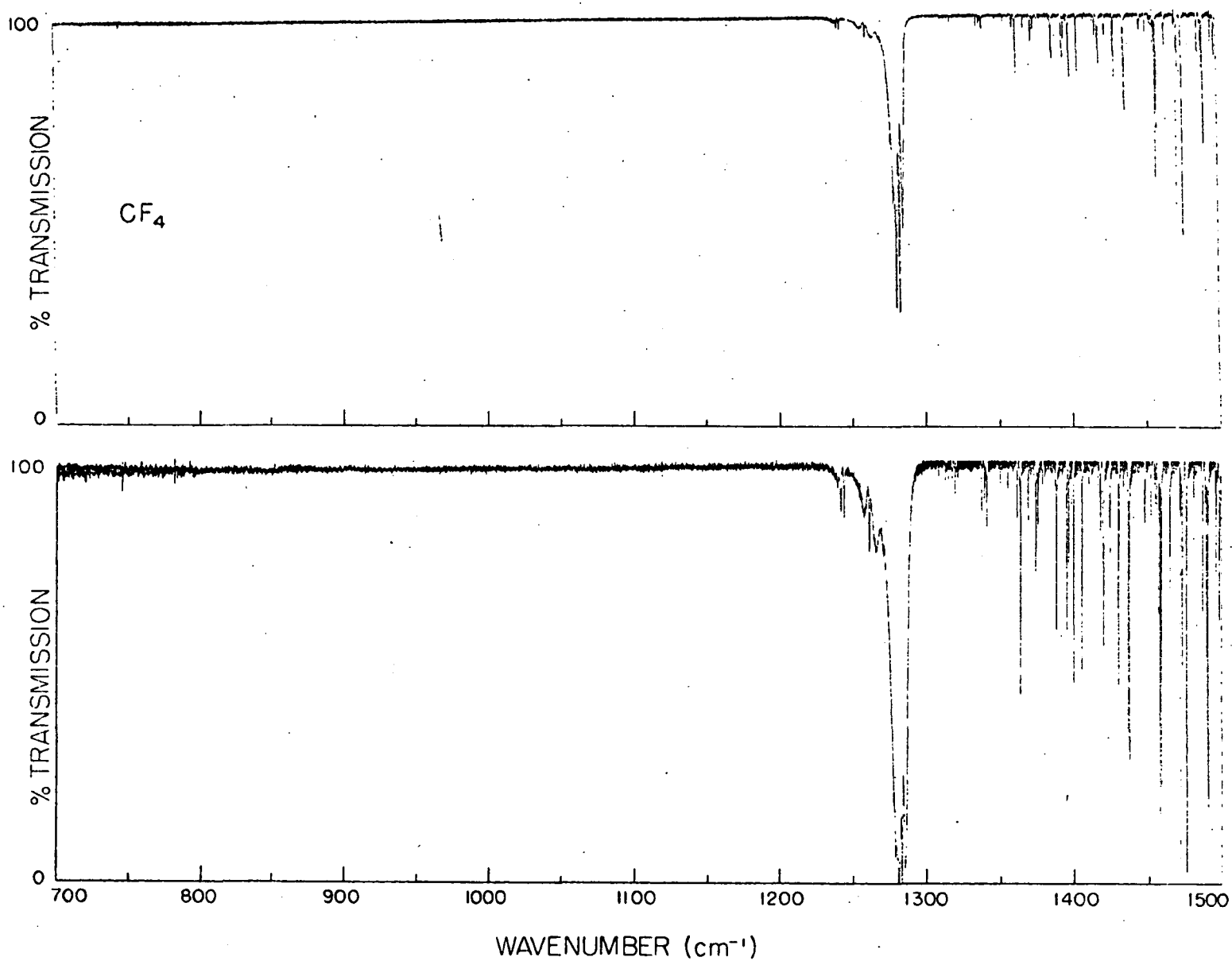

Figure 39. High-resolution spectra of carbon tetrafluoride

fluorocarbons is 0.125 cm^{-1}, and the spectral region extends from 700 cm^{-1} to 1500 cm^{-1} for all spectra.

Figures 40 through 53 show spectra of several compounds of interest in air pollution studies. These spectra were recorded at one wave number resolution over the spectral region from 600 to 3500 cm^{-1}, with the exception of a few compounds; only the region from 700 to 1500 cm^{-1} is shown in this library tabulation.

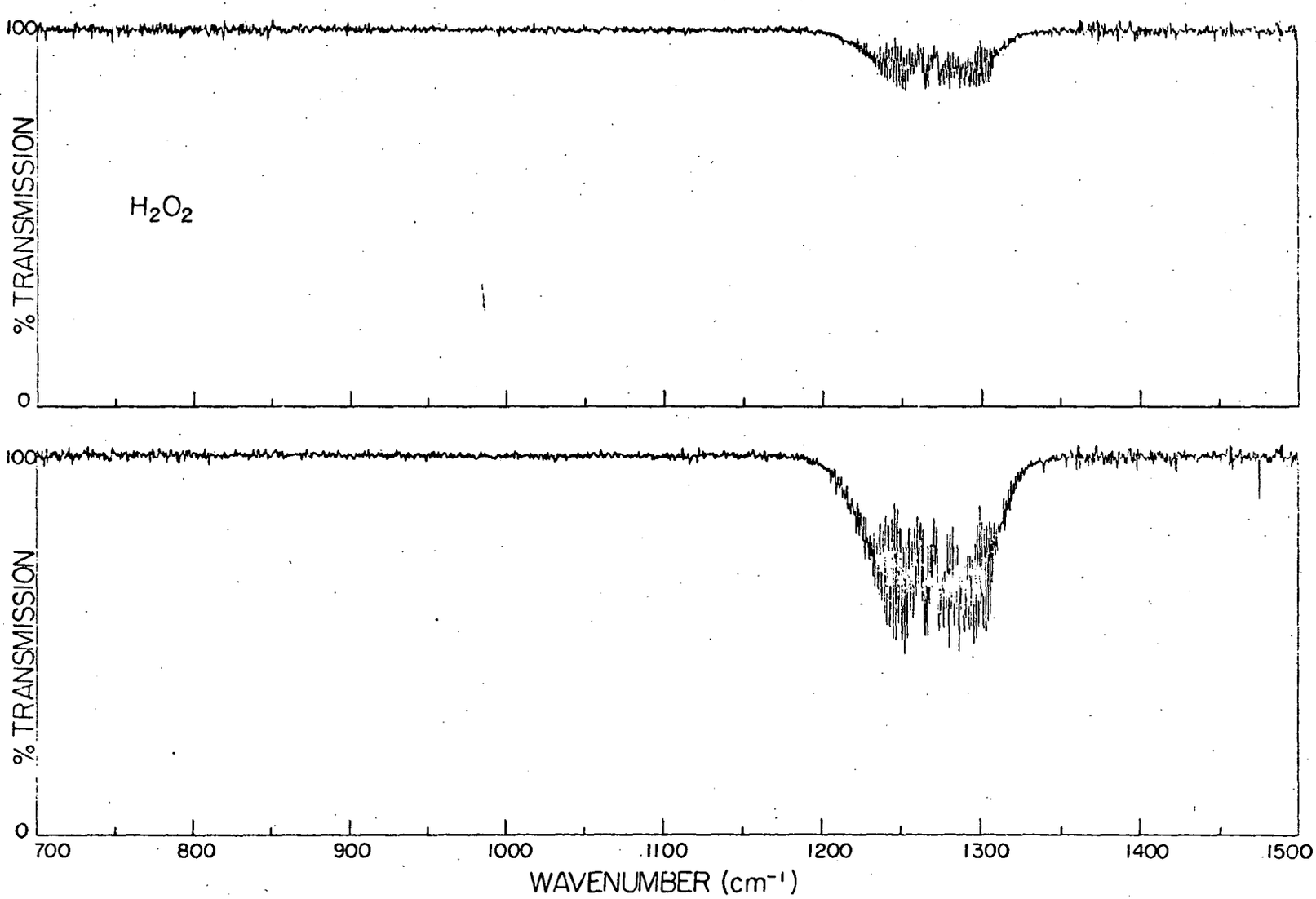

Figure 40. Infrared spectrum of hydrogen peroxide; Resolution = 1 cm^{-1}, top spectrum = 7.4 ppm, bottom spectrum =20.8 ppm, total pressure is less than 20 mm N_2, path length is 170 m

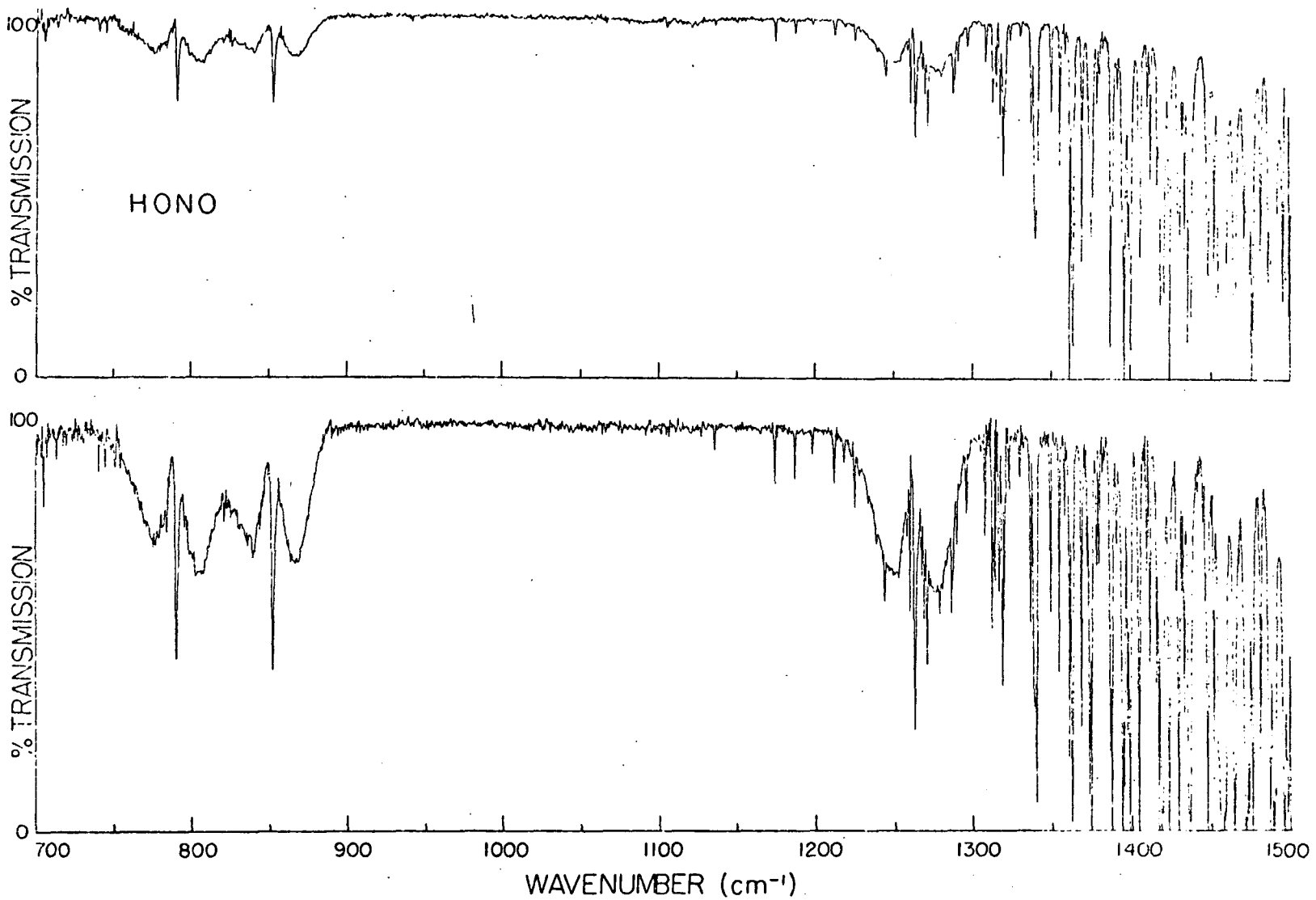

Figure 41. Infrared spectrum of nitrous acid; Resolution = 1 cm^{-1}, top spectrum = 0.9 ppm, bottom spectrum = 3.0 ppm, total pressure is 700 mm N_2, path length is 170 m

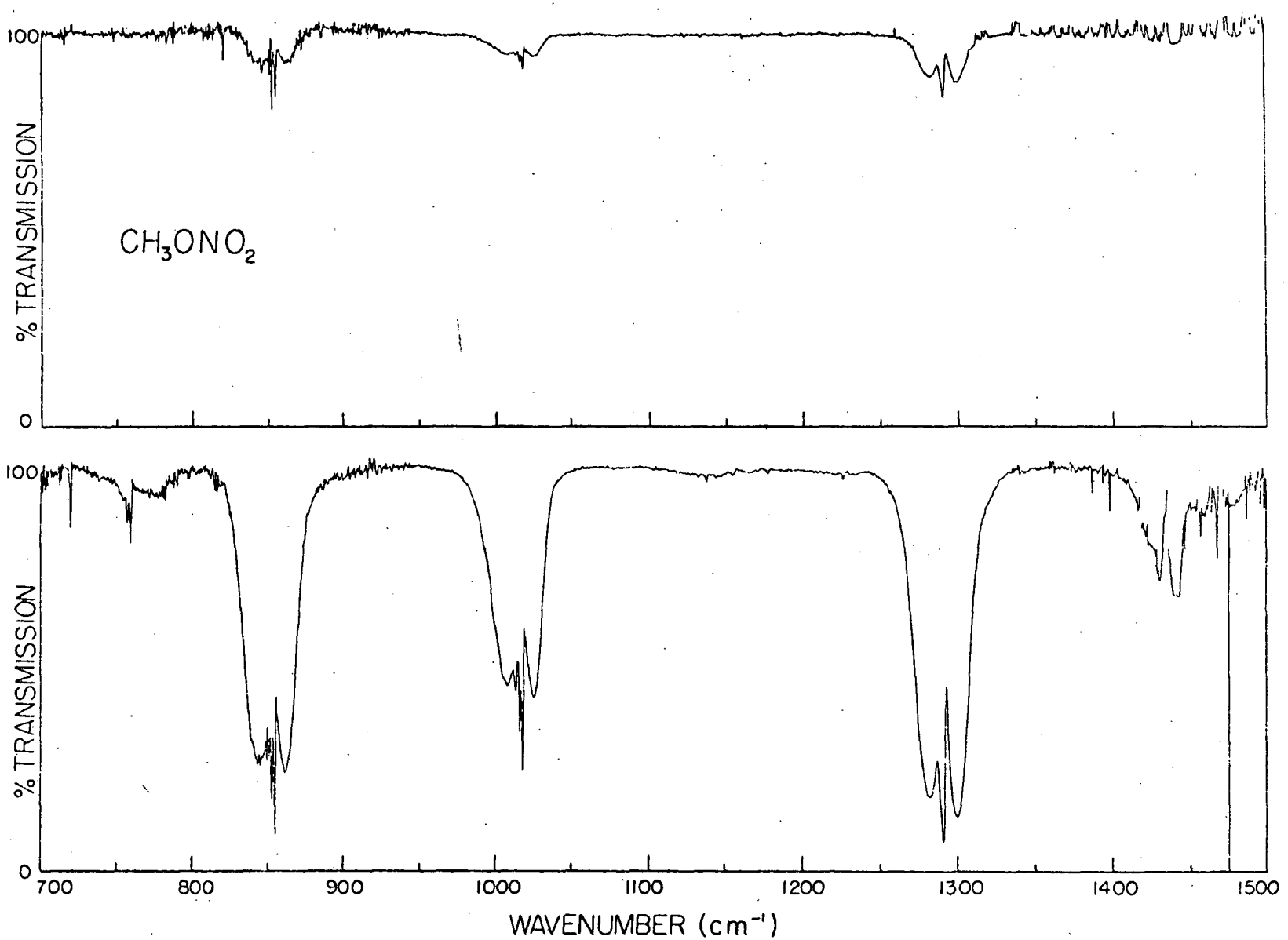

Figure 42. Infrared spectrum of methyl nitrate; Resolution = 1 cm^{-1}, top spectrum = 3.1 ppm, bottom spectrum = 19.0 ppm, total pressure is 700 mm N_2, path length is 85 m

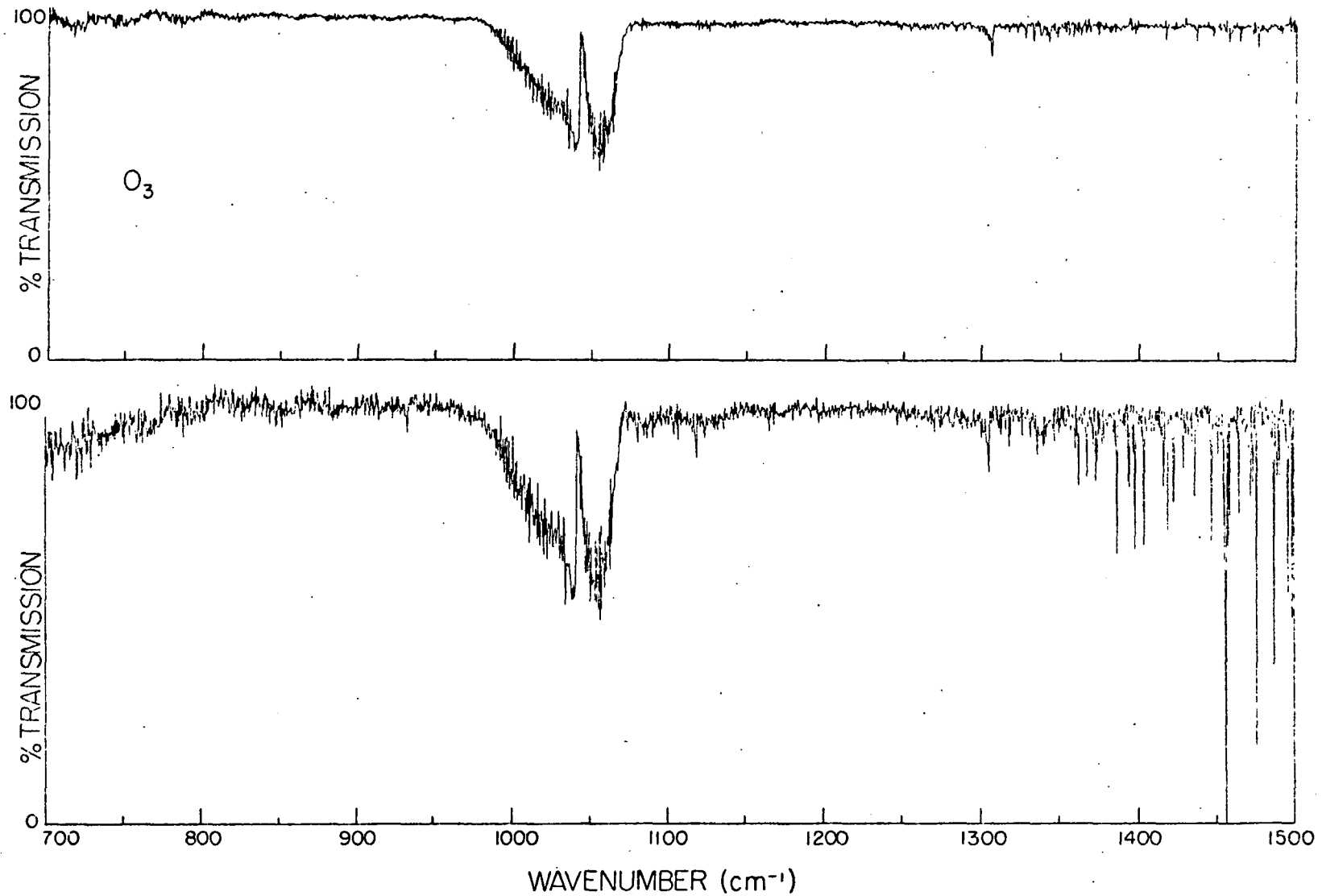

Figure 43. Infrared spectrum of ozone; Resolution = 1 cm^{-1}, concentrations unknown, total pressure is less than 20 mm N_2, path length is 170 m

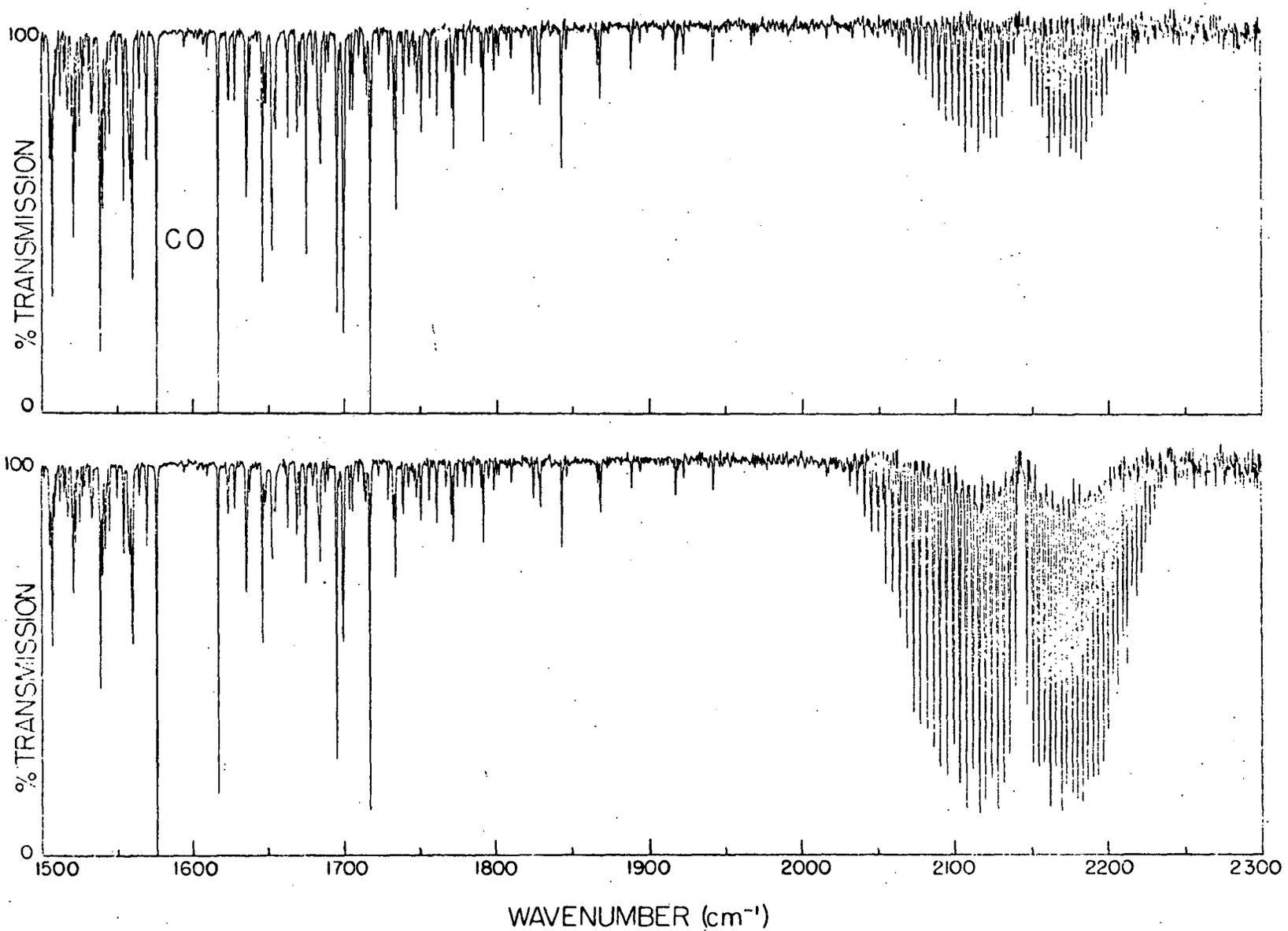

Figure 44. Infrared spectrum of carbon monoxide; Resolution = 1 cm^{-1}, top spectrum = 2.2 ppm, bottom spectrum = 20.2 ppm, total pressure is 700 mm N_2, path length is 255 m

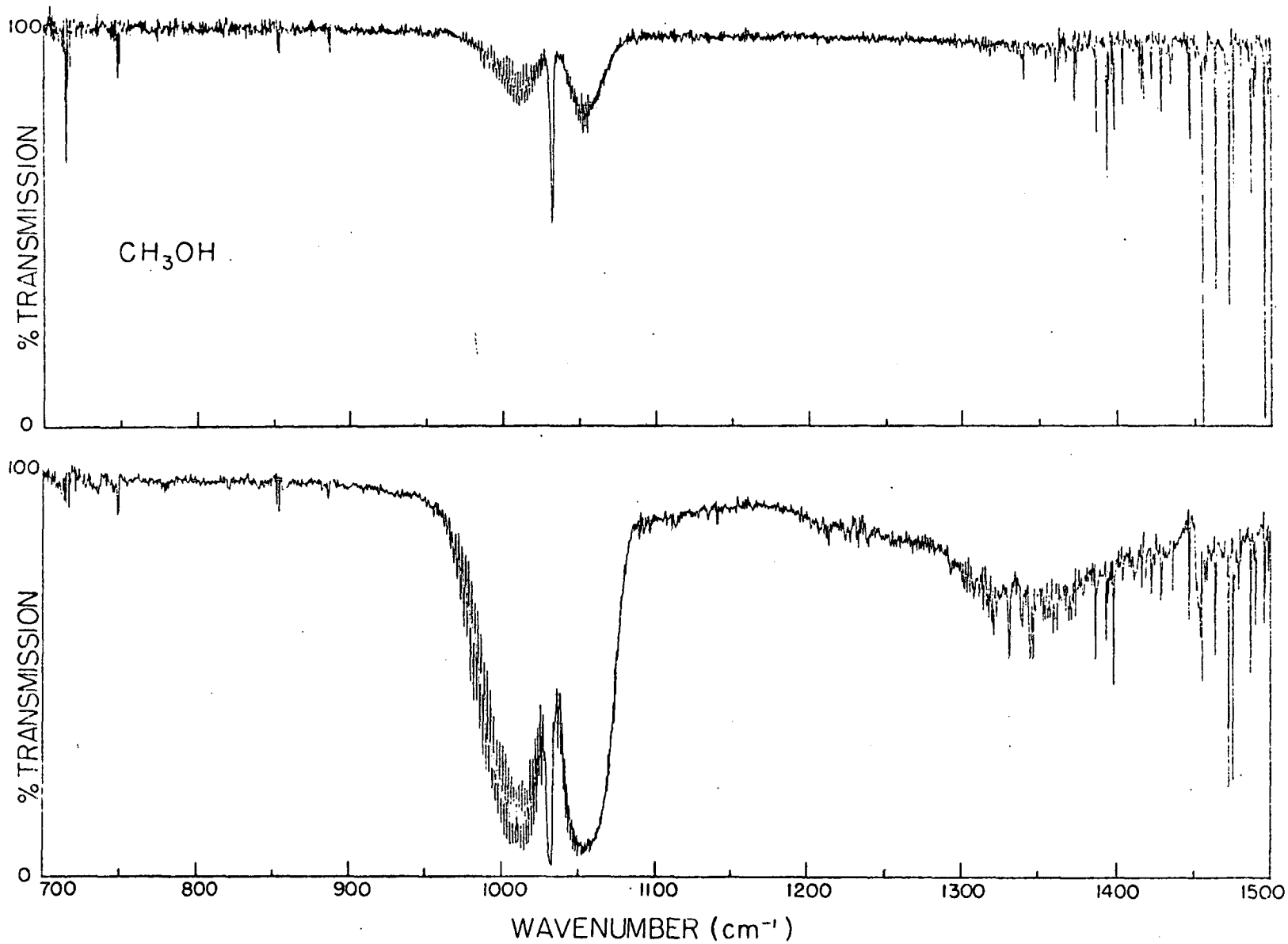

Figure 45. Infrared spectrum of methanol; Resolution = 1 cm^{-1}, top spectrum = 3.5 ppm, bottom spectrum = 19.6 ppm, total pressure is 700 mm N_2, path length is 255 m

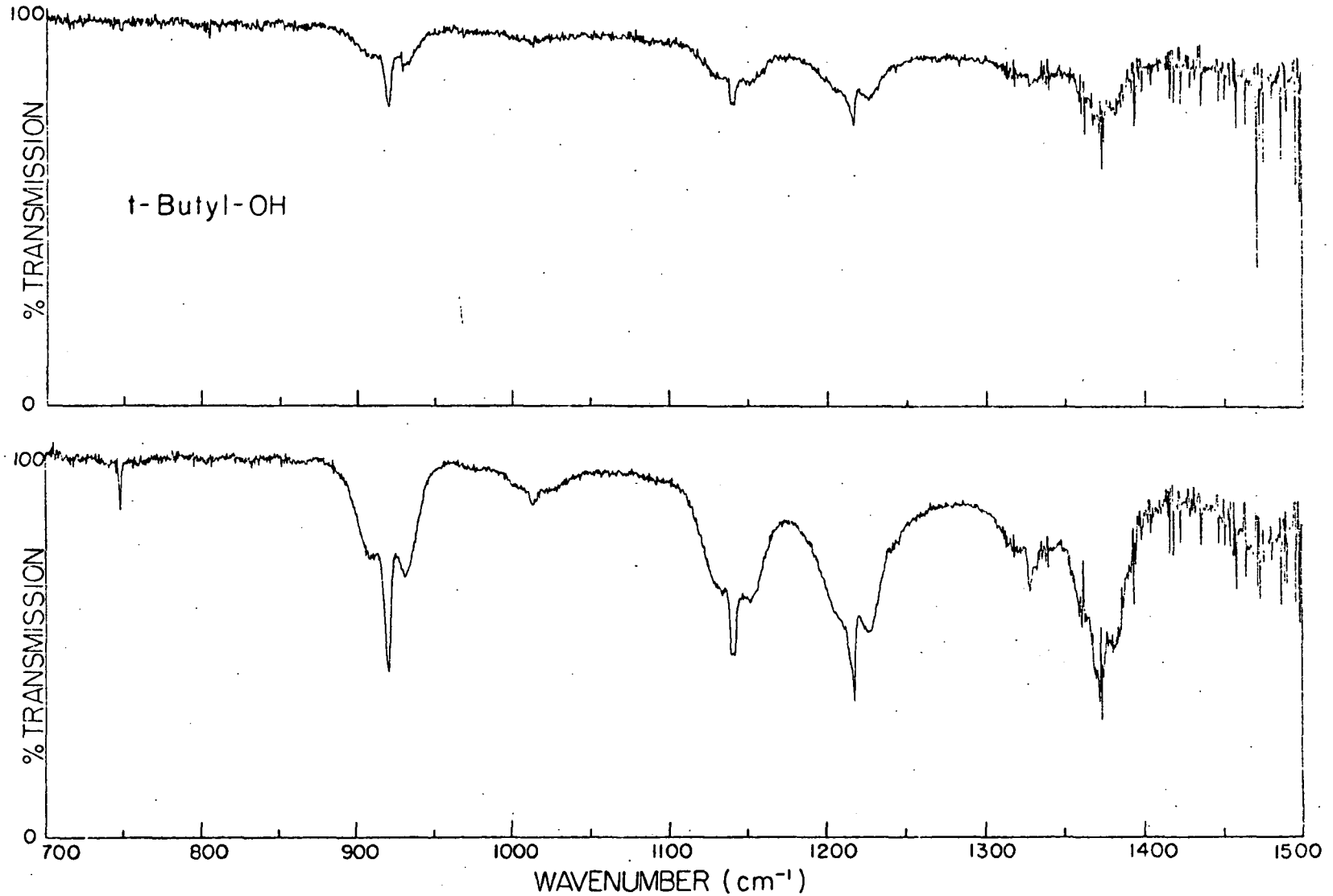

Figure 46. Infrared spectrum of t-butyl-alcohol; Resolution = 1 cm^{-1}, top spectrum = 1.9 ppm, bottom spectrum = 8.2 ppm, total pressure is 700 mm N_2, path length is 170 m

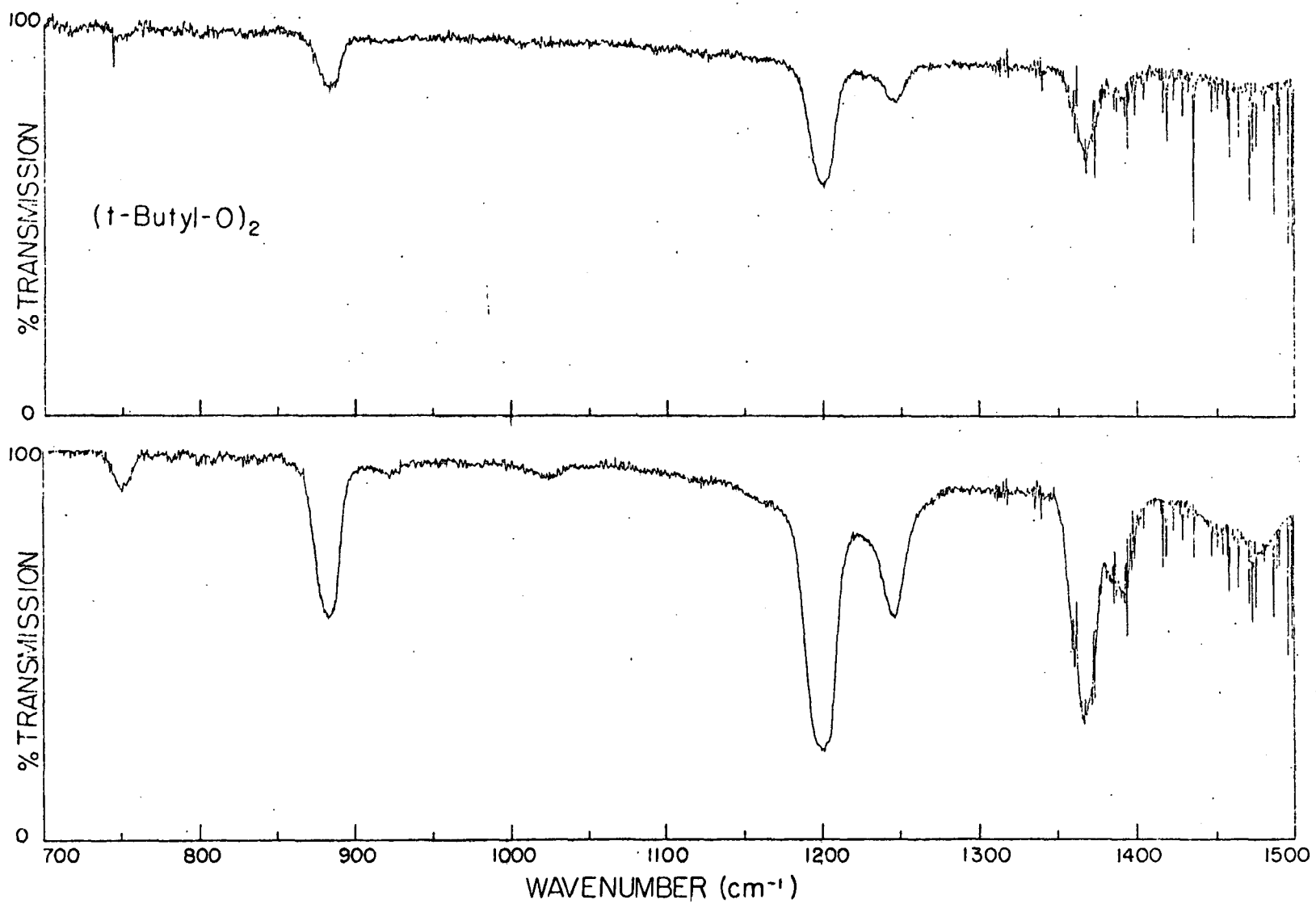

Figure 47. Infrared spectrum of di-t-butyl-peroxide; Resolution = 1 cm^{-1}, top spectrum = 1 ppm, bottom spectrum = 4.3 ppm, total pressure is 700 mm N_2, path length is 170 m

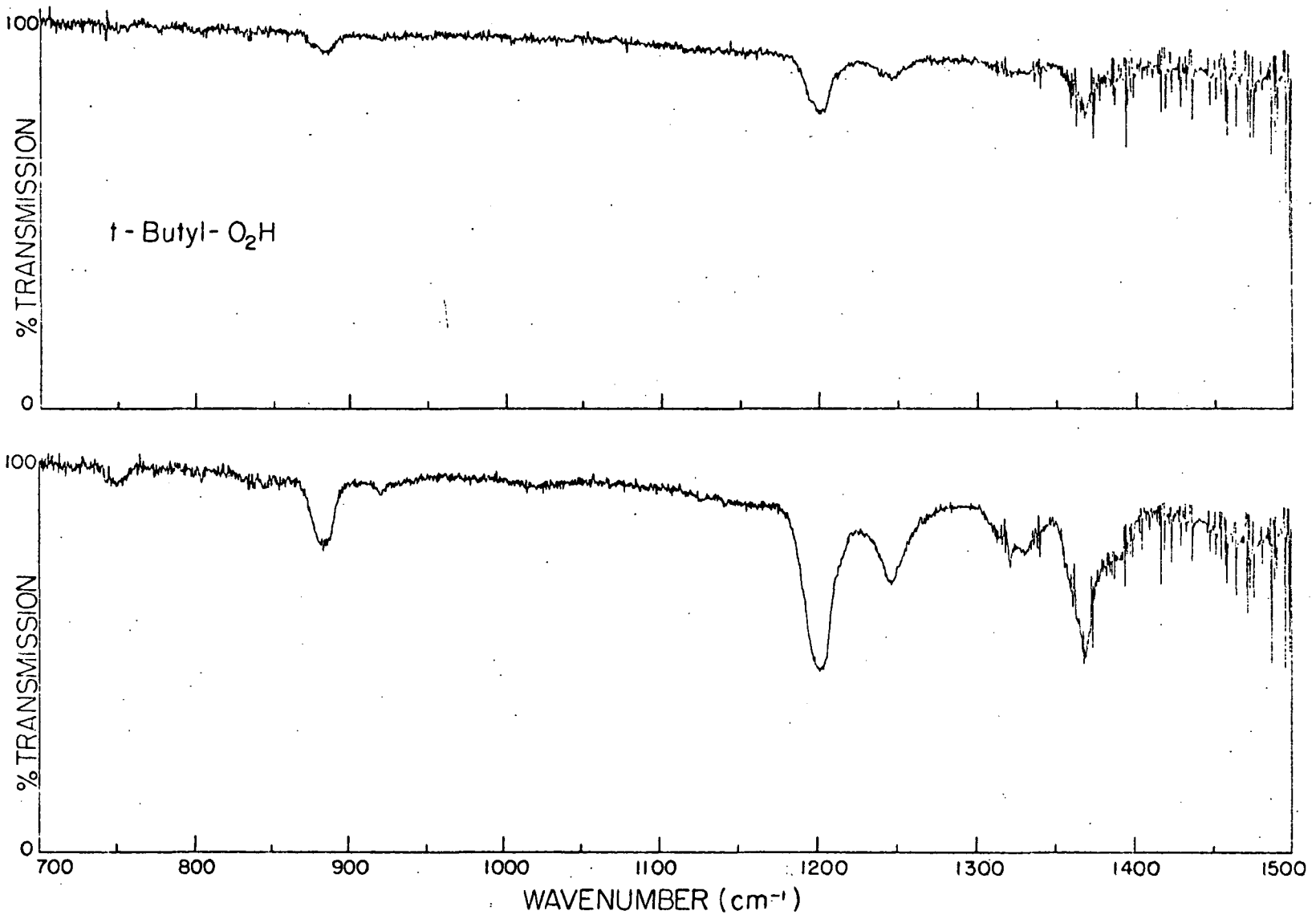

Figure 48. Infrared spectrum of t-butyl-hydroperoxide; Resolution = 1 cm^{-1}, top spectrum = 1.4 ppm, bottom spectrum = 6.0 ppm, total pressure is 700 mm N_2, path length is 170 m

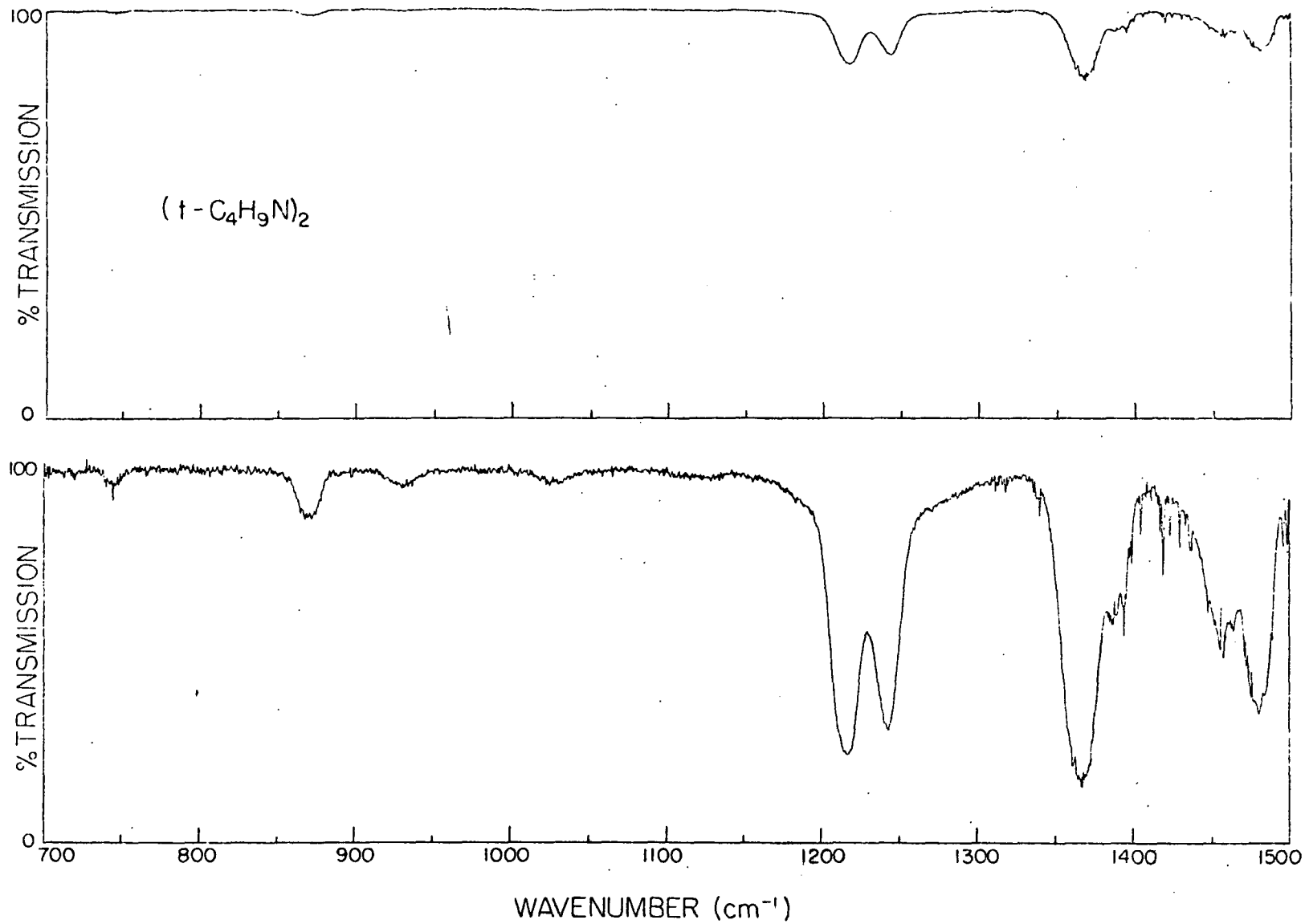

Figure 49. Infrared spectrum of 2, 2' - azoisobutane; Resolution = 1 cm^{-1}, top spectrum = 0.15 ppm, bottom spectrum = 15.4 ppm, total pressure is 700 mm N_2, path length is 170 m .

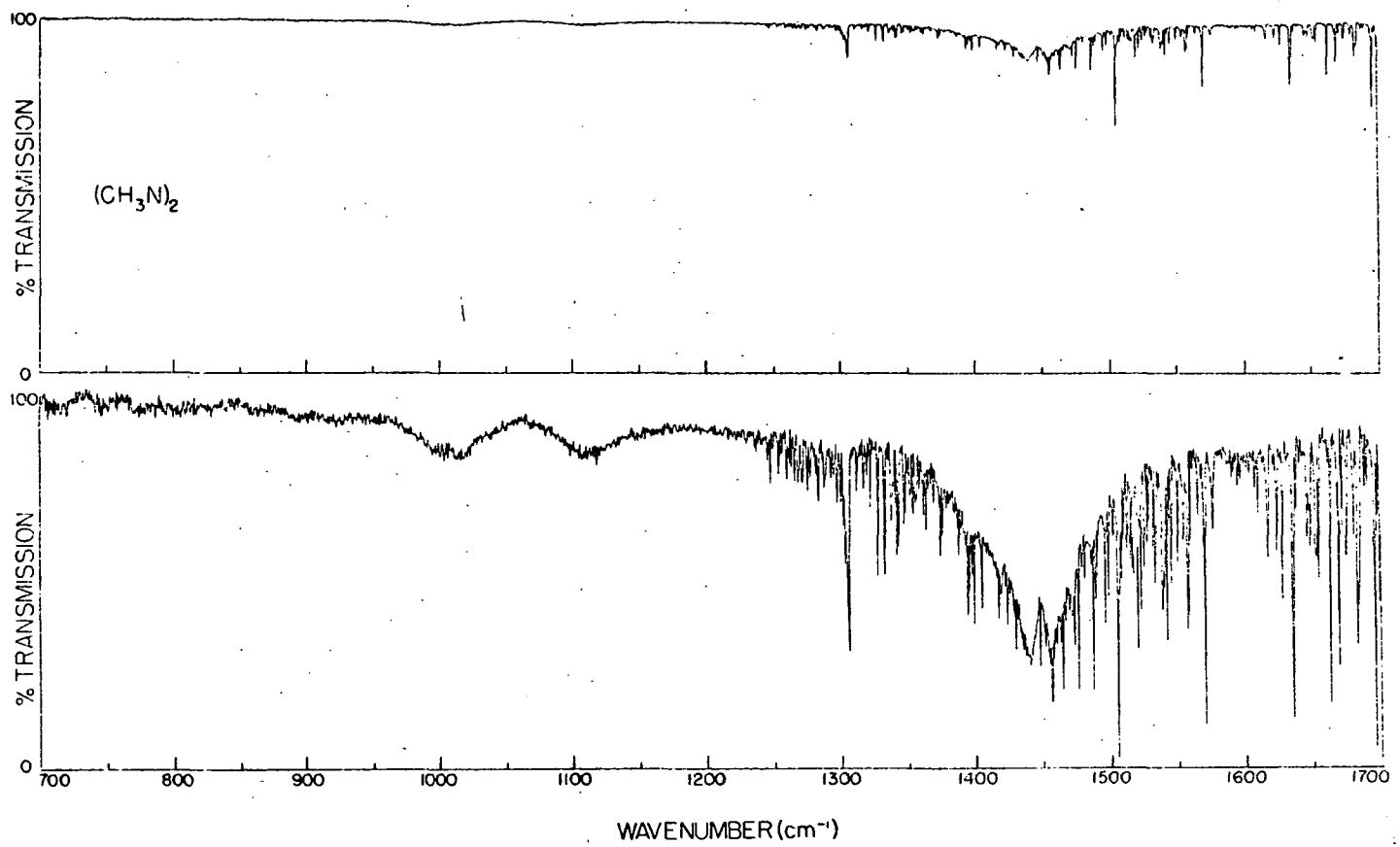

Figure 50. Infrared spectrum of azomethane; Resolution = 1 cm^{-1}, top spectrum = 3 ppm, bottom spectrum = 15 ppm, total pressure is 700 mm N_2, path length is 170 m; impurity band due to methane appears around 1300 cm^{-1}

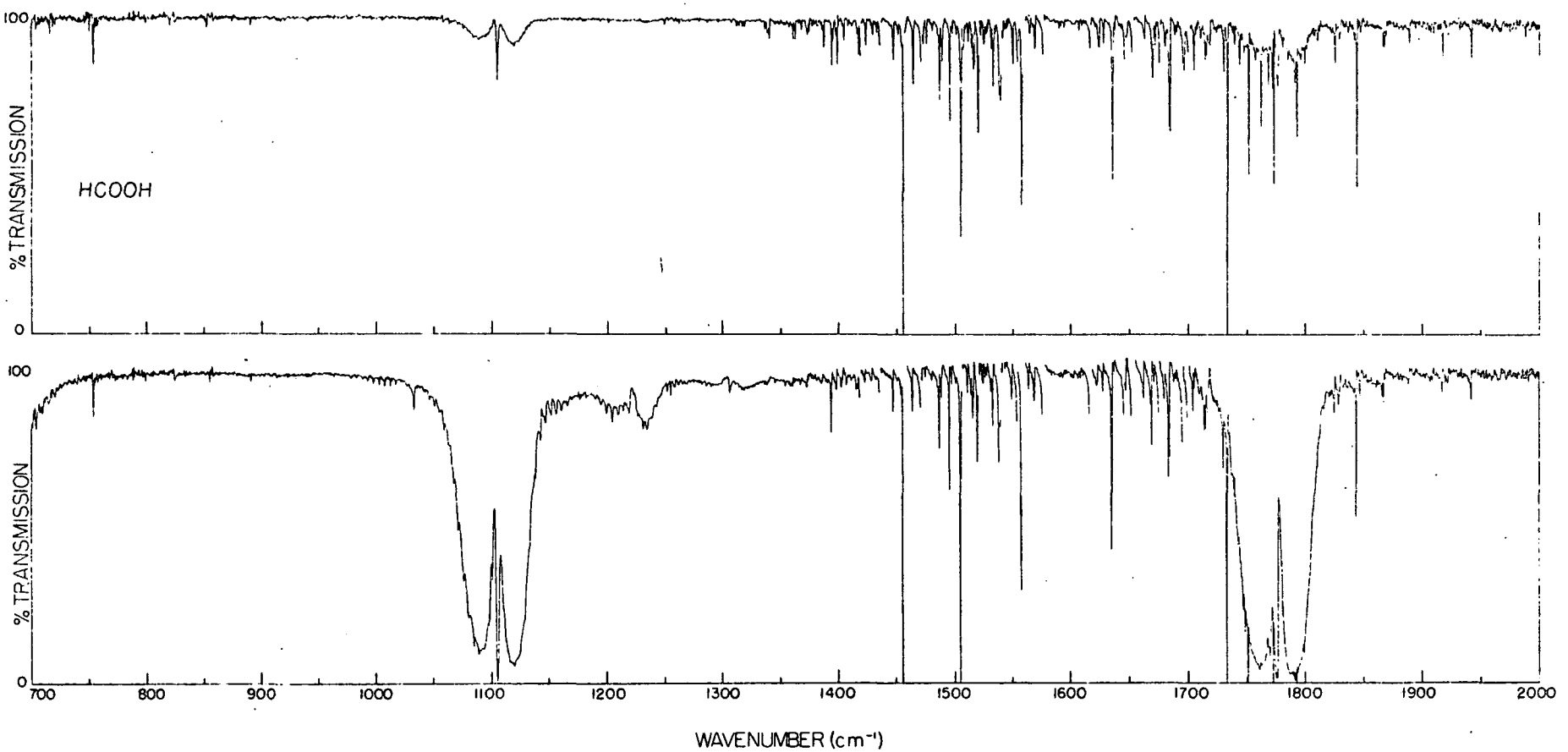

Figure 51. Infrared spectrum of formic acid; Resolution = 1 cm^{-1}, top spectrum = 0.52 ppm, bottom spectrum = 5.5 ppm, total pressure is 700 mm N_2, path length is 170 m

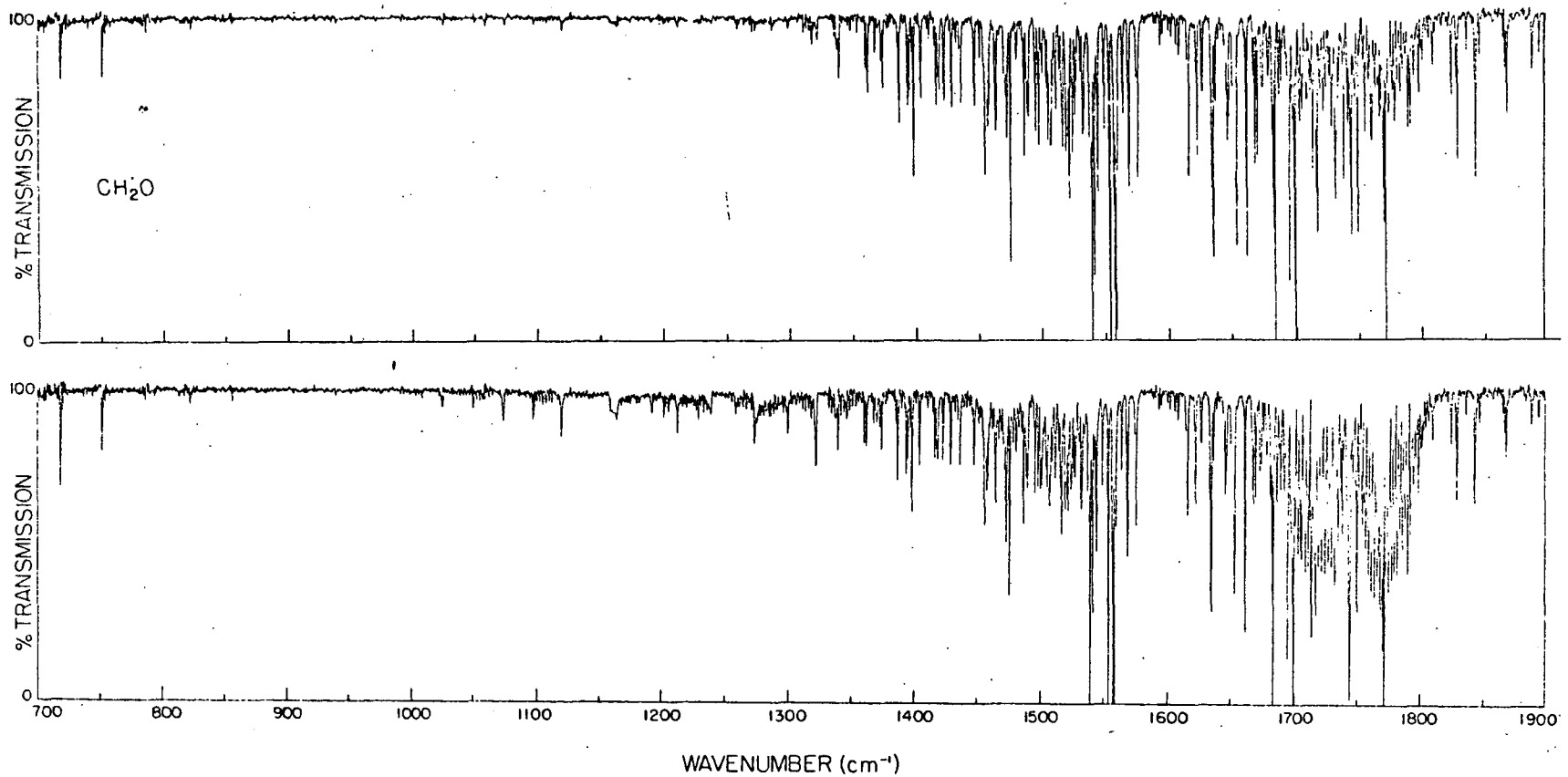

Figure 52. Infrared spectrum of formaldehyde; Resolution = 1 cm^{-1}, top spectrum = 4.6 ppm, bottom spectrum = 9.2 ppm, total pressure is 700 mm N_2, path length is 170 m

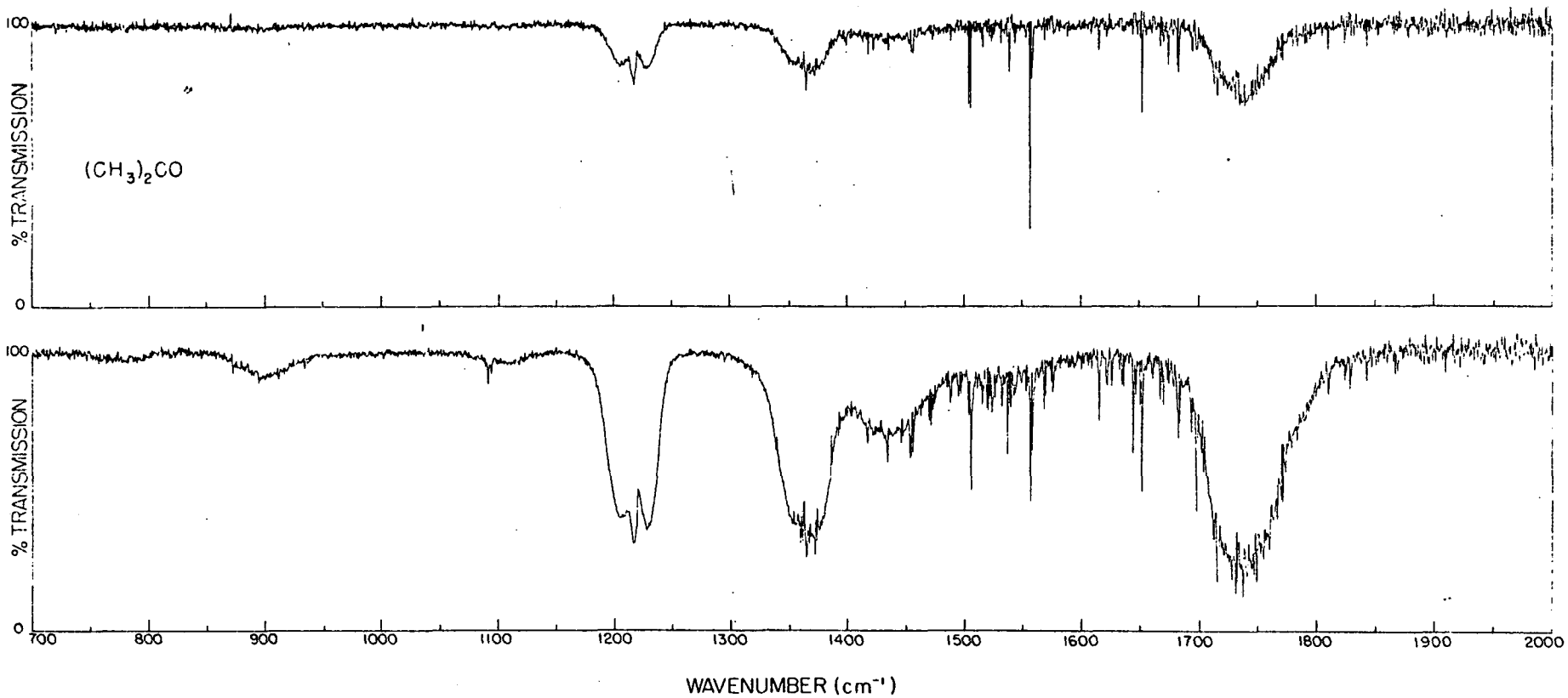

Figure 53. Infrared spectrum of acetone; Resolution = 1 cm^{-1}, top spectrum = 2.2 ppm, bottom spectrum = 16.4 ppm, total pressure is 700 mm N_2, path length is 170 m

CONCERNING PROBLEMS IDENTIFIED AS A RESULT OF THE PRESENT INVESTIGATION

SOLAR SPECTRA AND GROUND LEVEL AIR SPECTRA ANALYSIS

The comparison between these spectra and synthetic spectra calculated from the AFCRL line parameter testing has revealed that some of the line parameters need to be altered in order to improve the agreement between the spectra. We do not plan to improve the parameters throughout the entire spectral region investigated but it may be desirable to correct parameters associated with the lines of permanent gases which occur in spectral regions occupied by strong bands of possible atmospheric pollutants, in order to help in their identification.

We have attempted to estimate the abundance of fluorocarbon-12 (FC-12) from the appearance of its characteristic absorption features in solar spectra. We are currently attempting to derive line parameters for this molecule from laboratory spectra which will enable us to include the absorptance by this molecule in the synthetic spectra. Estimates of the abundances or upper limits to the abundances of these gases in the atmosphere can then be determined. Such a program requires first the generation of suitable quantitative spectra of known amounts of each gas and then the subsequent spectral analysis of the absorption bands. Such procedures are time consuming and will not be attempted unless they are of immediate concern to the program. It has already been found that the identification of FC-12 absorption features in solar spectra has been facilitated by the appropriate parameterization of its Q-branches and the subsequent use of these parameters to create synthetic solar spectra with varying amounts of FC-12 absorption.

In view of the possible importance of such studies we intend to cooperate with other workers in this area where possible. As part of this work analysis of the rotational structure of HNO_2 bands near 7.7-13.3 μm is being carried out. This work is described below.

In addition to these studies we also plan to investigate the low sun solar spectra which we have obtained and to identify as many H_2O lines as possible so that other remaining unidentified features can be located.

We also plan to use these synthetic spectra to monitor variations in the abundances of the permanent atmospheric gases, in particular of CO_2, N_2O, CO, and CH_4. We plan to investigate several spectral regions to locate those which show the greatest change in absorptance with the amount of gas present.

NITROUS ACID BAND ANALYSIS

It has been pointed out in a recent study on the chemical kinetics of HONO[41] that, contrary to previous belief, HONO formation in the free atmosphere can be of significance in environments which are rich in NO_x-H_2O. This is typical of conditions of power plant stacks and automotive exhaust pipes. Upon sunlight irradiation, HONO gives rise to HO radicals which play an important role in photochemical smog formation.

In order to facilitate the identification and detection of this molecule (HONO) in the atmosphere, moderately high resolution (0.125 cm^{-1}) spectra were obtained in the mid-IR region by Fourier transform spectroscopy using a path length of 42 m and a nitrous acid concentration of less than 5×10^{-5} atm.

The ν_4 bands of both the trans- and cis- isomers (at 790 and 852 cm^{-1}, respectively) and the ν_3 band of the trans-isomer (at 1263 cm^{-1}) are A-type transitions and are mildly degraded to higher energies. A partial rotational analysis of each of these bands has been carried out using Watson's Hamiltonian[42] and the lower state constants given by Cox et al.[43] Tentative assignments of transitions with quantum numbers up to $\overline{K} = \overline{6}$ and J = 20 have been made. The accuracy of the assignment is compromised by the fact that the present resolution does not allow us to resolve all the overlapping features to eliminate ambiguities. Intensity calculation of these bands will be carried out and comparisons between the observed spectra and the contours calculated will be made. With the determined upper state rotational constants, transition frequencies can be computed and they should facilitate detection with higher resolution tools such as laser spectroscopy.

A much weaker band of HONO has also been observed near 1068 cm^{-1}. This band exhibits B-type structure and is rather strongly degraded to lower energies. A preliminary analysis of the ^{p}Q and ^{r}Q heads suggests that it is an overtone band due to $2\nu_6$ of the trans-isomer. Rotational analysis of this band is intended to be carried out in the future. However, because of the very weak band intensity, unless HONO is present in a very large quantity, this band will be of little use for identification and detection purposes.

REFERENCES

1. M. J. Molina and F. S. Rowland, Nature 249, 810 (1974).

2. J. E. Lovelock, Nature 230, 379 (1971).

3. J. E. Lovelock, R. J. Maggs, and R. J. Wade, Nature 241, 194 (1973).

4. N. E. Hester, E. R. Stephens, and O. C. Taylor, J. Air Pollution Control Association 24, 591 (1974).

5. N. E. Hester, E. R. Stephens, and O. C. Taylor, Environ. Sci. Technol. 9, 875 (1975).

6. P. L. Hanst, L. L. Spillers, D. M. Watts, J. W. Spence and M. F. Miller, J. Air Poll. Control Assoc. 25, 1220 (1975).

7. D. G. Murcray, F. S. Bonomo, J. N. Brooks A. Goldman, F. H. Murcray, and W. J. Williams, Geophys. Res. Lett. 2, 109 (1975).

8. R. A. McClatchey, W. S. Benedict, S. A. Clough, D. E. Burch, R. F. Calfee, K. Fox, L. S. Rothman, and J. S. Garing, "AFCRL Atmospheric Absorption Line Parameters Compilation," AFCRL-TR-73-0096, Air Force Cambridge Research Laboratories Environmental Research Papers, No. 434 (1973).

9. E. K. Plyler and W. S. Benedict, J. Research NBS 47, 202 (1951).

10. J. C. Breeze, C. C. Ferriso, C. B. Ludwig, and W. Malkmus, J. Chem. Phys. 42, 402 (1965).

11. T. C. Kyle, Atlas of Computer Infrared Atmospheric Absorption Spectra, NCAR-TN/STR-112 (1975).

12. J. C. Fontanella, A. Girard, L. Gramont, and N. Louishard, Appl. Opt. 14 825 (1975).

13. M. T. Stier and W. A. Traub, Appl. Opt. 15, 364 (1976).

14. R. A. McClatchey, R. W. Fenn, J. E. A. Selby, J. S. Garing, and F. E. Volz, "Optical Properties of the Atmosphere," AFCRL-70-0527, (1970).

15. R. A. McClatchey and J. E. A. Selby, Atmospheric Attenuation of Laser Radiation from 0.76 μm to 31.25 μm, AFCRL-TR-74-0003, (1974).

16. W. L. Wolfe, Handbook of Military Infrared Technology, Government Printing Office (1965), pp. 228.

17. J. H. Shaw, M. L. Oxholm, and H. H. Claassen, Astrophys. J. 116, 554 (1952).

18. C. B. Farmer and P. S. Key, "A Study of the Solar Spectrum from 7 to 450 microns," EMI Report No. DMP 2160, (1965).

19. M. Migeotte, L. Neven, and J. Swensson, "The Solar Spectrum from 2.8 to 23.7 microns," Final Report under contract AF 61(514)-432, AFCRL Bedford Mass., (1965).

20. D. Murcray, private communication (1976).

21. W. S. Benedict and R. F. Calfee, "Line Parameters for the 1.9 and 6.3 micron Water Vapor Bands," ESSA Project Paper No. 2, Washington, D.C., (1967).

22. J. U. White, J. Opt. Soc. Amer., 32, 285 (1942).

23. D. J. McCaa, J. H. Shaw, J. Mol. Spec. 25, 374 (1968).

24. A. G. Maki, J. Mol. Spec. 57, 416 (1975).

25. W. E. Nexsen, Thesis, The Ohio State University, University Microfilms, Publication No. 16090, 53 pp.

26. D. Horn, and G. C. Pimentel, Appl. Optics, 10, 1892 (1971).

27. D. E. Burch, D. A. Gryvnak, R. R. Patty, J. Opt. Soc. Am. 57, 885 (1967).

28. R. Blickensderfer, G. Ewing, and R. Leonard, App. Opt. 7, 2114 (1968).

29. W. H. Chan, R. J. Nordstrom, J. G. Calvert and J. H. Shaw, Environ. Sci. Technol, 10, (1976), to appear June, 1976

30. J. P. S. Haarsma, G. J. deJong, J. Agterdenbos, Spect. Acta. 29B, 1 (1974).

31. Opthos Instrument Co., Rockville, Maryland.

32. Spectroscopic Studies of Photochemical Smog Formation and Trace Pollutant Detection, J. G. Calvert, W. H. Chan, R. J. Nordstrom, and J. H. Shaw, Final Report EPA Grant No. R803075, August 1975.

33. P. L. Hanst, "Spectroscopic Methods for Air Pollution Measurements," in Advances in Environmental Science and Technology, Vol. II, J. N. Pitts, Jr. and R. L. Metcalf Eds. (Wiley, New York, 1971), p. 91.

34. J. G. Calvert, Environ. Sci. and Technol., 10. 248 (1976).

35. J. R. Holmes, R. J. O'Brien, J. H. Crabtree, T. A. Hecht, J. H. Seinfeld, Environ. Sci. Techol., 7, 519 (1973).

36. D. H. Stedman and H. Niki, Envir. Sci. and Techol. 7, 735 (1973).

37. C. H. Wu and H. Niki, Environ. Sci. Techol., 9, 46 (1975).

38. K. L. Demerjian, J. A. Kerr, and J. G. Calvert, Adv. Environ. Sci. and Technol., 4, 1 (1974); see pp. 149

39. D. Garvin, "Chemical Kinetics Data Surveys" IV (NBSIR 73-203), V (NBSIR 73-206), VII (NBSIR 74-430).

40. H.S. Johnston and Graham, Can. J., Chem., 52, 1415 (1974).

41. W. H. Chan, R. J. Nordstrom, J. G. Calvert and J. H. Shaw, Chem. Phys. Letts., 37, 441 (1976).

42. J. K. G. Watson, J. Chem. Phys., 46, 1935 (1967).

43. A. P. Cox, A. H. Brittain and D. J. Finnigan, Trans. Faraday Soc., 67, 2179 (1971).

44. H. S. Johnston and L. Zafonte, quoted by A. C.Lloyd, Int. J. Chem. Kinet. in press.

45. D. D. Davis, W. A. Payne, and L. J. Stief, Sci., 179, 280 (1973).

46. R. Simonaites and J. Heicklen, J. Phys. Chem., 77, 1096 (1973).

47. J. G. Calvert and E. W. R. Steacie, J. Chem. Phys., 19, 176 (1951).

48. P. L. Hanst and J. G. Calvert, J. Phys. Chem., 63, 71 (1969).

49. B. A. DeGraff and J. G. Calvert, J. Am. Chem. Soc., 89, 2247 (1967).

50. R. D. McQuigg and J. G. Calvert, J. ibid., 91, 1590 (1969).

51. J. J. Bufalini and K. L. Brubaker, "Chemical Reactions in the Urban Atmospheres," C. S. Tuesday Editor, Elsevier Publishing Co., N.Y. 1971, p. 225.

52. B. Dimitriades and T. C. Wesson, J. Air Pollution Control Assoc., 22, 33 (1972).

APPENDIX I

SUMMARY OF OBJECTIVES FROM 1975 PROPOSAL

I. SUMMARY OF OBJECTIVES

The primary objective of the research outlined in this proposal is to develop infrared fourier transform spectroscopic (FTS) techniques to characterize certain key air pollutants, their precursors and reaction products, and to establish quantitative kinetic and mechanistic details of the interrelationships between these pollutants both in simulated and real atmospheres. We have chosen for study during the three year period of this research effort the following important, yet unresolved, problems related to the transformations of contaminants in both the troposphere and stratosphere. These systems are particularly well suited for study with the FTS system and associated equipment now in use at the Ohio State University laboratories.

1. Study of the natural removal mechanisms of the Freons and their influence on the ozone concentration in the stratosphere:

   a) The chlorine atom sensitized decomposition of ozone. The chemical kinetics and mechanism of interactions in the irradiated O_3, NO, NO_2, Cl_2 system.

   b) The fate of the organic free radicals formed by photodissociation of the Freons in the stratosphere. The chemical kinetics and mechanisms of the reactions of the CF_2Cl and CCl_2F free radicals in air at stratospheric pressures.

   c) The alteration of the stratospheric ozone concentration through Freon addition. The laboratory simulation of the photochemistry of the stratosphere perturbed by Freon addition.

2. Study of certain key reactions, seemingly important in photochemical smog systems:

   a) The role of nitrous acid in the development of the important free radical chain carrier, HO, and its relation to smog formation in the urban atmosphere. A kinetic study of the NO, NO_2, HONO, CO system. The quantum efficiency of HO radical formation in the sunlight photolysis of HONO in air. The determination of important rate constants for the HO reactions with NO and NO_2, and HO_2 with NO will be made.

b) The role of the aldehydes in smog development in the urban atmosphere. The nature and mechanism of the formation of the products formed in the photooxidation of formaldehyde. A kinetic study of the CH_2O, NO, NO_2, air, and the CH_2O, NO, NO_2, Cl_2, air systems. A search for the ellusive peroxyformyl nitrate.

c) A study of some potentially important SO_2 removal mechanisms in the lower atmosphere. The rates of the primary reactions of HO and HO_2 with SO_2 from the FTS study of the CH_2O, SO_2, CO, air and HONO, SO_2, CO, air systems. The nature of the SO_2-oxidizing species formed in the O_3-olefin dark reaction.

d) The determination of high resolution infrared spectra of the common atmospheric contaminants and their products. Cataloging of the absorption coefficient-wavelength data for use in this work and by other investigators in the field.

e) Direct observation of the infrared absorption spectra of air samples in Columbus, Ohio. We will employ both in situ samples, observed using solar infrared transmission spectra in long atmospheric paths near sunset and sunrise, and confined samples in the laboratory long-path system (up to 1.5 km); spectra will be taken at regular intervals throughout the period.

APPENDIX II

PAPERS PUBLISHED OR ACCEPTED FOR PUBLICATION

1. "An IRFTS Spectroscopic Study of the Kinetics and the Mechanism of the Reactions in the Gaseous System, HONO, NO, NO_2, H_2O." Walter H. Chan, Robert J. Nordstrom, Jack G. Calvert, and John H. Shaw, Chemical Phys. Letters, 37, 441-446 (1976).

2. "A Kinetics Study of HONO Formation and Decay Reactions in Gaseous Mixtures of HONO, NO_2, H_2O and N_2." Walter H. Chan, Robert J. Nordstrom, Jack G. Calvert and John H. Shaw, to appear in Environmental Science and Technology, July, 1976.

3. "A Spectroscopic Study of the NO_2-N_2O_4 System by the Infrared Absorption Technique," Robert J. Nordstrom and Walter H. Chan, J. Phys. Chem., 80, 847-850 (1976).

APPENDIX III

LIST OF PAPERS PRESENTED AT MEETINGS

1. "An IRFTS Spectroscopic Study of the Kinetics and the Mechanism of the Reactions in the Gaseous System, HONO, NO, NO_2, H_2O." Walter H. Chan, Robert J. Nordstrom, Jack G. Calvert and John H. Shaw, presented at the Centennial ACS meeting, New York City, April, 1976.

2. "A Partial Analysis of HONO Bands Between 750 and 1300 cm^{-1}". Walter H. Chan, C. Weldon Mathews and Robert J. Nordstrom, presented at the 31st Symposium of Molecular Structure and Spectroscopy, Columbus, Ohio, June, 1976.

3. "Infrared Spectroscopic Detection of Fluorocarbon-12 in the Atmosphere." Robert J. Nordstrom, W. R. Skinner, J. H. Shaw, W. H. Chan, W. M. Uselman, and J. G. Calvert, presented at the 31st Symposium of Molecular Structure and Spectroscopy, Columbus, Ohio, June, 1976.

4. "Comparison of Measured and Computer Spectra of Air Samples." R. J. Nordstrom, W. R. Skinner, J. H. Shaw, W. H. Chan, W. M. Uselman, and J. G. Calvert, presented at the 31st Sympsoium of Molecular Structure and Spectroscopy, Columbus, Ohio, June, 1976.

TECHNICAL REPORT DATA
(Please read Instructions on the reverse before completing)

1. REPORT NO. EPA-600/3-77-025	2.	3. RECIPIENT'S ACCESSION NO.
4. TITLE AND SUBTITLE APPLICATION OF FOURIER TRANSFORM SPECTROSCOPY TO AIR POLLUTION PROBLEMS Interim Report - 1976		5. REPORT DATE August 1977
		6. PERFORMING ORGANIZATION CODE
7. AUTHOR(S) J. G. Calvert, W. H. Chan, E. Niple, R.J. Nordstrom, J.H. Shaw, W.R. Skinner, and W.M. Uselman		8. PERFORMING ORGANIZATION REPORT NO.
9. PERFORMING ORGANIZATION NAME AND ADDRESS The Ohio State University Research Foundation 1314 Kinnear Road Columbus, Ohio 43212		10. PROGRAM ELEMENT NO. 1AA603
		11. CONTRACT/GRANT NO. R803868-1
12. SPONSORING AGENCY NAME AND ADDRESS Environmental Sciences Research Laboratory - RTP, NC Office of Research & Development U.S. Environmental Protection Agency Research Triangle Park, North Carolina 27711		13. TYPE OF REPORT AND PERIOD COVERED Interim
		14. SPONSORING AGENCY CODE EPA/600/09

15. SUPPLEMENTARY NOTES
See companion reports EPA-600/3-77-026, Computer-Generated Long-Path Air Spectra, and EPA-600/3-77-040, Comparison of Observed and Computed Air Spectra Between 700 and 2300 cm^{-1}

16. ABSTRACT

Spectra of air samples at ground level of approximately 10m, 100m, and 1km, and solar spectra obtained for solar zenith distances between 40° and 87° have been obtained. Examples of these spectra in the region from 1100 to 1200 cm^{-1} are presented together with spectra calculated from the atmospheric line parameter listing prepared by the Air Force Geophysical Laboratories. From the absorption features of fluorocarbon-12 near 1160 cm^{-1} in solar spectra, a mean tropospheric abundance of 0.34 ppb has been estimated.

A photochemical cell capable of approximating the solar noon irradiance at ground level between 300 and 400nm and in which path lengths in excess of 200m can be obtained is described. This cell has been used to study the photolysis of HNO_2 and a rate constant of 0.070 min^{-1} has been measured.

Spectra of more than 20 gases of importance to air pollution problems, obtained under controlled conditions covering the region from 700 to 1500 cm^{-1}, are presented.

Progress in the construction of a cell, coolable to $-60^{o}C$, and capable of being irradiated at wavelengths down to 170nm, is described.

17. KEY WORDS AND DOCUMENT ANALYSIS

a. DESCRIPTORS	b. IDENTIFIERS/OPEN ENDED TERMS	c. COSATI Field/Group
* Air Pollution * Infrared spectroscopy * Optical equipment Solar spectrum * Reaction kinetics * Photochemical reactions	Fourier transform spectrometer	13B 14B 20F 03B 07D 07E

18. DISTRIBUTION STATEMENT RELEASE TO PUBLIC	19. SECURITY CLASS *(This Report)* UNCLASSIFIED	21. NO. OF PAGES 113
	20. SECURITY CLASS *(This page)* UNCLASSIFIED	22. PRICE

EPA Form 2220-1 (9-73)